République Algérienne Démocratique et Populaire
Ministère de l'Enseignement Supérieur et de la Recherche Scientifique

Ecole Nationale Polytechnique
Department of Electronic
Laboratory of Communication Devices
and Photovoltaic Conversion

PhD Thesis in Electronic

Presented by:

Moussaab BOUNABI

Entitled:

Study of topologies and architectures of DC-AC photovoltaic converters connected to the grid

Members of jury:

Mourad. ADNANE	MCA , ENP	President
Linda. BARAZANE	Professor, USTHB	Examiner
Linda. HASSAINE	Research Director, CDER	Examiner
Mourad. HADDADI	Professor, ENP	Examiner
Mohammed. S. AIT-CHEIKH	Professor, ENP	Supervisor
Cherif. LARBES	Professor, ENP	Supervisor

ENP 2019

République Algérienne Démocratique et Populaire
Ministère de l'Enseignement Supérieur et de la Recherche Scientifique

Ecole Nationale Polytechnique
Department of Electronic
Laboratory of Communication Devices
and Photovoltaic Conversion

PhD Thesis in Electronic

Presented by:

Moussaab BOUNABI

Entitled:

Study of topologies and architectures of DC-AC photovoltaic converters connected to the grid

Members of jury:

Mourad. ADNANE	MCA , ENP	President
Linda. BARAZANE	Professor, USTHB	Examiner
Linda. HASSAINE	Research Director, CDER	Examiner
Mourad. HADDADI	Professor, ENP	Examiner
Mohammed. S. AIT-CHEIKH	Professor, ENP	Supervisor
Cherif. LARBES	Professor, ENP	Supervisor

ENP 2019

République Algérienne Démocratique et Populaire
Ministère de l'Enseignement Supérieur et de la Recherche Scientifique

Ecole Nationale Polytechnique
Département d'Electronique
Laboratoire des Dispositifs de Communication
et de Conversion Photovoltaïque

Thèse de Doctorat En Electronique

Option : **Electricité Solaire**

Présentée par :

Moussaab BOUNABI

Intitulée

Etude des topologies et architectures des onduleurs photovoltaïque connecter au réseau électrique

Proposée et dirigée par :

Mourad ADNANE	MCA à l'ENP	Président
Linda. BARAZANE	Professeur à l'USTHB	Examinatrice
Linda. HASSAINE	Directeur de Recherche au CDER	Examinatrice
Mourad HADDADI	Professeur à l'ENP	Examinateur
Mohammed. S. AIT-CHEIKH	Professeur à l'ENP	Directeur de thèse
Cherif. LARBES	Professeur à l'ENP	Co-directeur de thèse

ENP 2019

Laboratoire de Dispositifs de communication et de Conversion Photovoltaïque (LDCCP),
10 Avenue Hassen BADI, El-Harrach 16200
Alger Algérie

ACKNOWLEDGEMENT

This thesis has been conducted at the Laboratory of Communication Devices and Photovoltaic Conversion in the Department of Electronic of Ecole Nationale Polytechnique (ENP) of Algiers.

First of all, I would like to take this opportunity to express my deepest gratitude and thanks to my project supervisors, Professor **Mohamed Saleh Ait-Cheikh** and Professor **Cherif Larbes** for their constant guidance, assistance and support as well as all the knowledge they shared during the course of this research.

I also wish to thank the President of jury Mr **Mourad ADNANE**, Professor at ENP, and the members of the jury: Mr **Mourad HADDADI** Professor at ENP, Ms **Linda Barazane**, Professor at USTHB and Ms **Linda HASSAINE**, director of research at the CDER, for accepting to be members of the reading committee and for their constructive analysis of the present work.

Further, I sincerely thank Professor **Naeem Ramzan** for kindly inviting me to stay as a Ph.D. student visitor at the School of Engineering and Computing, University of the West of Scotland (UWS), in United Kingdom. The friendly and focused atmosphere at the UWS was a very memorable experience.

Last but not least, I would like to express my appreciation and gratitude to my family members, who have encouraged, motivated and supported me during my studies.

Abstract

ملخص—تقترح هذه الأطروحة بنية تحكم جديدة لنوعين من المحولات ثلاثية الأطوار متعددة المستويات المخصصة للأنظمة الكهروضوئية المتصلة بالشبكة الكهربائية. يشتمل مبدأ التحكم على استخدام تقنية "تحوير نبض العرض المتجه" للتحكم في طوبولوجيا العاكس المشبك والعاكس المتتالي، وكذا تطبيق لوغاريتمية "إستمثال عناصر السرب" لتشغيل النظام الكهروضوئي عند نقطة القدرة القصوى. في هذه الأطروحة إقترحنا تطبيق مصفوفة البوابات المنطقية القابلة للبرمجة مرتكزة على إستمثال عناصر السرب لحل مشكلة تتبع نقطة القدرة القصوى تحت شروط التظليل الجزئي، وتم التحقق من صحة هذه التقنية لمختلف التشكيلات الممكنة للوائح الضوئية من أجل تقييم سلوك كل تشكيل تحت توزيع إضائي غير موحد. يالإضافة إلى هذا تم استخدام استراتيجية تحوير نبض العرض المتجه لتوليد إشارات تحكم العاكس وتطبيقها على طبولوجيا العاكس المتتالية. كما أجريت دراسة مقارنة للنظم الكهروضوئية المتصلة مع كلا النوعين في بيئة MATLAB / Simulink وتقييمها على أساس تتبع القدرة القصوى والتشوه التوافقي والتكلفة. من أجل اختبار التنفيذ العملي لهيكل الرقابة المقترح، تم استخدام النهج القائم على الربط بين FPGA و Simulink لجعل النتائج أقرب ما يمكن إلى الواقع وبحد أدنى من القيود. ختاما تم وضع جدول مقارن على أساس تحليل النتائج التي تم الحصول عليها وتلخيص بعض المعلمات التجريبية.

الكلمات المفتاحية: الأنظمة الضوئية، المحولات المتعددة المستويات، استمثال عناصر السرب، تحوير نبض العرض المتجه.

Résumé—Cette thèse propose une nouvelle structure de contrôle de deux onduleurs triphasés multi-niveaux dédiés aux systèmes photovoltaïques (PV) connectés au réseau électrique. Ce principe de commande inclut l'utilisation de la technique de modulation de largeur d'impulsions vectorielles (SVPWM) pour contrôler les topologies d'onduleurs à diode clamper et des onduleurs en cascade. La recherche intègre la technique d'optimisation par essaims de particules pour faire fonctionner le système photovoltaïque au point de puissance maximale (MPP). Une implémentation sur FPGA, basée sur le PSO, est proposée pour résoudre le problème du suivi du MPP dans des conditions d'ombrage partiel. Cette technique est validée sous différentes configurations de générateur PV afin d'évaluer le comportement de chaque configuration PV sous un ensoleillement non uniforme. La stratégie de la SVPWM est utilisée afin de générer des signaux de contrôle de l'onduleur et implémentée pour les topologies d'onduleurs DCI et en cascade. Puis une étude comparative des systèmes photovoltaïques avec ces topologies d'onduleurs est réalisée dans l'environnement Matlab / Simulink et évaluée sur la base du MPPT, distorsion harmonique, coût, avantages et inconvénients. Afin de tester la mise en œuvre pratique de la structure de contrôle proposée, l'approche basée sur « hardware in the Loop » est utilisée pour rapprocher le plus possible les résultats obtenus de la réalité et avec un minimum de contraintes.

Mots clés : Système photovoltaïque ; Onduleurs multi-niveaux ; PSO ; SVPWM.

Abstract—This thesis proposes a new control structure for two multilevel three-phase inverter topologies for photovoltaic (PV) systems connected to the grid. This control scheme includes the use of the space vector pulse wide modulation (SVPWM) technique to control the Diode Clamped Inverter (DCI) and cascade inverter topologies and the integration of a particle swarm optimization (PSO) technique to operate the PV system at the Maximum Power Point (MPP). An FPGA implementation of PSO based MPPT is proposed to overcome the problem of MPP tracking under partial shading conditions. This MPPT technique is validated under various PV array configurations in order to evaluate the behavior of each PV configuration under non-uniform irradiation. An SVPWM control strategy is used in order to generate gate control signals for the inverter and implemented for both DCI and cascade inverter topologies. Then, a comparative study of photovoltaic systems with these inverter topologies is carried out under MATLAB/Simulink environment and evaluated on the basis of MPPT, harmonic distortion, cost, advantages and disadvantages. In order to test the practical implementation of the proposed control structure, FPGA/Simulink-based Hardware in the Loop approach has been used to bring the obtained results as close as possible to reality and with a minimum of constraints. Based on the analysis of the obtained results, some experimental parameters are summarized and a comparison table is synthesized.

Keywords: Photovoltaic systems; Multilevel inverters; PSO-MPPT; SVPWM.

CONTENTS

LIST OF FIGURES

LIST OF TABLES

CHAPTER 1

GENERAL INTRODUCTION

Contents

1.1 Introduction

In recent years, renewable energy systems have attracted remarkable attention and investment in many countries [1], due to concerns about environmental issues, ever-increasing world's energy demand and outlook of depletion of fossil fuel reserves [2]. Among renewable energy systems, photovoltaic (PV) systems are expected to play an important role in the future and, as such, a great deal of research effort is dedicated to enhancing their performance and efficiency, at both component and system levels. PV systems are either connected to a large independent grid and feed power to the grid or are separated from any grid and operate as the main power supply for a group of loads, mostly in remote buildings and communities [3].

1.2 Statement of problem and research objectives

The aim of this research is to study the factors that limit the capacity, efficiency, power quality, and the safety of the grid-connected large-scale PV systems, and to propose appropriate solutions to improve those factors:

- Capacity: Although large-scale PV farms have reached a capacity of up to several hundred MW, the single PV inverter capacity is limited to about 1 MW, and larger power ratings are achieved by parallel connections of the smaller inverter units [4]. Since one large inverter can offer better efficiency, lower cost, and easier implementation compared to the two parallel-connected (smaller) half-rated inverters, improving the capacity of the PV inverters can be one major contributing factor to further support the solar PV industries' fast growth.

- Efficiency: The efficiency of PV systems is affected by its components, which include the PV array and inverter, and the system configuration [5–7]. Different PV array configurations yield different levels of mismatch power loss, especially under partial shading conditions, and thus produce different total energy. Further, under normal operating conditions, the efficiency of different inverter and system configurations is affected by the switching power loss over the inverter

switches and by the conduction power loss all over the DC- and AC-side cables, switches, filter, and transformer [8].

- Power quality: With the fast growth of distributed generators, including the PV, the quality of their produced power needs to be further improved in order to not adversely affect the hosting network's performance. This can be achieved through utilizing appropriate inverter structures, inverter control schemes, and/or better filters [9].

- Safe grid-integration: Among the many grid-integration issues of PV systems, which includes the fault ride-through capability, islanding detection, and ancillary services provision, the over-voltage produced by PV systems (like other distributed generators) is one subject of interest in this thesis. With the widespread penetration of distributed generators (DGs) in power systems, the grid and DGs are facing the ever-increasing problem of temporary over-voltages produced by DGs and their damages on utility equipment and customer loads, especially the single-phase ones [10]. Appropriate solutions need to be worked out to prevent over-voltage formation and/or to suppress the produced over-voltage in the contributing DGs' structure.

Thus, this thesis aims to propose PV systems (consisting of array, inverter, and grid interface) which address all of the aforementioned characteristics and deliver better energy yield, higher capacity, better power quality, and safer integration with the utility network. To this end, PV array configurations and single- and two-stage as well as two- and multi-level inverter structures will be studied and appropriate structures and control strategies/schemes will be developed to achieve the defined goals. Therefore, more specific objectives of this thesis are:

- To develop a PV array model in order to study the efficiency of different PV array interconnection methods in central-configured PV systems, especially during partial shading conditions, and to search for methods to mitigate the disproportionate mismatch power loss during partial shading and characteristic mismatch conditions.

- To study the restrictions of the conventional single-stage converters for higher power ratings, to develop a two-stage conversion system, based on modular inverter technology, to further improve the capacity, efficiency, and output power quality, and to introduce multi-MPPT and distributed PV array structures.

- To study the grid integration issues of the PV systems, especially the temporary over-voltage (TOV) problem caused by PV systems in the power network, and to propose appropriate mitigation techniques.

1.3 Background and related works

According to the EPIA data, the total PV generation connected to the electricity grid surpassed 100 GW in 2012 and 300 GW in 2016 [11]. In 2017, cumulative solar PV capacity reached almost 398 GW and generated over 460 TWh, representing around 2% of global power output. Utility-scale projects account for just over 60% of total PV installed capacity, with the rest in distributed applications (residential, commercial and off-grid). Over the next five years, solar PV is expected to lead renewable electricity capacity growth, expanding by almost 580 GW under the Renewables 2018 main case. As stated in the same EPIA data report: **"Under optimal conditions, the world's solar generation plant capacity could reach up to 1,270.5 GW by the end of 2022, but we consider 1,026.2 GW more likely. Still, that means solar would reach the terawatt production capacity level in 2022. Reaching the 400 MW milestone already in 2017, we now expect in our Medium Scenarios the total global installed PV capacity to exceed 500 GW in 2018, 600 GW in 2019, 700 GW in 2020, 800 GW in 2021 and 1 TW in 2022"** [11].

The installed-system prices continue to fall, and PV is becoming increasingly more cost competitive across regions with high electricity consumption than the domestic power generation. This, together with the improved efficiency of PV system components, especially the solar panels, and the environmental concerns related with conventional and nuclear power plants given the Fukushima nuclear plant disaster of 2011, accelerate further growth of the PV industry, which in turn, further reduces the

prices in a positive feedback form [12].

To maintain this fast growth, on the one hand, and to deal with potential power network problems and complexity because of the high penetration of PV systems, on the other hand, much research is being conducted on improving the PV systems' performance and profitability and on the safe and supportive integration of them within the grid.

1.3.1 PV systems

Photovoltaic panels and the inverter are the two main components of a photovoltaic system, which determine the cost, efficiency and performance of the entire system. However, other system components, including cabling, maximum Power Point Tracking (MPPT), and the network interface, can significantly affect overall efficiency. In fact, the configuration of the system or the interconnection structure of the components plays an important role in the technical and financial characteristics of a PV system. Regarding the interconnection of the PV array and the inverter, PV systems are normally categorized into four or five main groups [13–16]. Central structure, String structure, Multi-string structure, AC modules, micro-inverters and Power optimizers. These last are small DC-DC converters dedicated to every module. They perform the MPPT task for their connected single module to eliminate the mis-match power loss and, therefore, are considered in the same category with the AC modules [17]. However, since a central inverter is required to connect them to the grid, they can also be considered in the multi-string structure category. AC modules are normally rated around 180-250 W, and therefore they are used in low-power (not more than a few kW) roof-top residential applications where the possibility of shading from neighboring buildings and trees is high [18]. The string inverters are rated around 2-3 kW, or slightly higher for the 1000 VDC standard (in Europe), and as such are utilized in low- to medium-power residential and commercial/industrial roof-top applications. Their shading performance is low compared to the AC modules but is high compared to the central structures. The multi-string and central structures' rating can reach up to about 1 MW, so are utilized in medium- to high-power com-

mercial/industrial and utility-scale applications. The multi-string structure has better partial shading performance but can be expensive compared to the central structure, which is the most commonly practiced structure in large-scale applications, since it also offers lower installation and maintenance costs, simplicity of grid interconnection and central monitoring [19].

1.3.2 Grid integration of PV systems

With the proliferation of distributed generators, the utility grid faces new possibilities including increased transmission and distribution network capacity, improved reliability, and provision of ancillary services by DGs, and new challenges including possible instability, protection complexity, and over-voltage problems caused by DGs. Not long ago, distributed generators had to meet some few conditions and standards for connection to the grid, in order not to adversely affect grid performance. These conditions included production of high-quality power with harmonic contents less than specific levels defined by IEEE Std.519 [20], and detection of islanding and de-energizing the utility line during a predefined time window to avoid damage to the utility and customer equipments and personnel [21]. However, recently, it was realized that distributed generators, especially the inverter- based ones, can support the grid more actively in order to improve the performance and the capacity of the network. Therefore, the grid codes in most countries were redefined to include the new requirements for DGs to provide dynamic and static support during network faults and normal operations [22]. For instance, the German grid code for connection of PV systems to the medium-voltage power grid requires dynamic grid support, or fault ride-through (FRT) capability, demanding that the generating plants have to stay connected during a fault, support the voltage by providing reactive power during the fault, and consume the same or less reactive power after the fault clearance [23].

In PV systems, the control task is normally performed in synchronous dq frame synchronized with the grid voltage, which results in decoupled real and reactive power control through the decoupled d- and q-axis current control-loops [24, 25]. During the normal operation of a PV system, the d-axis current control-loop is uti-

lized for the DC-link voltage regulation which results in maximum power production (operation of PV array at MPP voltage). In the case of over-frequency in the network, however, the power set-point is calculated depending on the network frequency and is applied to the current control scheme, which results in the operation of a PV array with an operating voltage different than the MPP voltage. On the other hand, the reactive power set-point for PV systems, in normal operating condition, is set to zero or a small value to deliver unity power factor at the network connection point. However, in case of required dynamic or static voltage support, the reactive power set-point is calculated accordingly, depending on the network voltage [26].

1.4 Major contributions

The goal of the research presented in this thesis is to help increase the penetration level of PV systems in the electric network. This goal can be achieved by accurately evaluating the performance of the PV system without overestimating or underestimating its impacts on the electric network. Upon performing this analysis, the impacts of the fluctuating output power of PV systems should be considered. The main reason behind this consideration is the intermittent nature of the output generated from these systems. Another important factor that can help increase the penetration level of PV systems is to investigate the suitability of different methods that can improve the performance of the PV system and mitigate its negative impacts, especially due to power fluctuations. Accordingly, the following are the most significant contribution of this thesis:

- A PSO-MPPT algorithm for centrally configured PV systems is proposed to reduce the mismatch power loss over the PV array during partial shading, modules' aging, and characteristic mismatch conditions, which improves the energy yield of the entire PV system.

- The thesis then proposes a two-stage three-phase (still centrally configured) PV system that, utilizing an interface, applies the distributed-MPPT structure to the

central inverter, and thus, features an enhanced maximum power point tracking capability, and an improved energy yield under partial shading conditions.

- The thesis further proposes the two-stage PV system (for large-scale grid-connected applications) which consists of multiple DC-DC boost converters and one large central inverter. The inverter is based on the modular technology. The boost converters independently control the DC voltages of their corresponding PV arrays, while their output voltages are regulated by the inverter. Further, they limit the DC-link voltage of the inverter if the power cannot be dispatched to the grid, for example, due to network faults or failure of the inverter. The proposed PV system also offers an enhanced MPPT performance and energy yield, due to its multi-MPPT capability. The modular technology permits the employment of low-voltage switches for the inverter, despite the doubled net DC voltage.

- The thesis also presents a comparative study of two types of multilevel inverters that comprise of diode clamped and cascaded H-Bridge multilevel inverter for reduction of harmonics in the multilevel inverter output. The proposed system is designed using MATLAB/SIMULINK and it consists of diode clamped and cascaded H-Bridge multilevel inverters. The controller is based on the space vector pulse width modulation (SVPWM) technique which is applied to the proposed three phase multilevel inverters. The various performances of simulation results of the diode clamped and cascaded H-Bridge multilevel inverters were investigated. The Total harmonic distortion (THDv) of the output voltage was measured for the two types of multilevel inverters.

- In this thesis, an innovative simplified feedback linearization (SFL) control strategy is proposed for the PV inverter with the LCL filter, which offers satisfactory performance, particularly, in decoupling the control system, improving the dynamic performance, and enhancing the adaptability. Furthermore, the SFL controllers are simpler than the high-order tracking controllers used in conventional feedback linearization control. The detailed simplification process and accurate transfer functions for SFL control strategy have been presented, and the perfor-

mance comparisons between the proposed SFL control strategy and the classical dual-loop method are carried out to show the characteristics of the proposed control algorithm

- Finally, a new semi-modular multi-level photovoltaic inverter (SMMLI) is introduced. The adopted approach exploits the properties of modular topology mixed with central topologies and interfaced by several photovoltaic panels assembled into sections. Two control algorithms; Particle Swarm Optimization (PSO) algorithm for maximum power extraction and SVPWM technique for inverter control; are implemented into FPGA chip to improve the proposed model efficiency. Using MATLAB/Simulink, characterization tests are successfully compared to other configurations reported in the literature. The obtained results are also validated against experimental prototype under various test conditions.

1.5 Thesis outline

To achieve the aforementioned objectives and facilitate the presentation of the results obtained in this research, the thesis is organized as follows:

- In this chapter, an introduction to the subject and related works together with the research objectives and the major contributions of the thesis were outlined.
- Chapter 2 provides a general overview of grid-connected PV systems. This chapter looks at different components of a grid-connected PV system from the solar irradiance received by the PV arrays to the AC power injected into the grid, and makes a review of the recent achievements and current research activities in the field.
- Chapter 3 is divided into three sections as follows:
  - Section 3.1. of this chapter begins by brief overview of meta-heuristics algorithms. Then, the key feature of the PSO algorithm is described. Further-

more, the formulation of MPPT as an optimization problem is presented and the application of the proposed technique for MPPT is discussed.

  - Section 3.2. present the SVPWM technique in general. Then presents the control of three-phase multilevel cascaded H-bridge inverter for photovoltaic (PV) grid utility system with an LCL filter using Space Vector Pulse Width Modulation (SVPWM) scheme. This technique (SVPWM) is an attractive control candidate for any multilevel inverter, since it can create a greater output power by reducing Total Harmonic Distortion (THD) and commutation losses.
  - In order to filter the harmonics produced by the inverter we use an LCL filter, which is a powerful solution for the interconnection between the inverter and the grid. The control of a grid-connected inverter with LCL filter is studied thru conventional direct-current dq vector control strategy and presented in Section 3.3.

- In Chapter 4, a comparative study of photovoltaic systems with different inverter topologies is carried out under Matlab/Simulink environment and evaluated on the basis of MPPT, harmonic distortion, cost, advantages and disadvantages.

  In order to test the practical implementation of the proposed control structure, FPGA/Simulink-based Hardware in the Loop approach has been used to bring the obtained results as close as possible to reality and with a minimum of constraints. Based on the analysis of the obtained results, some experimental parameters are summarized and a comparison table is synthesized.

CHAPTER 2

REVIEW OF PHOTOVOLTAIC SYSTEM CONNECTED TO THE GRID

Contents

2.1 Introduction

ENERGY handling is one of the greatest challenges faced by the world today. In the global power supply, it is important to balance three factors: competitiveness, security of supply, the environment and climate. No single source of energy is perfect according to these three angles. Currently, we use polluting energies that will dry up in the near future such as oil and gas. Therefore, it will be necessary to develop more renewable energy to enlighten us, heat us, run the various engines and many other functions. The advantages of renewable energies are numerous, as they are generally clean, safe and above all renewable. They also generate little waste, which can even be recyclable. These energies respect the environment during their manufacture, their operation and at the end of their life, at the moment of their dismantling. In any case, all renewable energies reduce CO2 in the same way as the non-renewable energies they are supposed to replace [27].

To summarize, these renewable energies can significantly reduce the emission of CO2, they would not generate any dangerous radioactive waste and their resources would be infinite thanks to the wind, the water and the sun. The responsibility for global warming of renewable energies is a major disadvantage. They are often presented and accepted to solve this problem, but for it to be real, the consumption of fossil fuels such as oil, coal or gas should be considerably reduced and renewable energy must be better managed to save more. Solar energy is part of so-called renewable energies in the sense that the sun is a resource almost inexhaustible. In addition to the sun, a photovoltaic system consists of two main elements: modules composed of a large number of cells converting photons of light into electrical energy and the electric converter, in particular the inverter, whose role is to transform electricity generated upstream in electricity usable daily [28].

The chapter begins by an overview of photovoltaic generation systems. Then, the PV array characteristics under partial shading are critically examined. It is followed by the brief presentation of partial shading mitigating techniques. Finally, a review of MPPT techniques and inverter topologies that have been prominently used in the grid connected PV system is presented.

2.2 Overview of photovoltaic system

2.2.1 Historical overview

The photovoltaic effect has been discovered in the first half of the 19th the century. In 1839, a young French physicist Alexandre Edmond Becquerel observed a physical phenomenon or effect that allows the conversion of light into electricity [29]. The solar cells' work is based on this principle of photovoltaic effect. In the following years, a number of scientists have contributed to the development of this effect, the most relevant among them are Charles Fritts, Edward Weston, Nikola Tesla and Albert Einstein, who has been awarded the Nobel Prize for his work on "photoelectric effect" in the year 1904 [30]. However, due to high production rates, a greater development of this technology has begun only along with the development of semiconductor industry in the late fifties of the 20th century. During the sixties, the solar cells are used exclusively for supplying electricity to orbiting satellites in Earth orbit, where they prove themselves as very reliable and competitive technology. In the seventies there are improvements in production, performance and quality of solar cells, while the coming oil crisis helps to reduce production costs of solar cells and open up many possibilities for their practical implementation. Solar cells have been recognized as an excellent replacement for the supply of electricity at locations distant from the electricity grid. The energy is supplied to wireless applications, lighthouses' batteries, telecommunication equipment and other low power electricity dependent equipment. During the eighties, solar cells have become popular as an energy source for consumer electronic devices including calculators, watches, radios, lamps and other applications with small batteries. Also, after the crisis in the seventies, great efforts have been made in the development of solar cells for commercial use in households. Independent solar cell systems (off-grid) have been developed, as well as network connected systems (on-grid). In the meantime, a considerable increase in wide use of solar cells has been recorded in rural areas where electricity network and infrastructure have not been developed. Electricity produced in these areas is used for pumping water, cooling energy, telecommunications and other household appliances [31].

2.2.2 Types of solar photovoltaic cells

Solar cells are made of various materials and with different structures in order to reduce the cost and achieve maximum efficiency. There are various types of solar cell material, single crystal, polycrystalline and amorphous silicon, compound thin-film material and other semi-conductor absorbing layers, which give highly efficient cells for specialized applications [32]. Among silicon-based solar cells, crystalline silicon cells are most popular, though they are expensive whereas the amorphous silicon thin-film solar cells are less expensive. Monocrystalline solar panels have the highest efficiency rates since they are made out of the highest-grade silicon. The efficiency rates of monocrystalline solar panels are typically 15-20%. A variety of compound semi-conductors can also be used to manufacture thin-film solar cells like cadmium telluride (CdTe) and copper indium gallium diselenide (CIGS) [33].

2.2.3 photovoltaic system types

A solar cell constitutes the basic unit of a PV generator. In fact, a photovoltaic module is a packaged interconnected assembly of photovoltaic cells. The electrical output of the module depends on the size and number of cells, their electrical interconnection and the environmental conditions to which the module is exposed. To achieve the desired voltage and current, modules are usually wired in series and parallel into what is called a PV array. The flexibility of the modular PV system allows designers to create solar power systems that can meet a wide variety of electrical needs, no matter how large or small. PV systems can be classified into three types: stand-alone, grid-connected and hybrid systems [34]. Stand-alone photovoltaic systems are designed to operate independent of the electric utility grid, and are generally designed and sized to supply certain DC and/or AC electrical loads. The two types of stand-alone photovoltaic power systems are direct-coupled system without batteries and stand alone system with batteries. The simplest type of stand-alone photovoltaic system is a direct-coupled system, where the DC output of a photovoltaic module or array is directly connected to a DC load. Since there is no electrical energy storage (batteries)

in direct-coupled systems, the load only operates during sunlight hours, making these designs suitable for common applications such as ventilation fans and water pumps. However, in stand-alone photovoltaic power systems, the electrical energy produced by the photovoltaic panels cannot always be used directly. As the demand from the load does not always equal the solar panel capacity, battery banks are generally used for energy storage [35]. The second category is the grid-connected systems. Grid-connected or utility-interactive photovoltaic systems are designed to operate in parallel with and interconnected with the electric utility grid. The primary component in grid-connected photovoltaic systems is the inverter. The inverter converts the DC power produced by the photovoltaic array into AC power consistent with the voltage and power quality requirements of the utility grid, and automatically stops supplying power to the grid when the utility grid is not energised. In addition, these PV systems are used to reduce the consumption from the electricity grid and, in some instances to feed the surplus energy back into the grid. This system can produce significant quantities of high-grade energy near the consumption point, avoiding transmission and distribution losses [36]. The third category is the hybrid systems that combine solar power from a photovoltaic system with another power generating energy source such as a diesel, gas or wind generator [37].

2.3 Modelling of the photovoltaic system

2.3.1 PV module model

To develop an equivalent model of a photovoltaic cell, it is necessary to make a judicious choice of the electrical circuits that constitute it and to understand the physical configuration and the electrical characteristics of the elements of the cell. For this, several mathematical models are developed to represent the nonlinear behavior of semiconductor junctions [38]. Fig. 2.2 shows the equivalent circuit of a solar cell, realized by the parallel connection of two saturation current diodes I_1 and I_2, a current source producing the short-circuit current of the cell that depends on solar illumination. The R_s series resistor takes into account the resistivity of the material and the

semiconductor-metal contact. Its value can be determined by the inverse of the slope of the characteristic I(V) for the open-circuit voltage V_{co}. The parallel resistance R_p reflects the presence of a leakage current in the junction. The PV module is composed by N_s PV cells associated in series. The current I delivered by the cell is given by the following expression:

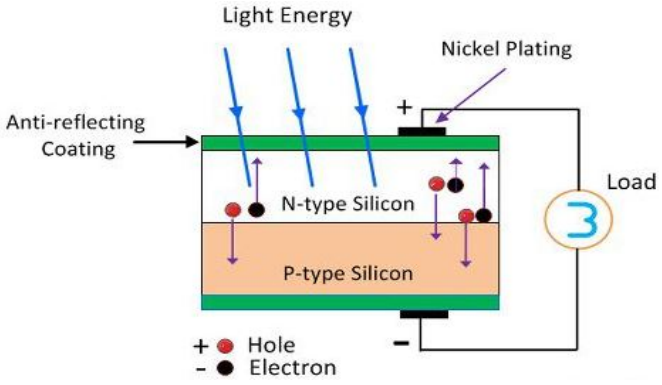

Figure 2.1: Solar cell.

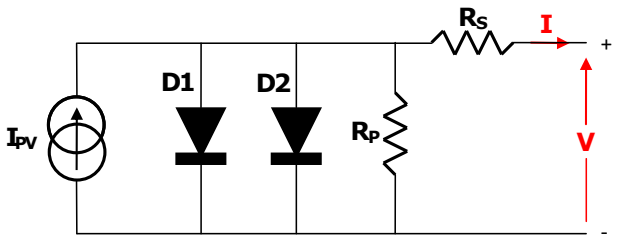

Figure 2.2: Equivalent circuit of a solar cell.

$$I = I_{PV} - I_{01}\left[exp\left(\frac{V + IR_sN_s}{a_1V_TN_s}\right) - 1\right] - I_{02}\left[exp\left(\frac{V + IR_sN_s}{a_2V_TN_s}\right) - 1\right] - \left(\frac{V + IR_sN_s}{R_pN_s}\right) \tag{2.1}$$

where I and V refer to the output current and the output voltage of the PV array, respectively. V_T (equal to KT/q) is the thermal voltage of the diodes, k is the Boltzmann constant ($1.3806503 \times 10^{-19}$ J/K), q is the electron charge ($1.60217646 \times 10^{-19}$ C) and T is the temperature in Kelvin. a_1 and a_2 are the ideality factors of the diodes D1 and D2, respectively.

Table 2.1: SM55 module specifications

Parameters	Value
Number of series cells in the module (N_s)	36
Number of bypass diodes	2
Open circuit voltage(V_{oc})	21.7 V
Short circuit current (I_{sc})	3.45 A
Voltage at P_{max} (V_{mpp})	17.4 V
Current at P_{max} (I_{mpp})	3.15 A
Maximum power (P_{max})	55 W
Temperature coefficient of V_{oc} (K_V)	-77$\times$ 10-3 V/AC
Temperature coefficient of I_{sc} (K_I)	1.2 $\times$ 10-3 A/AC

2.3.2 Uniform irradiance condition

The PV module, SM55, is used in this work. The parameters of this module under the standard test conditions (STC) ($T = 298$K and $G = 1000\,\mathrm{W/m^2}$) are given in Table 2.1.

Fig. 2.3 and Fig. 2.4 show the corresponding static I-V and P-V curves for different values of irradiance G and temperature T. The module receives a uniform solar insulation, thus, the P-V curves exhibit a unique maximum power point (MPP).

The effect of the irradiance on the current-voltage (I-V) and power-voltage (P-V) characteristics is depicted in Fig. 2.3. As was previously mentioned, the photo-generated current is directly proportional to the irradiance level, so an increment in the irradiation leads to a higher photo-generated current. Moreover, the short circuit current is directly proportional to the photo-generated current; therefore it is directly proportional to the irradiance. For this reason the current-voltage characteristic varies with the irradiation. In contrast, the effect in the open circuit voltage is relatively small, as the dependence of the light generated current is logarithmic.

The temperature, on the other hand, affects mostly the voltage and the open circuit voltage is linearly dependent on the temperature. Fig. 2.4 shows how the voltage-current and the voltage-power characteristics change with temperature. The effect

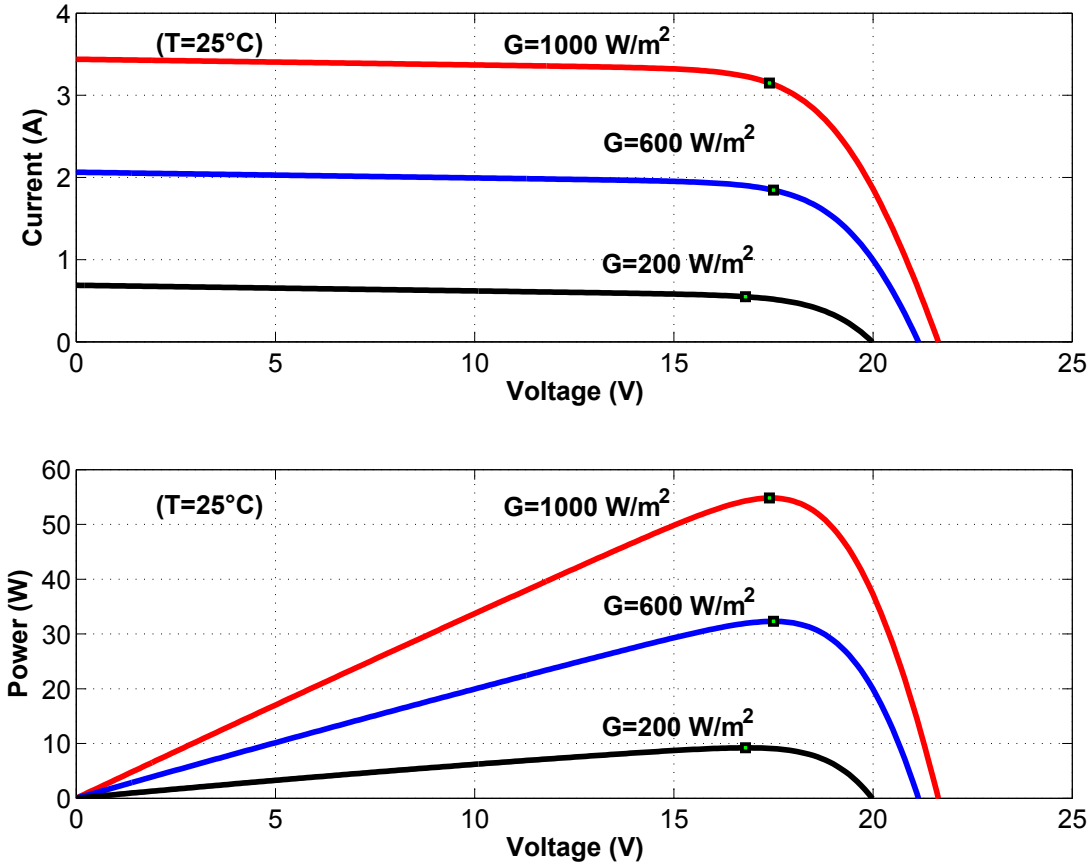

Figure 2.3: The characteristic of PV system under uniform variation in irradiance.

of the temperature on V_{OC} is negative, i.e. when the temperature rises, the open circuit voltage decreases. The current increases with the temperature but very little and it does not compensate the decrease in the voltage caused by a given temperature rise. That is why the PV power also decreases. PV panel manufacturers provide in their data sheets the temperature coefficients (K_v and K_i), which are the parameters that specify how the open circuit voltage, the short circuit current and the maximum power varies when the temperature changes.

2.3.3 Influence of partial shading

Shade

Photovoltaic modules are very sensitive to shading. Unlike solar thermal panels that can tolerate some shading, photovoltaic modules cannot be obscured, mainly because

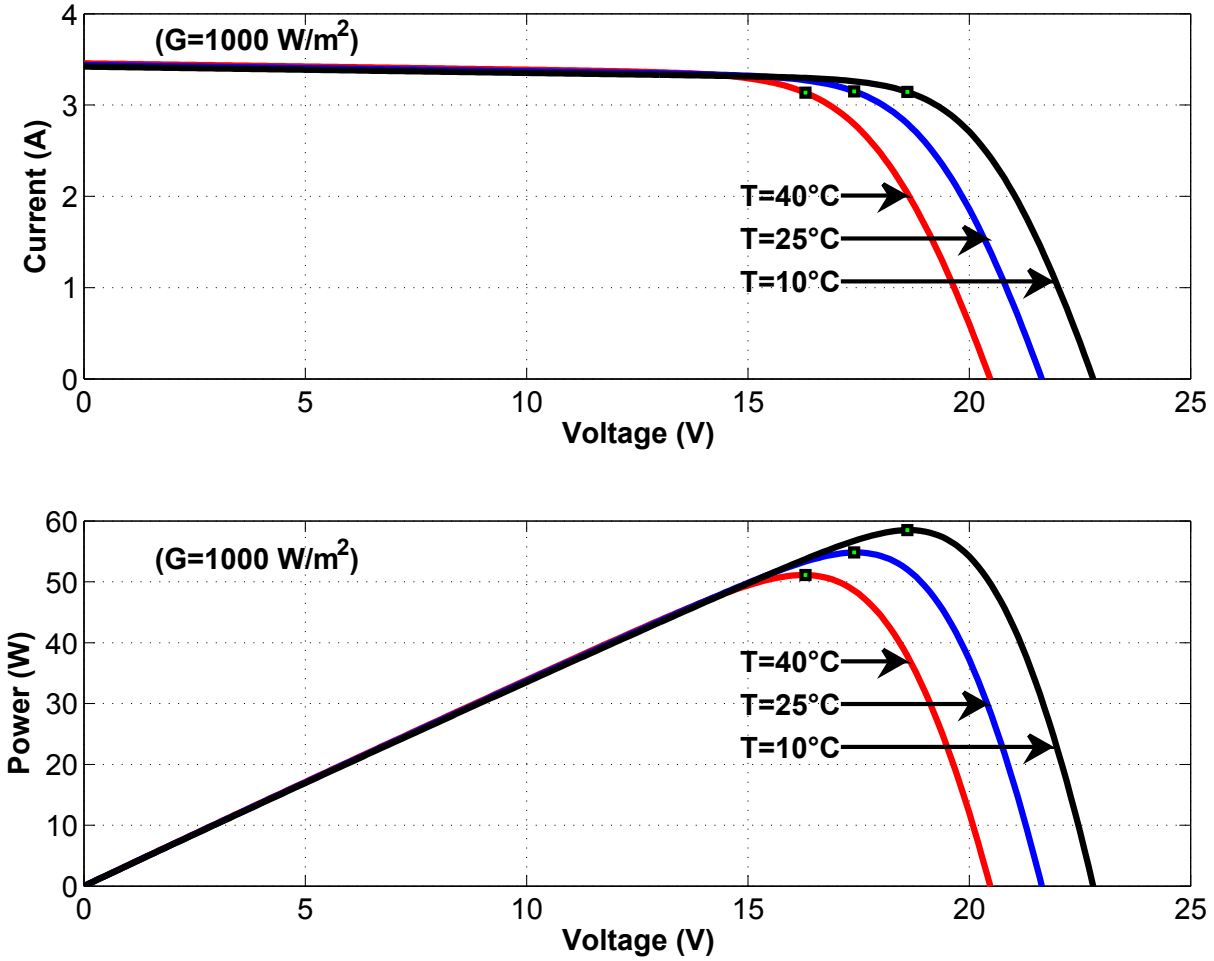

Figure 2.4: The characteristic of PV system under variation in temperature.

of the electrical connections (in series) between the cells and between the modules. There are two types of shading: total shading and partial shading. The complete shading prevents any radiation (direct and indirect) from reaching a part of the photovoltaic cells. Partial shading only prevents direct radiation from reaching part of the photovoltaic cells. Often, the cells of a photovoltaic module are connected in series. Thus, the weakest cell will determine and limit the power of other cells. Shading half a cell or half a row of cells will decrease the power proportionally to the percentage of the shaded area of a cell, in this case by 50%. Total shading of a row of cells can reduce the power of the module to zero [39]. To avoid the misuse of a photovoltaic installation, it is necessary, from the planning stage, to minimize the yield losses due to the shading conditions. Factors such as the arrangement of photovoltaic modules,

their connection and in particular the choice of the suitable inverter, play an essential role. By taking into account some important rules during planning, these factors can be adapted to different photovoltaic installations, so the energy that can provide can be exploited completely [40].

Effects of partial shading on photovoltaic installations

Each PV generator has a single point of work where it can provide the maximum possible electrical power, called the Maximum Power Point (MPP). This power depends mainly on the intensity of radiation. If different modules of a "String" in a photovoltaic generator are in the shade, its electrical properties are significantly altered: the photovoltaic generator now has different points of work "favorable". Fig. 2.5(a) demonstrates a PV array containing of two modules associated in string. Fig. 2.5(b) demonstrates the comparing static P-V characteristic curves for two distinctive shading designs. For the principal case, the PV panel gets a uniform sun based irradiance, therefore, the P-V curve shows one MPP. In the second case, the following of the GMPP becomes a more challenging task, we can see the presence of four MPPs whose GMPP is $P = 52,89$ W at $V = 27.59$ V. Thus, the P-V characteristic can take different structures according to the shading design.

Shade: A special roles of the inverter

Each photovoltaic inverter has what is called an MPP tracker. It provides a photovoltaic generator service always at its optimum working point. Controlled in this way, the photovoltaic generator can exploit at its maximum efficiency the available power for a given solar radiation. In our proposed semi-modular inverter, the control supports this function and thus guarantees maximum energy efficiency. However, two or more different points occur due to the shading of some PV modules within a PV generator as described above. Then, the connected inverter must decide which of these working points, the local MPP(LMPP) or the global MPP(GMPP), it must operate the photovoltaic generator.

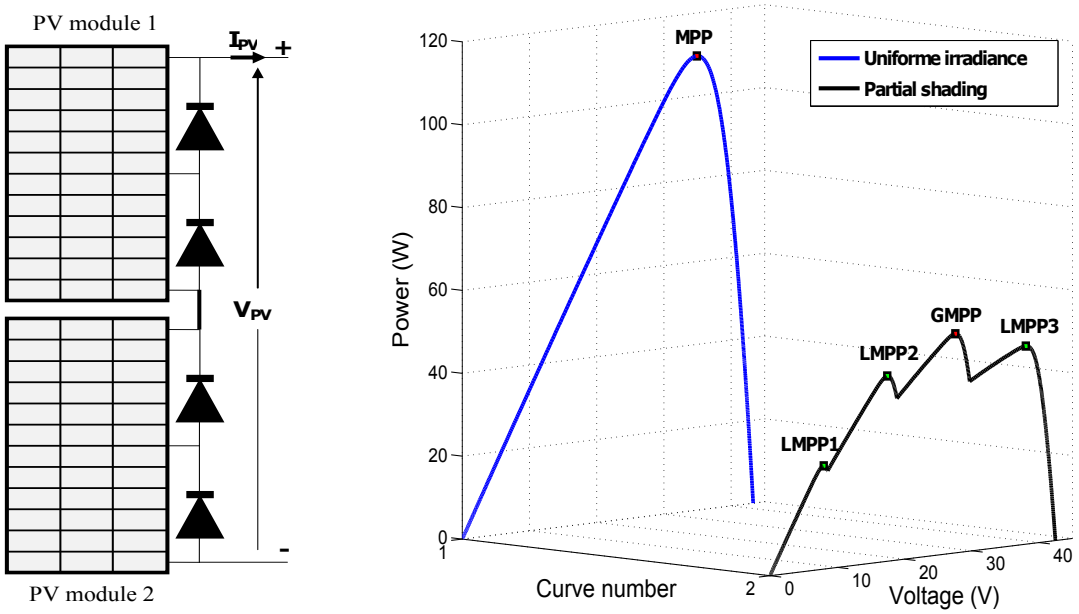

(a) Two PV modules associated in series

(b) The P-V curves of two PV modules under uniform and partial shading conditions.

Figure 2.5: Effects of partial shading on photovoltaic installations

2.4 Mitigation control against partial shading effects in large-scale photovoltaic power plants

Partial shading in photovoltaic (PV) arrays renders conventional maximum power point tracking (MPPT) techniques ineffective. The reduced efficiency of shaded PV arrays is a significant obstacle in the rapid growth of the solar power systems. Thus, addressing the output power mismatch and partial shading effects is of paramount value. Extracting the maximum power of partially shaded PV arrays has been widely investigated in the literature. The proposed solutions can be categorized into four main groups. The first group includes modified MPPT techniques that properly detect the global MPP. They include power curve slope, load-line MPPT, dividing rectangles techniques, the power increment technique, instantaneous operating power optimization, Fibonacci search, neural networks, and particle swarm optimization. The second category includes different array configurations for interconnecting PV modules, namely series–parallel, total-crosstie, and bridge-link configurations. The

third category includes different PV system architectures, namely centralized architecture, series-connected micro-converters, parallel-connected micro-converters, and micro-inverters. The fourth category includes different converter topologies, namely multilevel converters, voltage injection circuits, generation control circuits, module-integrated converters, and multiple-input converters. This section surveys the proposed approaches in each category and provides a brief discussion of their characteristics.

2.4.1 Maximum power point tracking techniques for shaded photovoltaic arrays

Maximum power point tracker is a power conversion system with an appropriate control algorithm to extract the maximum power from the PV source irrespective of the changes in the operating conditions. The objective of the MPPT algorithm is to govern the voltage or current or duty cycle in a way that the PV system will always deliver the maximum power. Up to date there are numerous MPPT techniques have been reported in the literature. Despite the fact that these methods are designed for the same objectives, they differ markedly in terms of complexity, convergence speed, steady state oscillations, cost, range of effectiveness and flexibility. Furthermore, each technique may work best in certain conditions while not in others. For instance, some MPPT techniques yield better performance under uniform irradiances but under partial shading conditions, the results are found to be unsatisfactory. A review of different MPPT techniques that address the partial shading condition is presented below.

Several MPPT techniques are presented in the literature to handle the multimodal *P-V* characteristic in partial shading conditions. These methods vary in complexity, in the types and the number of sensors used and the equipment used for the implementation. [41] proposed a two stage MPPT algorithm for tracking the GMPP. The authors introduce an analytic condition to distinguish partially shaded conditions from normal conditions. This condition is based on the comparison of the sensed photovoltaic current around $(0.8 \times N_{SS} \times V_{oc})$ and a reference value calculated at uniform insola-

tion conditions with $G = 1000\ \mathrm{W/m^2}$, where N_{SS} is the number of series photovoltaic module and V_{oc} is the open circuit voltage. When the region of GMPP is located, the algorithm calls a hill climbing subroutine to reach the GMPP. However, in the first stage, $(N_{SS} + 1)$ points should be tested each time the partial shading conditions are detected before calling the hill climbing algorithm to locate the GMPP. This method will become time-costly if the number of series module is large [42]. In addition, temperature sensors must be used to determine the open circuit voltage.

It is shown in [43] that the function describing the PV power as a function of the PV voltage is a Lipschitz function. Therefore, [43] adopted the dividing rectangles (DIRECT) algorithm to search for the GMPP. Although the presented experimental results showed the efficiency of this method in tracking the GMPP under partial shading conditions, an appropriate choice of the first sampling interval is primordial for the GMPP tracking performance [44].

[45–47] employed two-stage search methods to track the GMPP, which first scanned the $P - V$ characteristic curve and then recorded the GMPP. In the second stage, these methods applied either the P&O method [45] or fuzzy logic control [46,47] to maintain the operating point at the GMPP.

[48] proposed a three stage tracking technique to find the GMPP under partial shaded condition. In the first stage, the control space of PV array voltage is subdivided into predetermined n number of partitions based on the measured open circuit array voltage, where n is the number of PV modules connected in series. Then, the slopes on the P-V characteristic in the portioned regions are computed. In the second stage, the sector or interval wherein the GMPP is located is determined based on the estimation of local maximum PV power in the portioned regions. In the third stage, the conventional P&O technique is used in the optimal partitioned region to finally reach the GMPP and this technique continues to track the MPP until a change in the irradiation pattern is observed.

Evolutionary algorithms and metaheuristics: In partial shading conditions , many traditional maximum power point tracking methods like perturbation and observation, and incremental conductance may become invalid due to involvement in the

local maximum power point. Many advanced methods based on the artificial intelligence like artificial neural network, and fuzzy logic control can track the global maximum power point. However, they need massive training and broader experience to familiarize with real complex environment. Alternatively, bio-inspired maximum power point tracking algorithms deal properly with such situations. In recent years, researchers have widely applied bio-inspired algorithms to track the global maximum power point of photovoltaic system during partial shading situations [49]. Various tracking methods are discussed and compared in terms of their characteristics and corresponding improved methods. It also presents the advantages and disadvantages of each method. The modified and combined forms of these methods found to have better performance than original algorithms. Overall, the performance of swarm intelligence based algorithms and evolutionary algorithms are discussed.

Evolutionary algorithms (EAs): Evolutionary algorithms are originated from the study of natural evolution in living things. These are used for solution of complex optimization problems. Few optimization problems like multimodal, non-differentiable, or discontinuous cannot be solved by traditional methods. They are appropriately solved using evolutionary algorithms. Generally, an evolutionary algorithm evolves a population of possible solutions and returns a population of solutions simultaneously. Typical evolutionary algorithms are genetic algorithm [50], evolutionary programming [51], evolution strategy [52], differential evolution [53], and biogeography-based optimization [54]. There are several advantages of evolutionary algorithms like relative simplicity of implementation, high-dimensional solution spaces, and inherent parallel architecture [55].

Genetic algorithm (GA) Genetic algorithm is based on stochastic optimization with a global search potential capacity developed by Holland [56]. It is the most successful class among evolutionary algorithms which is originated from the idea of biological evolution of living things. Due to its excellent performance for solution of optimization problems, it has been known as a function optimizer.

[57] proposed to use genetic algorithm based method for tracking MPP in the PV

array system during partial shading situation. The results indicated the robust tracking capability of the proposed method under rapidly varying irradiance which shows the improvement in efficiency of grid-connected system. [58] showed that genetic algorithm tracks the global power point which was matched with the binary search result and the error did not exceed 2%. [59] presents GA algorithm for MPPT in PV panels and performed simulation experiments to check the performance. They concluded that GA is simple to apply for MPPT in PV panels and shows good tracking accuracy. The proposed method is called by changes in power output of PV array. [60] developed a modified genetic algorithm based method without taking the step of mutation into account. This was done to eliminate the effect on convergence and oscillations. The algorithm is restarted by resetting the early population when there is variation in temperature, solar irradiance, and load, to look for new MPP. The genetic algorithm is restarted upon satisfaction of following two conditions. [60] also compared the developed method with perturbation & observation, and incremental conductance methods under the conditions of irradiance variation, temperature changes, and load changes. The comparison results showed better performance of proposed approach. [61] performed a comparison between the continuous genetic algorithm and the hybrid particle swarm optimization algorithm used for MPPT in a PV array system. It was observed that the hybrid particle swarm optimization algorithm outperforms continuous genetic algorithm in terms of global power tracking during partial shading situations. The tracking time of continuous genetic algorithm is 2.82 s while hybrid particle swarm optimization algorithm is faster with tracking time of 2.69 s.

Differential evolution algorithm DE: Differential evolution algorithm appears to be one of the most promising population-based problem optimization approach, as it is very simple. In this approach, firstly, the initial population is chosen randomly if there is no information about the system. Then the DE optimises the means of creating new candidates on the basis of different formulas of different methods while the population size is maintained simultaneously. New candidates and the existing ones with the best fitness remains in the population, while, other candidates will be

replaced. Three main advantages exhibited by differential evolution algorithm during MPP tracking in PV systems are: ability to find the true GMPP without depending on initial parameter values, less convergence time and requirement of few control factors [62]. A modified differential evolution algorithm was also proposed as a solution for optimisation problems. It does not consist of an arbitrary number. It involves only one factor i.e. mutation. Its performance was comparatively, as PSO converges to local MPP often. The evolutionary algorithm and differential evolution algorithm have almost same stages. The only difference between them is the population members.

[63] proposed a MPP tracking algorithm based on differential evolution in 2010. This algorithm could track global MPP during partial shading situations. This proposed algorithm track the GMPP quickly without any fluctuation. A comparison was made between the proposed approach and traditional Perturb and observe algorithm during normal and abrupt varying partial shading conditions, and the performance of proposed approach was found satisfactory. It was observed from simulated results, that the DE algorithm converges to MPP quickly and perfectly, while the response speed of P&O algorithm was very slow even under constant conditions. It was therefore concluded that, P&O approach requires more time to track MPP under constant conditions, however it may oscillate and never converges to real MPP due to its slow speed during abrupt varying conditions.

[64] proposed a method that could converge to the real MPP in most of the external situations like normal partial shading situation, and abrupt varying solar insolation situation. The proposed method was observed to be accurate and fast. It was able to track the GMPP using a wide-space searching technique, thereby more solar power could be harvested from the PV system, particularly during partial shading circumstances. The planned technique offers rapid and precise convergence of the system to optimum operating point for gaining maximum power in most of external circumstances like normal partial shading situation, and abrupt varying solar insolation situation. Additionally, it avoids the fluctuation, once the optimum operating point is reached. [65] proposed a modified hybrid evolutionary method i.e. differential evolution-particle swarm optimization technique to track MPP during partial shading

situations. In the PSO method, the diversity of particles decreases with increasing iteration, which may lead to convergence to LMPP [66]. In DE algorithm, differential information is utilized to find the local optimum point of search space, but the search quality disproves in exploring the global optimum point [53]. But, when these two algorithms are combined as above proposed technique, it prevents the convergence to LMPP by diversifying the PSO algorithm [67]. The literature review of relevant work done by different researchers reveals that it is better in performance than both DE and PSO algorithms, especially in terms of search quality and converging speed [68]. In searching process of PSO technique, each individual tries to make its position towards the best one G_b found by swarm. After certain number of iterations, the diversity reduces due to decremented weighted velocity of the individuals. This drawback was overcome in the hybrid approach. The diversity was increased by combining with DE which avoids the convergence towards local optima [67]. In every odd iteration step, PSO technique is implemented, while DE is applied in every even iteration step [65]. The simulated and experimental results of above proposed method prove the system as a reliable, fast, and accurate system. This method differentiates the GMPP from LMPP. Few major benefits of this method are: 1) a pure MPPT technique due to its stochastic nature, 2) maintains its metaheuristic characteristic due to random numbers and thus track GMPP during any shading situation, 3) reliable and fast in finding true GMPP, and 4) easy to implement with an economical micro-controller and less computational burden.

[69] introduced an improved differential evolution algorithm for tracking the GMPP. The proposed algorithm is simulated in the PSIM electronic simulation software to ensure its capability to handle the partial shading and its faster respond against load variation. The improved DE algorithm is implemented on the PIC18F4520 micro-controller and the feasibility of the approach is validated through experimentation using solar array simulator from Chroma (Model: 62150H-1000S) and single-ended primary-inductance converter (SEPIC). The experimental results shows the that the proposed improved DE technique performs faster than the conventional DE algorithm and it is able to track the GMPP rapidly (within 2s) with MPPT accuracy of

above 99%. Moreover, the proposed algorithm can respond to load variation rapidly (within 0.1s) which ultimately reduce undesirable fluctuations at the output of PV array.

Particle swarm optimisation PSO: Particle swarm optimization (PSO) algorithm is a swarm intelligence based optimization technique. It was developed by Eberhart and Kennedy in 1995. The idea of this algorithm originated from the study of swarm behavior of social animals like torus pattern observed in fishes and flock pattern observed in birds. The major benefits of PSO are simple computation, reliable true global convergence, and simple application with less expensive controller [70].

Authors in [71] used conventional PSO algorithm to control several PV arrays with one pair of voltage and current sensors. Rather than using individual MPPT blocks to control each of the PV arrays, the authors proposed a single PSO MPPT scheme to control multiple PV arrays. The scheme has the advantages of providing lower cost, higher efficiency and simplicity with respect to its implementation. The proposed scheme tracking capability is tested with experiment for both normal and partial shading patterns. In addition, the PSO MPPT dynamic response of the PV system under the partial shading condition is analysed and compared with other MPPT methods (conventional fixed voltage MPPT , Hill-climbing algorithm, Fibonacci search MPPT). A DSP-TMS320C32 is used to realise the proposed scheme. The average tracking time of the PSO algorithm is 2 s, and it was observed that this response time was almost independent of the shape of the partial shading pattern.

[72] proposed a dual-algorithm search method based on dormant particle swarm optimization (DPSO) and incremental conductance (INC) algorithm to track the MPP. When the occurrence of partial shading conditions is confirmed, DPSO is activated and applied to search the area of global peak, and then the algorithm will be switched to conventional INC algorithm to track the maximum output power of photovoltaic arrays. A comparative study including the analyses of convergence time and the power losses is performed in order to choose the initial number of particles in the first population (initial size of population) and to determine the optimal searching sequence of particles. In order to enhance the tracking speed and improve efficiency, the par-

ticles in DPSO have two states: dormant state and active state. During iteration, the particles are turned into dormant state (not participate in the next iteration) one after one until there is no active particle. Simulation and experimental results show that this scheme reduces the fluctuation of PV voltage and presents good performance, no matter how complex shaded conditions the PV arrays are under. In addition, it performs better than conventional PSO which take longer time to converge to the GMPP and conventional INC technique which falls to handle partially shaded conditions.

[73] proposed a modified PSO algorithm based MPPT to enhance the tracking capability of the conventional PSO method and improve it's dynamic performance. The proposed methods is verified under very challenging conditions, namely large step change in (uniform) solar irradiance, step changes in load, and partial shading conditions. The results reveal that this method presents the advantages of fast tracking speed and reduction of the steady-state oscillation (to practically zero) once the maximum power point (MPP) is reached, thus improving the MPPT efficiency. The proposed method is implemented on a TMS320F240 digital signal processor and verified experimentally using a buck-boost converter fed by a solar array simulator. Furthermore, the simulation and experimental results highlight the superiority of the proposed method over the conventional HC in terms of tracking speed and steady-state oscillations.

In [74], the authors have improved their algorithm (PSO) by removing random factors from the conventional PSO velocity equation. The proposed algorithm becomes deterministic and its structure becomes simpler. However, a restriction is imposed on the maximum of particle velocity to not fall into a LMPP. The value of limiting velocity factor is determined based on a critical study of P-V characteristics during partial shading. In this paper, the complete algorithm is divided on two modes: global mode and local mode. The DPSO algorithm was used only when partial shading conditions is occurred. The local mode is activated in two cases; when uniform insulation is detected or when the convergence criterion of DPSO in global mode is reached. In this case, variable step-size HC method is employed minimize the energy loss due to oscillations in the vicinity of MPP. The DPSO method is implemented

by the TMS320F240 DSP on the Dspace DS1104 environment. The simulation and experimental results have shown that the proposed technique offers remarkable accuracy and tracking speed compared to conventional HC under several scenario of irradiance including uniform insulation, partial shading conditions, slow variation of partial shading conditions and extreme partial shading. The proposed method yields an average efficiency of 99.5% when tested using the measured data of a tropical cloudy day.

[75] presented a FPGA implementation of PSO based MPPT for PV systems under partial shading conditions. First, Matlab/Simulik simulations are presented to demonstrate the accuracy of PSO for global peak tracking and its superiority over the P&O technique. After that, the PSO method has been designed using very high speed integrated circuit hardware description language (VHDL) and implemented on Xilinx Virtex5 (XC5VLX50-1FFG676) FPGA in order to achieve a high degree of flexibility and robustness for the MPPT algorithm. The developed architecture is tested in real time application on a buck-boost converter and the experimental results confirm the efficiency of the PSO scheme and its high accuracy to handle the partial shading.

[76] proposed an improved MPPT strategy for PV systems based on PSO algorithm. To increase the tracking speed, a variable sampling time strategy (VSTS) based on the investigation of the dynamic behaviour of DC-DC converter current is deployed. To insure that particles (the duty cycle) don't exceed the interval [0,1], the velocity is controlled by using the inverse tangent function which permit to retain the speed of particles within a safe margin. In order to access the superiority of the proposed approach over the fixed sampling time strategy (FSTS), Matlab/Simulink simulations and experimentation, in which a TMS320F335 DSP is used to implement both tracking strategies on a real boost converter connected to a an Agilent E4360 Modular Solar Array Simulator, are performed under uniform irradiance, fast transient changes in insulation, and partial shading conditions.

[77] combined P&O and PSO to form a hybrid method to reduce the search space of the PSO. Initially, the P&O method is employed to identify the nearest local maximum. Then, the PSO method is used to search for the GMPP. The advantage of this

method is the improvement of the time that is required for convergence since the search space for the PSO is reduced in the early stage. The proposed controller was implemented in a 32-bit digital signal processor (DSP-TMS320F28035) and has been validated with experiments for three static *P-V* characteristic curves. In addition, the dynamic tracking capability was investigated for two scenarios of changing sequences of the shaded patterns. The experiments results have shown that the proposed hybrid method can track the GMPP dynamically, requires less tracking time and exhibits better dynamic response than the conventional PSO method.

[78] proposed a combined algorithm that integrates the benefits of PSO approach and Proportional-Integral (PI) control technique. The proposed combined algorithm works in two phases. In the first phase, the algorithm uses PSO approach to locate the global power. To increase the efficiency of the proposed algorithm, an Adaptive Sampling Time Strategy is integrated using a comparator between the reference voltage computed by the PSO based controller and the output voltage of PV system. Once the reference voltage is attained, the corresponding power is measured and stored, and the next agent is set as a new reference voltage to the power converter. Thus, the convergence speed towards the global power is greatly increased. In the second stage of this algorithm, once the global power is attained, the algorithm switch to a PI based MPPT controller in order to increase the tracking precision and to deal with slow variations in the global power location, if existed. The above proposed algorithm was tested through simulations under different environmental conditions. Simulation results show that it could track global power peak with high accuracy and convergence speed. The algorithm is simple and involve rapid computations.

Authors in [79] integrated the PSO technique in a new control structure for two multilevel three-phase inverter topologies for photovoltaic (PV) systems connected to the grid. This control scheme includes the use of the space vector pulse wide modulation (SVPWM) technique to control the Diode Clamped Inverter (DCI) and cascade inverter topologies and the integration of the PSO technique to operate the PV system at the maximum power point (MPP). PSO method is used to overcome the problem of MPP tracking under partial shading conditions. This MPPT technique is implemented

into FPGA and validated under different shading patterns for two PV architectures; string and modular, in order to select the optimal PV system architecture and circuit topologie offering the highest performance and to evaluate the behaviour of each PV inverter setting due to non-uniform irradiation. In these conditions, it is observed that the modular connection is dominant but, the results also highlight the benefit of inserting an adaptation stage with PSO-based MPPT between the PV array and the load in order to optimize the produced power at any time.

BAT algorithm: In [80], a MPPT algorithm based on a bat algorithm (BA) is proposed to deal with the multi-modal characteristic of photovoltaic panel under partial shading conditions. The bat algorithm is a swarm intelligence based method which was inspired by the echolocation behaviour of bats. Simulations are carried out in Matlab/Simulink environment under extreme shading patterns to confirm the global search ability and the good dynamic performance. The simulations results have shown that the proposed method tracks the GMPP with a high accuracy and yields a static efficiency above 99.9% for the most cases studied. In addition, the proposed scheme outperforms the P&O and the PSO methods in terms of accuracy and oscillations in PV power at the transient time. The BA based MPPT is implemented on Xilinx Virtex-5 (XC5VLX50-1FFG676) Field Programmable Gate Array (FPGA) and tested experimentally for four partial shading patterns.

Ant colony Optimization algorithm ACO: The ant colony optimization is a probabilistic algorithm for solution of optimization problems. This idea was originated from the study of collective behavior of ants looking for their food [81, 82]. It was proposed in the early 1990s. Initially it was applied for solution of complex combinatorial problems, which gives a set of discrete feasible solutions. In last few years, this approach has been extended to solve continuous problems [83, 84] In combinatorial problems, the social behaviour of numerous ants was involved. The ants search for the food in a collective way. Initially, few ants follow random paths to search for food and lay down pheromone, which act as a communication signal for other ants. The other ants follow this pheromone path. More the ants follow that path, more is the

pheromone density on that path. This results in a trend that large number of ants will choose that path to reach the food. In the meantime, pheromone starts to evaporate. The longer the distance, more pheromone will evaporate. Finally, an individual ant find a shortest route to the food through this communication process. Now this results in less evaporation of pheromone comparatively. Now, few other ants started to follow this new route. Finally, the overall result is that all the ants started to follow this new shortest route having high pheromone density. The same idea gives the solution of combinatorial optimization problems. The idea for solution of continuous optimization problems is little different [85].

[85] proposed an ant colony optimization based method to search for MPP in large-scale PV systems during partial shading situations. They also proposed a centralized controlled PV array configuration to work with this new technique. Only one pair of sensors were used in this configuration, which reduces the overall system cost and adds up simplicity. This PV configuration enhance reliability and efficiency of the system. The proposed system was also tested using MATLAB simulation. The simulation results showed that, the average execution time of this algorithm is 7.3 min after 30 repetitions of the algorithm, when sampling period was set at 0.01 s. And this algorithm takes average running time of less than 0.4 s to track global optimal point. It was observed that, ant colony optimization based MPPT controller meets global point in less number of iterations as compared to PSO based MPPT. Furthermore, the convergence does not depend upon initial conditions.

[86] propose a new bio-inspired MPPT controller based on the Ant colony Optimization algorithm with a new pheromone updating strategy (ACO NPU MPPT) that saves the computation time and performs an excellent tracking capability with high accuracy, zero oscillations and high robustness. Several tests are performed under standard conditions for the selection of the appropriate ACO NPU parameters (number of ants, coefficients of evaporation, archive size, etc.). To evaluate the performances of the obtained ACO NPU MPPT, in terms of its tracking speed, accuracy, stability and robustness, tests are carried out under slow and rapid variations of weather conditions (Irradiance and Temperature) and under different partial shading

patterns. Moreover, to demonstrate the superiority and robustness of the proposed ACO NPU MPPT controller, the obtained results are analyzed and compared with others obtained from the Conventional Methods (P&O MPPT) and the Soft Computing Methods with Artificial intelligence (ANN MPPT, FLC MPPT, ANFIS MPPT, FL GA MPPT) and with the bio-inspired methods (PSO) and (ACO) from the literature. The obtained results show that the proposed ACO NPU MPPT controller gives the best performances under variables atmospheric conditions. In addition, it can easily track the global maximum power point (GMPP) under partial shading conditions.

Cuckoo search: Cuckoo Search is a soft computing method used for solution of complex optimization problems. The idea of this algorithm originates from the study of natural reproduction behavior of cuckoo birds. These birds follow a parasitic and aggressive strategy during their reproduction process. They lay down eggs in nests of other birds (communal nests) instead of their own nests. The other birds are termed as host birds. The cuckoo mother bird find other suitable nest to hatch its own eggs in a search space just like other animals find food. This parasitic behavior of cuckoo bird is followed in cuckoo search algorithm [87,88].

[87] proposed cuckoo search algorithm for MPPT in 2013. They also conduct performance evaluation of the proposed algorithm. They made a performance comparison between cuckoo search based MPPT and P&O based MPPPT under same environmental conditions. It was observed that, cuckoo search algorithm takes less tracking time as compared to P&O algorithm. Cuckoo search takes 22 ms while, P&O takes 45 ms at standard test conditions to track MPP. In addition to fast convergence speed, the cuckoo search algorithm tracks MPP without any steady state oscillations. While, P&O algorithm shows oscillations. The P&O algorithm oscillates but cuckoo search algorithm remains on Vmpp and Impp. Initially, cuckoo search shows oscillations before final tracking, as samples are randomly placed over the entire region. But, the convergence takes place with high speed. Once the voltage samples come closer to optimal point, the oscillation decreases. Finally, oscillations disappeared at steady state and cuckoo search remains at MPP. Furthermore, the cuckoo search algorithm is capable to track true global power even during abrupt varying solar irradiation

distribution.

Ahmed and Salam [88] stated that cuckoo search algorithm can handle partial shading conditions appropriately because it has natural ability to track global optimal point. They verified the algorithm using simulation approach. A partial shading condition is developed in the simulation. The sampling rate was 10 ms during simulation of 2s. At 1s (partial shading point), the P&O algorithm moves towards local peak point. In contrast, cuckoo search algorithm tracks true global optimal point after searching of 300 ms. Large oscillations are observed during searching process of cuckoo search algorithm due to Levy flight distribution. performance comparison between cuckoo search and PSO algorithms during partial shading situations was elaborated. The comparison shows that, both the algorithms are capable to handle partial shading situations, as both involve searching mechanism. However, cuckoo search exhibits high convergence speed. Cuckoo search tracks maximum power in 300 ms, while, PSO takes 520 ms. Apart from this, PSO shows large oscillations in transient state.

[89] proposed an optimized FLC algorithm for hybrid power system based on cuckoo search to operate under different environmental conditions. In present approach, the cuckoo search algorithm adjusts the functions of FLC. It tunes design variables of fuzzy algorithm to obtain more accurate controller. Hourly solar irradiation, temperature, and load profile data is used to tune the fuzzy controller. This adjustment facilitates better performance as compared to traditional FLC algorithm and fuzzy controller with PSO.

2.4.2 Array configuration

The partial shading effects can be alleviated by employing different array configurations for interconnecting PV modules [90–92]. PV array configuration pertains to the interconnections of individual PV modules which are Series (S), Parallel (P), Series-Parallel (SP), Total-Cross-Tied (TCT), Bridge-Linked (BL), and Honey-Comb (HC) [2]. The two configurations Series (Fig. 2.6(a)) and Parallel (Fig. 2.6(b)) are basic configurations for the interconnection of PV modules. The series coupling of the modules

makes it possible to increase the voltage of the PV field. In the parallel connection the global current is the sum of all currents. Serial-to-Parallel (SP) connection is the most commonly used and is achieved by serialising the PV modules to form a string or branch in order to achieve the required voltage. These strings are then connected in parallel in order to increase the total output current, as shown in Fig. 2.6(c). In the TCT configuration (Fig. 2.7(c)), the modules are first linked in parallel to form parallel-connection groups; these will then be connected in series. So in this type of coupling the PV modules are fully connected. The two BL and HC configurations are shown in Fig. 2.7(a) and Fig. 2.7(b).

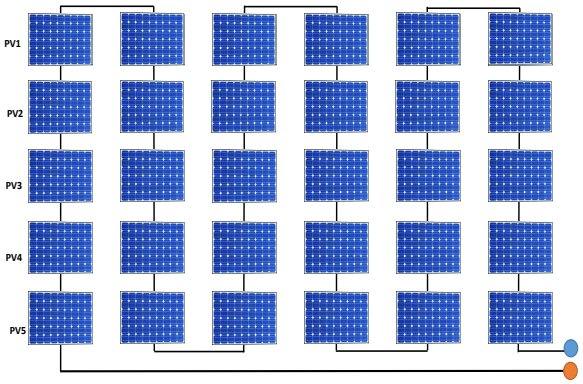

(a) Serie connection

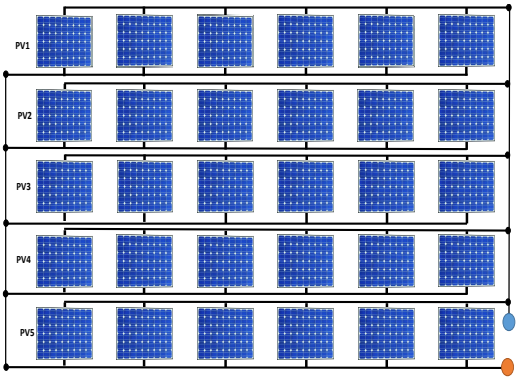

(b) Parallel connection

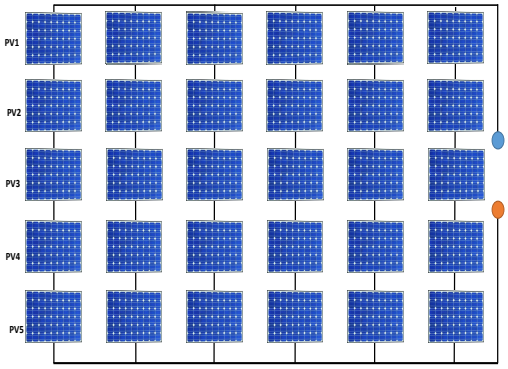

(c) Serie-parallel connection

Figure 2.6: Traditional connection schemes for PV array.

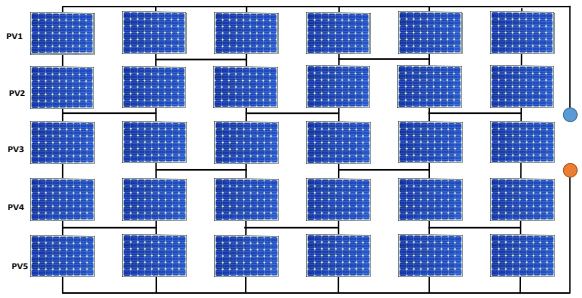

(a) BL connection

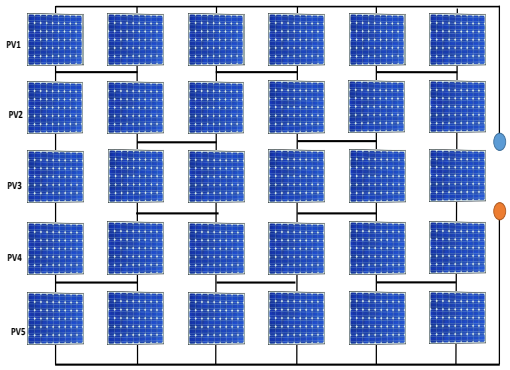

(b) HC connection

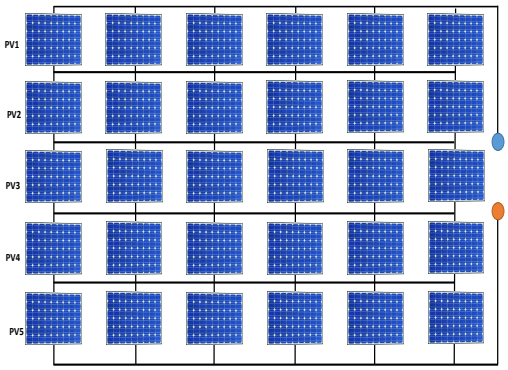

(c) TCT connection

Figure 2.7: Alternative connection schemes for PV array

They reduce the number of connections between the adjacent strings modules by approximately half, compared to the TCT configuration, which significantly reduces the amount and duration of PV field wiring. Reconfigurable PV arrays are another viable solution to compensate the power loss due to the partial shading condition [93]. In [93], Adaptive reconfiguration of solar PV arrays under shadow conditions has been presented. A matrix of switches is used to connect a fixed TCT PV array with a solar adaptive bank that can be reconfigured. Simple control algorithms that determine how the switches can be controlled to optimize output power are presented and implemented in real time. Once shading is detected, the switching matrix reconfigures the PV modules. The shaded modules in the fixed part are compensated by the modules in the adaptive bank. Thus, the PV system produces a constant power even when shaded. An experimental adaptively reconfigurable solar PV array has been built and tested to verify the proposed configurations.

2.4.3 Photovoltaic inverter topologies and architectures

Photovoltaic inverters are essential for connection of photovoltaic solar panels to the network. They make it possible to adapt the direct current coming out of the photovoltaic generator into an alternating current injectable in the public network. But they also play a role in the performance of the photovoltaic system. The optimization of the production of an installation goes through a choice adapted to the type of inverters and their dimensioning. We will define five criteria in order to make a comparison between different architectures that can answer the problems mentioned above.

- The first criterion is the level of leakage current generated by the structure. The latter depends directly on the switched voltage level across the parasitic capacitances of the modules. The amplitude of the current generated during the operation of each structure will then be analysed.

- The second criterion concerns the capacitive decoupling of the DC-link. This is to identify the amplitude of the DC-link, as well as the number of capacitors necessary to ensure the operation of the inverter.

- The number of sources (PV fields or subfields) at the input, as well as the number of switches constituting the structure, define the third and fourth criteria. This will provide an initial assessment of the cost of achieving the power structure.

- Finally, the fifth criterion is to evaluate the harmonic distortion rate THD of the output voltage. This quantity makes it possible to quantify the variation of a signal with respect to a reference, here a sinusoid of frequency equal to 50 Hz.

2.4.3.1 Photovoltaic inverter topologies

The topologies which represent the different possible configurations that link the modules PV to inverters are described below:

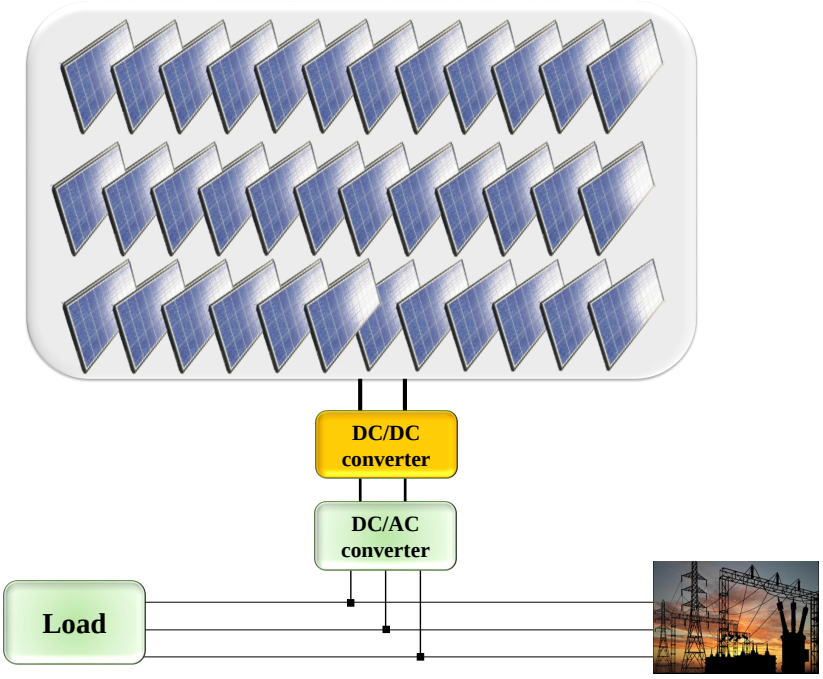

Figure 2.8: Central inverter topology.

A. Central topology This topology (see Fig. 2.8), which appeared in the 1990s, is the oldest and most known topology. Networks (called rows or "strings") of several PV modules associated in series then in parallel are connected to a single inverter. Applications that use this topology are high power level, from a few kilowatts to a hundred kilowatts [1]. Such topology has many advantages. First of all, its simplicity, the installation cost is the most attractive of all configurations, its performance which is also the most efficient, but on the other hand, can be quickly penalised by the existence of shading on the PV-field. Indeed, because of the many associations in series of modules, if only one of them is in the shade, not only the whole row will be penalized (current limited by the least irradiated module), but also the whole of production, since MPP research is common to the entire installation. Given the large area of the field and the high DC bus voltage (300 V - 600 V), anti-return diodes are required. Continuous losses due to DC cable lengths are also important (about 0.43 Wm^{-1} for a current of 10 A on a 4 mm^2 copper cable). another problem of central topology is redundancy. In case of failure of the inverter, the entire installation will be out of order and will not produce anything. In summary, this topology is dedicated to

installations of high power and under conditions where the entire field of PV modules is subjected to a uniform light intensity and without disparity. Towards the 2000s, to alleviate the various problems mentioned, the installations turned towards string configurations.

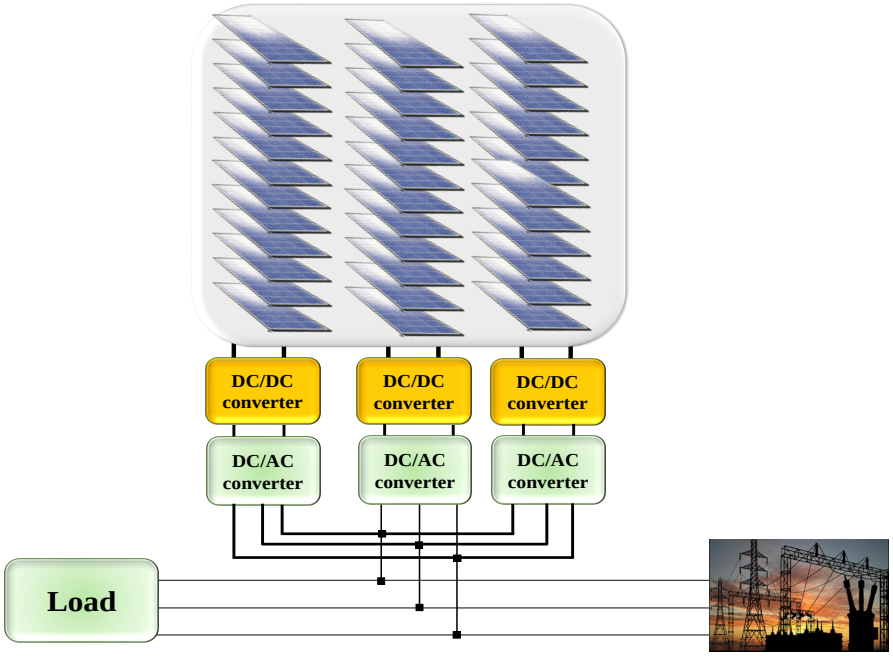

Figure 2.9: String inverter topology.

B. String topology The string topology (see Fig. 2.9) is widely used in applications from 1 kW to 3 kW [94]. It has the advantage of having one inverter per string and thus one MPPT stage per row. The productivity gain (which depends on the size of the shading and its homogeneity) is positive in case of shading. Redundancy is also improved because if there is a failure on one of the inverters, the rest of the installation continues to produce power. The anti-return diodes are also no longer needed. The major disadvantage here is the cost, which is increased in comparison with the previous topology. An example of application could be that of a house with two different orientations (south-east and south-west). In this case, the optimum operating point at a given time is different for both orientations. Two MPP Trackers would then bring a gain with maximum productivity.

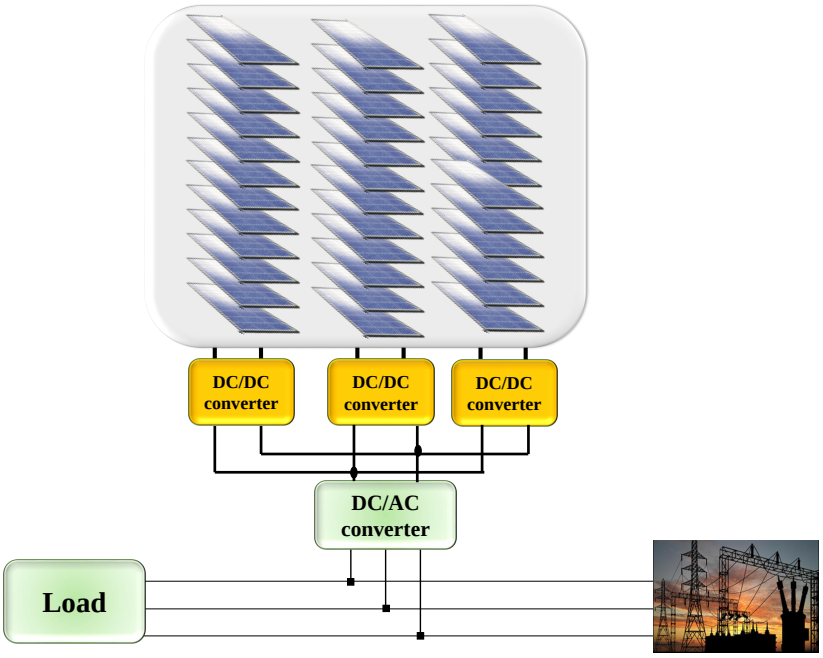

Figure 2.10: Multistring inverter topology.

C. Multistring inverter topology The multi-string inverter (see Fig. 2.10) has been developed to provide a compromise between the two previous topologies [95,96]. The interest is to reduce the costs of the topology ranked by the use of only one inverter (fewer components), to reduce DC losses compared to the central topology, but also to be less sensitive to shading by the existence of a MPPT per row. This topology, also called string converter (using a DC/DC converter per string) is still penalizing in case of malfunction. The range of power of this topology which is democratized more and more are between 3 kW and 10 kW.

D. Central inverter topology with Remote MPPT Always in the optics of discretization the production and being the least sensitive to shading (problematic mainly in urban environment), new concepts have recently emerged. This is to integrate a MPPT stage by module [97]. The assembly is then connected to a conventional central inverter (see Fig. 2.11) The objective is to have PV modules able to provide their maximum power whatever the uniformity and the level of sunshine. This problem has been dealt within the work of Stéphane VIGHETTI [98]. It exposes the problem of

voltage rise on conversion efficiency of DC/DC converters. Thus, work is carried out on several identical DC/DC converters whose outputs are first connected in parallel, then in series (has better performance for a high voltage gain) to study the impact of the type of association on Total Return. A balancing structure is also proposed. It allows a better discretization of the energy conversion and presents better performances in case of shading (+ 2% on the European yield). A similar study of this topology is carried out in the works of Cédric CABAL where the association of the outputs of converters is made in parallel and not in series (mode inter leaving). This study demonstrates once again the gain brought by the discretization in case of shading [99]. The major disadvantage of this topology is the increase in the number of components which induces an additional cost.

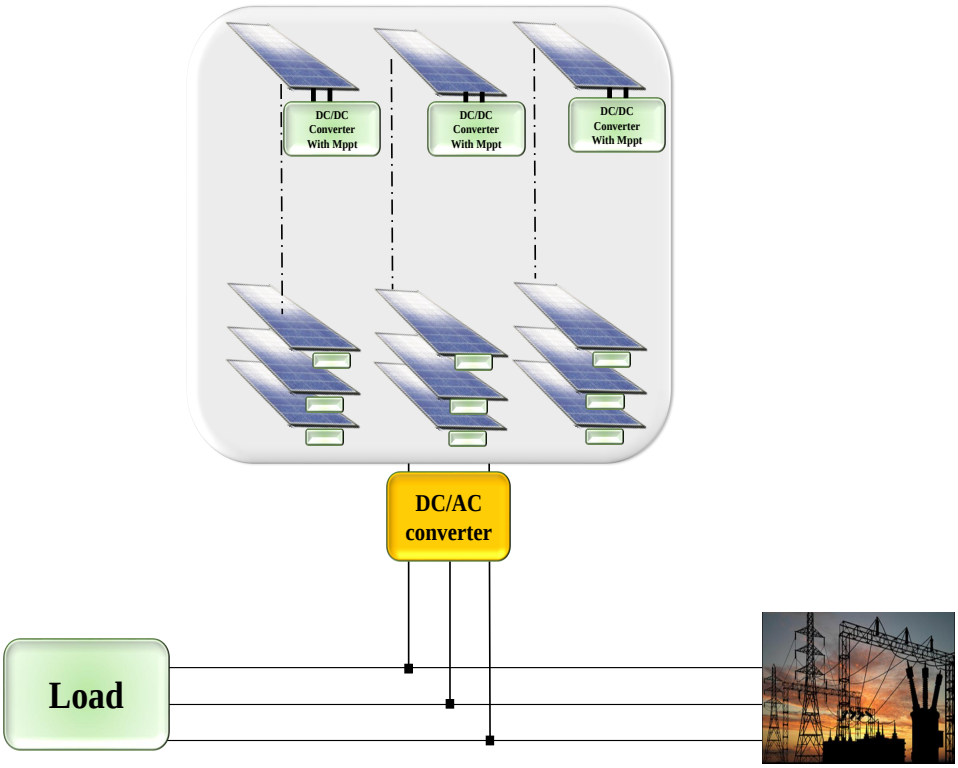

Figure 2.11: Central topology with remote MPPT.

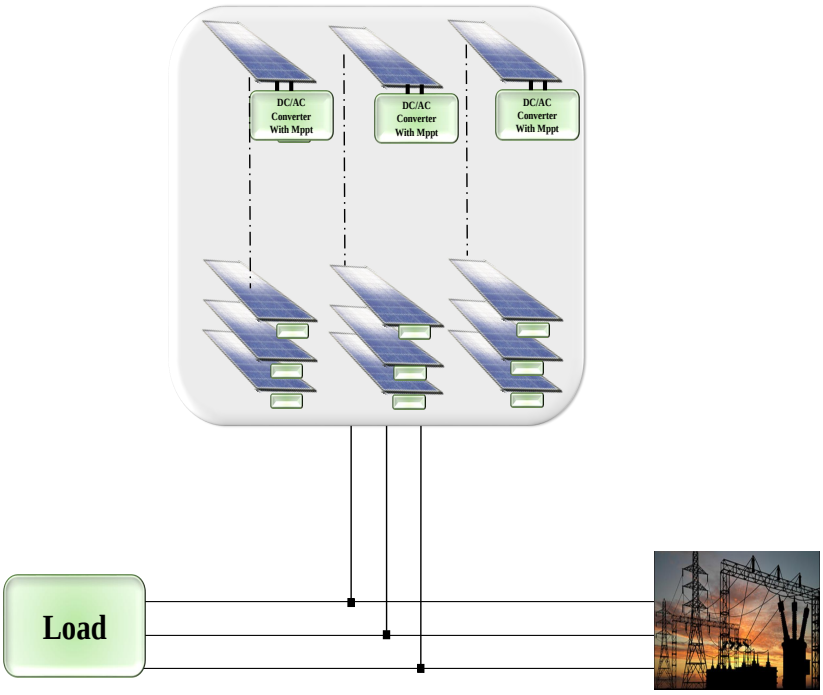

Figure 2.12: Modular inverter topology.

E. Modular topology Unlike the previous topology, the purpose of the integrated inverter (see Fig. 2.12) is not to integrate a DC/DC converter per module, but directly a DC/AC converter [100]. We are moving towards the Plug and Play concept. Each module is stackable with another. It is enough to associate them judiciously between them to increase the production of energy [101]. We therefore have directly alternative generators optimized and usable either individually or in groups. This concept certainly seems very attractive, but costs and performance are penalized. Indeed, a strong increase of the input voltage of the modules (about 45 V for a surface of 1.5 m^2) towards the mains voltage (230 V) induces losses (the European efficiency of a micro-inverter of 240 W of the manufacturer Enecsys worth 92%). The applications are limited and reserved to date for small local applications. We have seen that the trend is to discretize production [102]. As an indication, it would be possible to push it even further, until the cell. The goal is to always produce maximum energy, whatever the operating conditions.

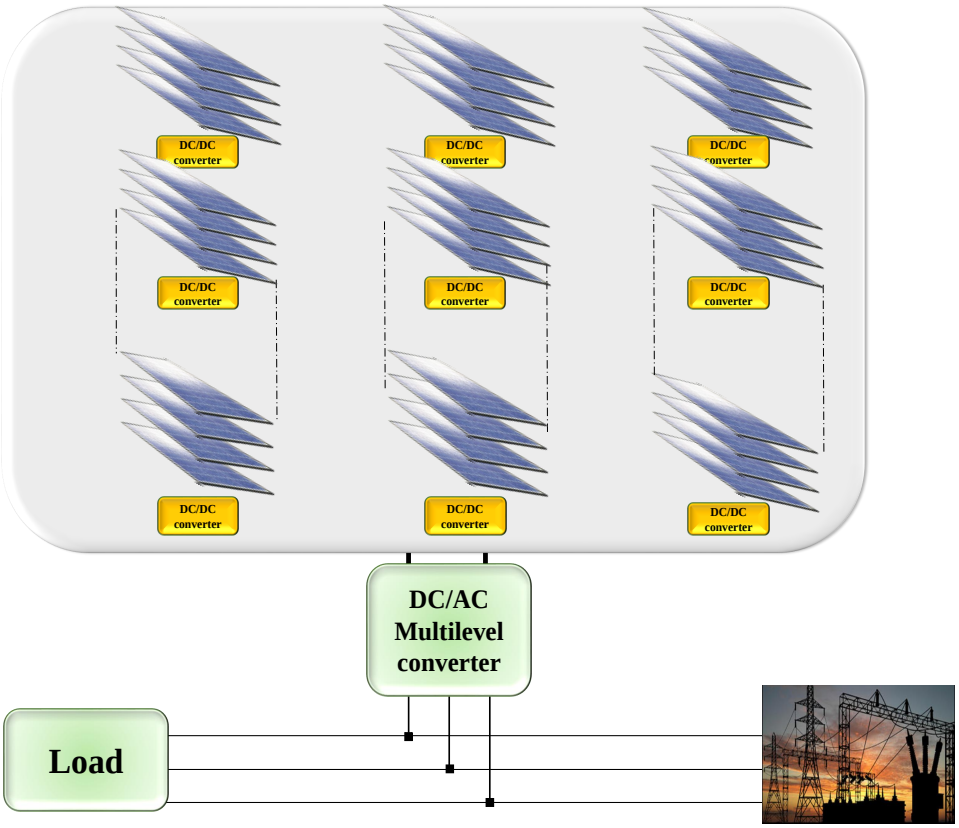

Figure 2.13: Proposed semi-modular inverter topology .

F. Proposed photovoltaic inverter topologie Fig. 2.13 describes a new semi-modular photovoltaic inverter topology based on several DC-DC converters interfaced by one multilevel inverter. This configuration is obtained by the combination of the central inverter and multistring inverter configurations. The principle of this method is based on the fact that each string is divided into sections (2-10 modules per section). Each section is connected to a DC/DC converter with its own MPPT command allowing each section to operate at its maximum power point. These DC/DC converters are connected to a central multilevel inverter through a continuous bus as shown in Fig. 2.13. The advantage of this architecture is , first of all, to have the ability to detect and locate the failed GPV which disturbs the operation of the installation. In addition, the use of DC/DC converters allow to work at lower GPV voltages. By using its modularity property, in case of several peaks on the PV-characteristic of the sections due to the partial shading, the DC/DC converters can adapt the different PV modules

of the system whatever the condition of shading. In contrasts with modular topology, this proposed topology extract the maximum power from PV modules while reducing installation costs by reducing the cable connection and the number of converters to use. The cost can be competitive for this installations which incorporate a monitoring system.

2.4.3.2 photovoltaic module/inverter interconnection

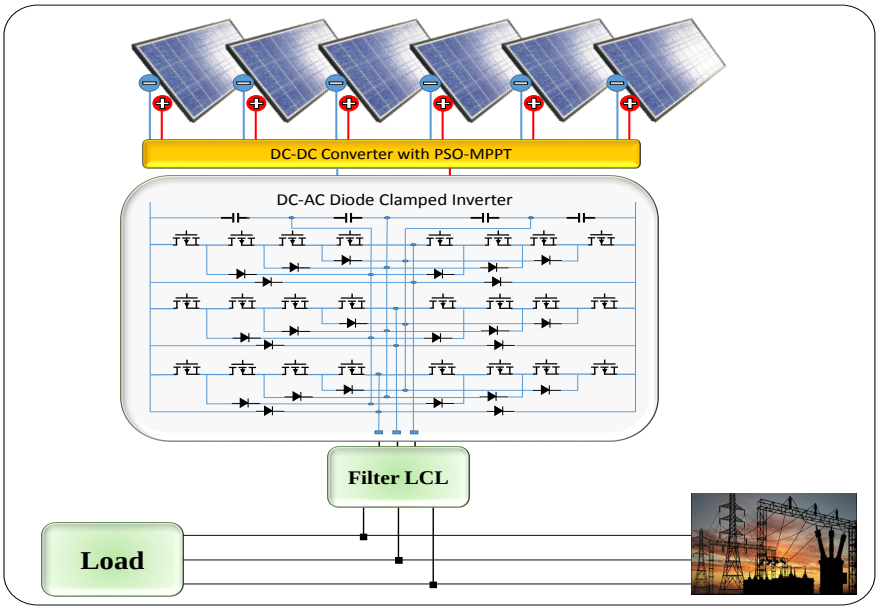

Figure 2.14: Diode clamped inverter integrated with common DC sources (Centralized).

A. Common DC sources Common DC sources presented in Fig. 2.14 was based on centralized inverters (Diode clamped inverter) that interfaced a large number of PV modules to the grid. The PV modules were distributed into strings, each one producing the required high voltage to avoid further amplification. Through string diodes, these strings were connected in parallel. A centralized system has many advantages in the case of projects with large homogeneous photovoltaic generators. Their watt-peak cost may be lower and maintenance can be facilitated because of the centralized setting. However, they still have some limitations such as high voltage in DC cables, power losses due to a centralized MPPT, mismatch losses between the PV modules and losses in the string diodes. Above a certain size of a PV installation, it becomes

more practical to opt for a centralized topology in order to avoid complications due to the use of a decentralized topology.

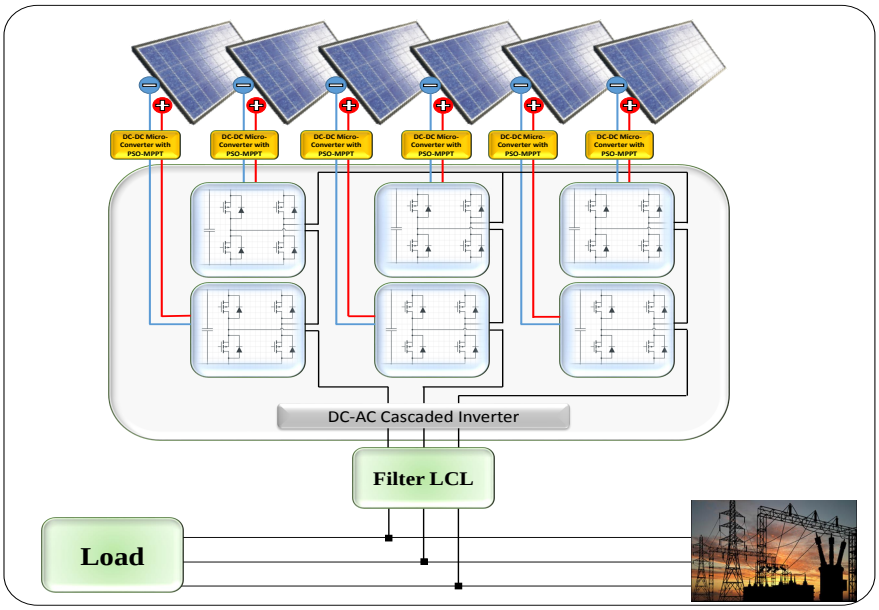

Figure 2.15: Cascade inverter integrated with separate DC sources (Decentralized).

B. Separate DC sources For PV installations with heterogeneous configurations such as different inclinations and orientations, modules and strings of different sizes, modules with high manufacturing tolerance or shaded modules, it is preferable to opt for decentralized concept using several DC-DC converters as shown in Fig. 2.15. With several DC-DC converters, it is possible to adapt to the different operating points of the various PV modules of the system. A string inverter is then connected with a series of PV modules with the same characteristics. The characteristics of the PV modules are relatively constant, the modules are all more or less different from each other. However, the yield of a string is directly dependent on the module having the lowest yield. So, if a module is partially shaded by tree leaves, dust or if it has a slight defect, the whole string will suffer. The use of a micro-converters can solve this problem as the PV modules are independent of each other. A module having a defect can also be disconnected while waiting to be cleaned or fixed without affecting the rest of the modules. The major disadvantage still faced by micro-converters is their cost. It is indeed obvious, that it is more costly to put one converter per PV module

than one converter for 10 modules. Nevertheless, the cost can be competitive for complex installations which incorporate a monitoring system. Decentralized systems still have the option of replacing only one element in case of failure of one PV module or string or a drop in efficiency, while keeping the PV system in operation; thus reducing downtime and it is even better and more advantageous when using micro-inverters.

2.5 Inverter for photovoltaic modules connected to grid: circuit-topologies

2.5.1 Design of grid-connected PV inverters

The inverter in a grid-connected PV system functions as the interface between energy sources with the utility grid on one side and the PV module on the other side. As the inverter transforms DC power into AC power, it controls the amount of power that should comply the requirement by different standards, e.g., EN 50106, IEEE 1547.1–2005, IEC61727 and VDE0126-1-1 in various regions. These standards handle issues like total harmonic distortion (THD), leakage current, injected DC current level, range of frequency and voltage for regular operation, power factor (PF), automatic reconnection of the system [103]. Table 2.2 shows the summary of two remarkable standards. Grid-connected PV inverters are grouped into isolated or non-isolated ones based on the galvanic isolation between the power grid and the PV module. A high-frequency transformer or a line frequency transformer can be used to monitor the galvanic isolation that adjusts the DC voltage of the converter [104–106]. In general, galvanic isolation is detected through a transformer that considerably affects the DC to AC efficiency of grid-connected PV systems [107]. The occurrence of galvanic isolation in a grid-connected PV system depends on the regulations of a country [108]. In countries such as Italy and the UK, galvanic isolation is a requirement and is implemented using either a high frequency transformer on the DC side or a low-frequency step-up transformer on the grid side, as shown in Fig. 2.16(a) and (b).

Table 2.2: Summary of two prominent standards in grid-connected PV systems.

Issue	IEEE1547	IEC61727
Nominal power	30 kW	10 kW
Maximum current THD	5%	5%
Power factor at 50% of rated power	-	0.9
DC current injection	Less than 0.5% (rated output current)	Less than 0.% (rated output current)
Voltage range (normal operation)	88–110% (97–121 V)	85–110% (196–253 V)
Frequency range (normal operation)	59.3–60.5 Hz	50±1 Hz

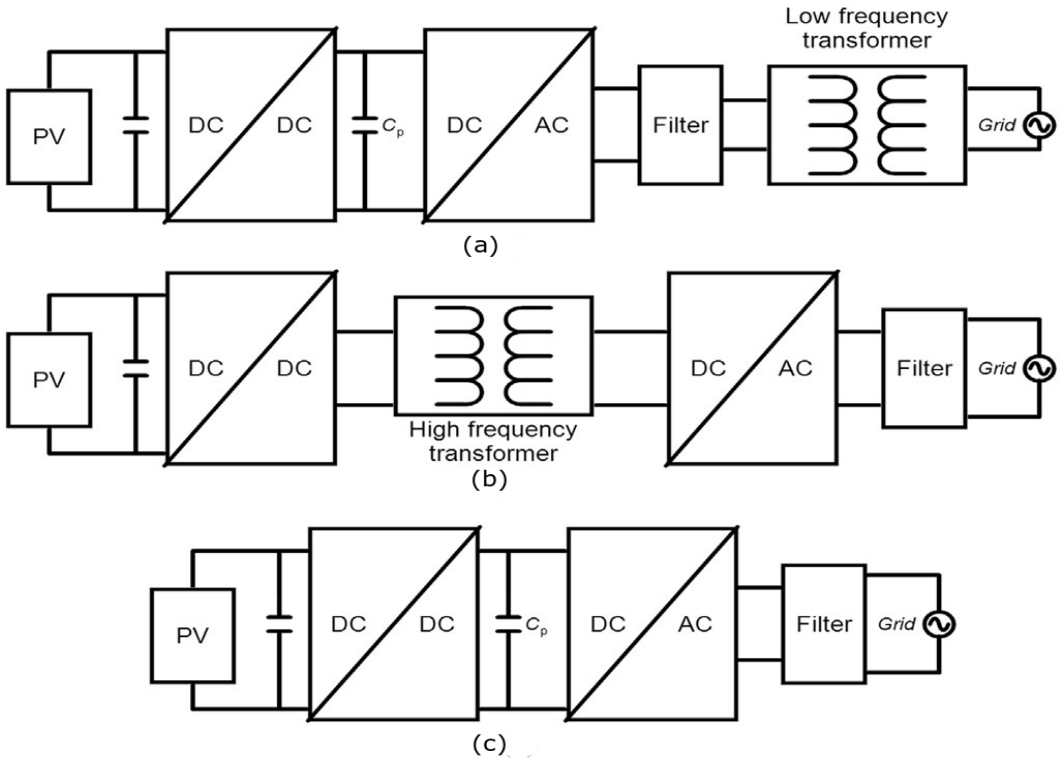

Figure 2.16: Grid-connected PV systems with (a) a transformerless inverter, (b) a high-frequency transformer, and (c) a low-frequency transformer.

A summarized criteria of existing standards in some IEA countries is given in Table 2.3 [109]. Considering weight, size, and cost, line frequency transformers are preferably removed at the time of designing a new converter. Moreover, a high-frequency transformer necessitates numerous power stages, which make increasing efficiency and reducing cost challenging [110]. On the contrary, in countries such as Spain and Germany, galvanic isolation is not required if other technological solutions are used to separate the electrical grid and the PV array. Fig. 2.16(c) shows a typical transformerless PV system, which decreases the installation complexity, weight, cost, and size of the whole system. One drawback of these systems is that DC current may be produced by the inverter to the injected AC current due to the missing line frequency transformer, thereby causing overheating and failure [111,112]. Meanwhile, one of the advantages of these systems is the remarkable 2% increase in total efficiency [113–115].

Table 2.3: Existing standards in some IEA countries.

Countries	Voltage fluctuation (V)	Isolation Transformer	Harmonic	Power factor
Austria	184–253	NO	EN61000-3-2-A	> 0.9
Denmark	207–253	HPFI Relay-30 mA	EN61000-3-2-A	> 0.95
Germany	216–244	NO	EN61000-3-2-A	> 0.9
Italy	207–253	DC Monitoring	EN61000-3-2-A	> 0.9
Japan	182–222	DC Monitoring	THD $< 5\%$	> 0.85
Holland	207–244	NO	EN61000-3-2-A	> 0.9
Portugal	187–253	NO	EN50160	-
Switzerland		DC Monitoring	EN61000-3-2-A	-
United Kingdom	226–254	DC Monitoring	EN61000-3-2-A	> 0.85
United States		DC Monitoring	THD $< 5\%$	> 0.95

2.5.2 Single-phase transformerless inverter topologies

Proper understanding on the strengths and weaknesses of different inverters can possibly be achieved by examining their configurations and operations. Inverters have many configurations, which exhibit their own characteristics, to address the issues of CM noise and ground leakage current. Most transformerless inverters can be categorized according to the number of required switches, such as two-switch, three- switch, four-switch, five-switch, six-switch and multilevel inverters.

2.5.2.1 Two-switch inverters

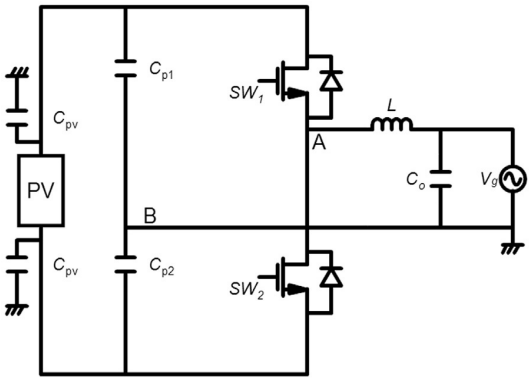

Figure 2.17: Half HB inverter topology.

The half H-Bridge (HB) topology involves a capacitive divider coupled with the PV module and two transistors (Fig. 2.17). The grid neutral wire connection to the midpoint of a capacitive divider warrants a relatively constant voltage that inhibits leakage current through the parasitic capacitance of the module [116]. The half HB topology uses only half of the semiconductors, and thus, is simple and low-cost compared to the full HB topology [117]. However, the former is seldom used because of its drawbacks. For example, the switches should support twice the voltage than the full HB topology, the output waveform only has two levels, and the output current is extremely distorted and generates a high amount of electromagnetic interference emissions [116,118]. Thus, the half HB topology requires high blocking voltage power transistors, which increase switching losses. The specifications of a half bridge topology are listed in Table 2.4 [118].

Table 2.4: Parameters of two-switch topologies.

	Half HB [118]
Power (KW)	5.5
Input voltage (V)	700
Switching frequency (KHz)	5
Grid voltage (V)	230
Filter inductor (mH)	3
Filter capacitor (uF)	-

2.5.2.2 Three-switch inverters

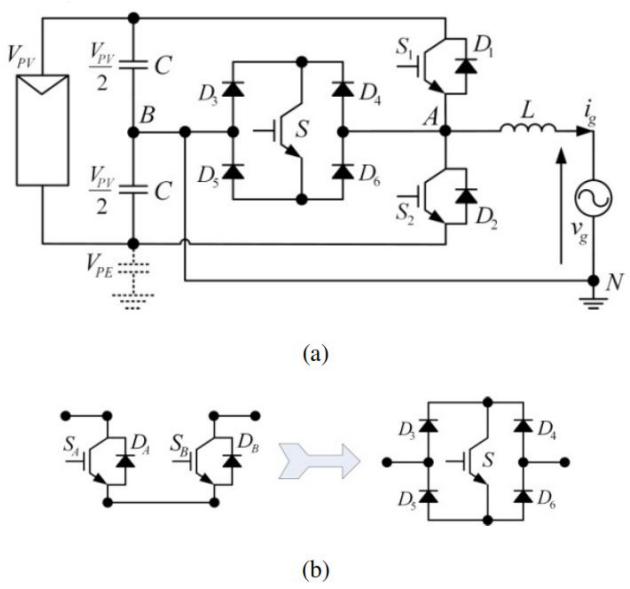

Figure 2.18: Conergy NPC topology.

Conergy neutral point clamped (NPC) topology is illustrated in Fig. 2.18, in which voltage output is clamped to the neutral point through bidirectional switches [119], where the clamping circuit has four diodes and one switch. Zero voltage can be attained in this topology by clamping the ground to the output voltage (midpoint of the DC bus) via S_A and S_B. Switches S_1 and S_A commutate complementary at a high frequency during the positive half cycle, whereas during the negative half cycle,

S_2 and S_B commutate complementary at a high frequency. CM voltage is clamped to $V_{PV}/2$ during the entire process, and consequently, low leakage current streams into the parasitic capacitance [120]. This topology has higher efficiency, which makes it appropriate for low-power PV applications [121]. The specifications of a conergy NPC topology [119] is listed in Table 2.5.

Table 2.5: Parameters of three-switch topologies.

	Conergy NPC [119]
Power (KW)	0.225
Input voltage (V)	-
Switching frequency (KHz)	10
Grid voltage (V)	-
Filter inductor (mH)	-
Filter capacitor (uF)	-

2.5.2.3 Four-switch inverters

Full HB topology is commonly used in grid-connected PV inverters. This topology has four transistors, which are linked as shown in Fig. 2.19(a). Numerous commercial inverters adopt this topology along with a low-frequency transformer; thus, studying its usage in transformerless inverters is beneficial. A uni-polar pulse width modulation (PWM) is the most commonly used modulation for this topology because it offers several advantages, such as improved efficiency, reduced electromagnetic interference emissions, and lower current ripple at high frequencies as compared with bipolar modulation [122]. Nevertheless, a high-frequency CM voltage of amplitude $V_{DC}/2$ is applied to the PV panels in uni-polar PWM, which generates a considerable amount of leakage current because of the parasitic capacitance of PV panels. Thus, this modulation is not recommended for transformerless inverters [123]. In the PV inverter with a full HB topology, bipolar PWM is used to solve the problem of leakage current. Thus, the high-frequency components of the applied CM voltage to the panels are eliminated [124].

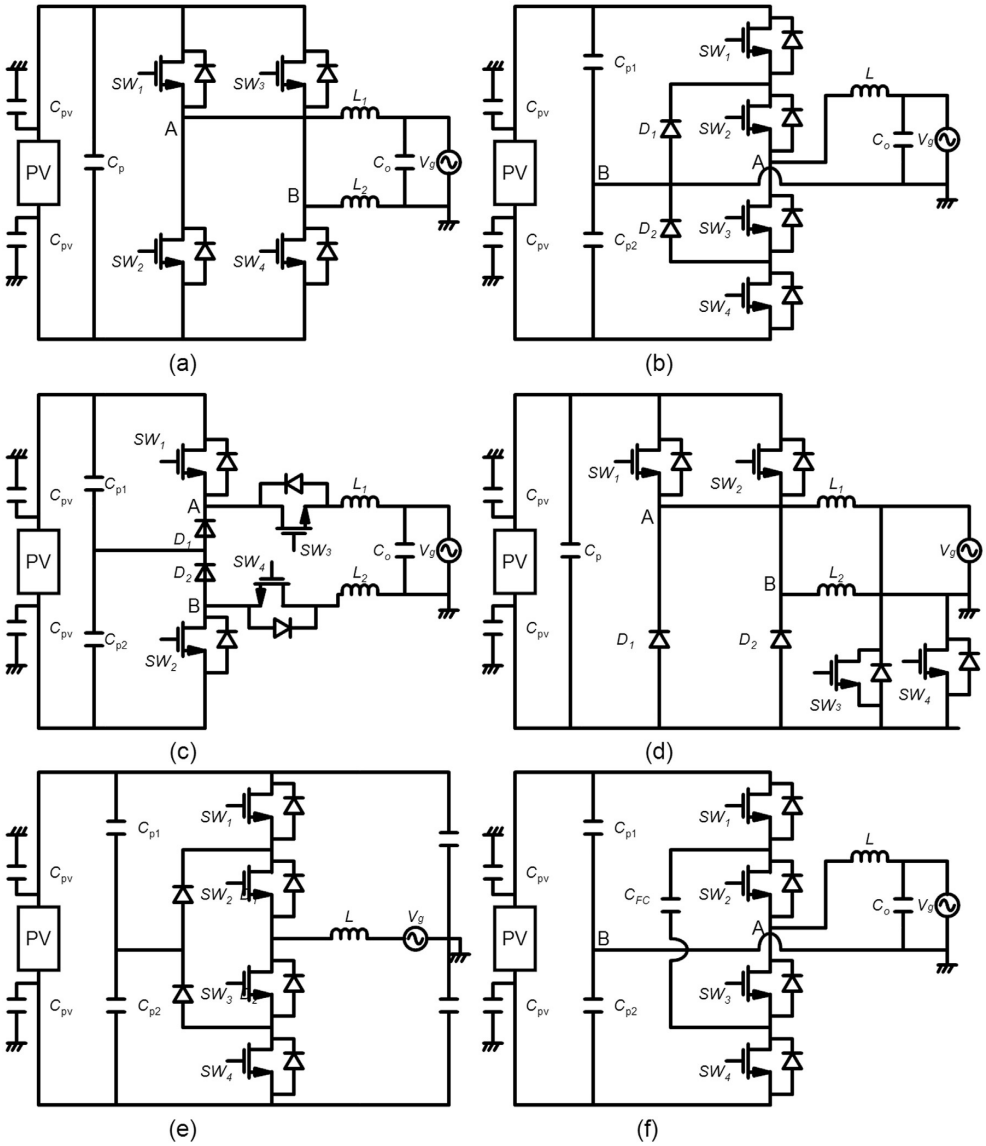

Figure 2.19: Full HB topology (a), NPC half-bridge inverter (b), dual-buck transformerless inverter with, series configuration (c), parallel configuration (d), NPC three-level voltage source inverter (e), flying capacitor topology (f).

CM voltage only has the low-frequency component of the first harmonic, and leakage current is reduced [125–127]. However, good synchronization is required among the gate signals of the bridge transistors to limit peak leakage current. If not, then leakage current may increase significantly [128]. Therefore, this topology is not suitable for transformerless PV inverters, even when bipolar PWM is used [129]. Another four switches inverter, NPC half-bridge topology is a single-phase version of the multilevel topology for high-power applications [130]. Recently, it has

been introduced as an alternative for the design of PV inverters. This topology has a branch with two clamping diodes and four transistors (Fig. 2.19(b)). The diodes provide a freewheeling path for the output current, which results in a state of zero output voltage [124]. The NPC half-bridge topology functions similarly as the half HB topology, but has less current ripple, better efficiency, and a constant CM voltage [118], which inhibit leakage current. The voltage derivative and performance of the NPC half-bridge topology are also similar to those of the full HB topology with uni-polar PWM, that is, a three-level output inverter voltage. Therefore, the performances of the converter and the output filter are comparable with that of a uni-polar PWM full HB topology [127]. The main disadvantages of the NPC half-bridge topology are its high input voltage, use of several power semiconductors, and a high capacity bank for capacitors [126, 131], which generate twice the full HB input voltage [123]. Another issue is the transient overvoltage in internal transistors because of the lack of parallel capacitors [132]. However, this issue can be solved by using a snubber circuit. Moreover, power loss is not consistently scattered across all the semiconductors [133].

Another four switch topology can be generated as displayed in Fig. 2.19(c) and (d). If dual-buck converter modules are combined, a transformerless inverter is obtained. Here, one buck is responsible for the negative half cycle voltage, whereas another buck is used to generate a positive half cycle voltage. These modules are either in parallel or in series configuration. In series configuration, the split-inductor NPC inverter is used [134], as shown in Fig. 2.19(c). D1 and S_{w1} comprise the upper buck module, whereas D2 and S_{w2} form the lower buck module. Switch S_{w3} remains turned on during the positive half cycle, whereas S_{w1} functions in high frequency to produce the positive half cycle voltage. To disconnect the lower buck module, this module is turned off. Furthermore, the upper buck module does not work during the negative half cycle, and only the lower buck converter operates to generate a negative half cycle voltage. To block the reverse inductor current, S_{w3} and S_{w4} change direction with line frequency. The dual-buck inverter with series configuration does not experience the shoot-through problems of the half-bridge inverters, and thus, system reliability is improved. Nevertheless, the DC-link voltage should be twice the grid peak voltage.

Parallel configuration is used to reduce the DC-link voltage. Fig. 2.19(d) shows the dual-buck inverter with parallel configuration in analogous working modes [123]. The required DC-link voltage is split to decrease the number of series PV panels and enhance safety. Two inductors, which work alternately, are necessary in dual-buck inverters. Filter inductors have a significant role in power density and cost [135]. The interleaved dual-buck inverter reduces inductor size [136]. The coupled inductors further decrease the size of the magnetic core.

A NPC topology was introduced for single-phase grid-connected PV systems. This topology has one leg with two diodes D1–D2 and four switches S_{w1}-S_{w4} (Fig. 2.19(e)). The diodes provide a freewheeling path for the output current, which leads to a zero-voltage output state [118, 124]. This topology has an operating principle that is comparable with that of the half-bridge topology, but its current ripple is less and its efficiency is higher. Moreover, a high-frequency CM voltage remains constant, and thus, leakage current is reduced. Similar to the full-bridge topology, uni-polar sinusoidal PWM (SPWM) is used with a three-level output voltage [127]. The main disadvantage of this topology is the higher input voltage (800 V) requirement. Consequently, a high capacity bank of capacitor is necessary [126, 131]. Flying Capacitor (FC) is another four switch topology that can function as an exceptional solution for transformerless PV inverters (Fig. 2.19(f)). The clamping diodes in this topology are substituted with a capacitor that "floats" relative to the DC source reference. Extra levels are attained through the capacitor, and maintaining a constant voltage across the capacitor at the preferred level is required, mainly when loading the outer DC-link capacitor. Nevertheless, imbalances may generate a high voltage that can destroy the inverter [137,138]. Thus, an exceptional circuit is required for pre-charging the floating capacitor to solve the overvoltage problem. This circuit will increase the complexity of the control circuit of the FC inverter [131, 139]. Furthermore, several capacitors are necessary for large structures. Fault-tolerant operation is the most remarkable feature of FC inverters. This feature enables the inverter to remain functional even if multiple faults occur in different phases or if a single switch fault occurs per phase [140]. The specifications of some four-switch topologies are listed in Table 2.6.

Table 2.6: Parameters of four-switch topologies.

	Full HB [122]	Dual-Buck [123]	3-Level NPC [118]
Power (KW)	1.7	4.5	5
Input voltage (V)	400	376–537	700–1100
Switching frequency (KHz)	10	16	16
Grid voltage (V)	240	230	230
Filter inductor (mH)	-	3	3
Filter capacitor (uF)	-	3.3	-

2.5.2.4 Five-switch inverters

Compared with the FB topology, the H5 topology only requires an extra transistor. SMA Solar Technology introduced H5 topology [141]. In this topology, the PV panel is disconnected from the grid during current freewheeling periods to inhibit the switching of frequency ripples in the voltage of the panel poles to the ground, and consequently, maintaining a nearly constant CM voltage. The H5 topology shown in Fig. 2.20(a) uses a FB inverter that involves a DC-bypass S_{w5} switch and four switches (S_{w1},S_{w2},S_{w3}, and S_{w4}). Here, S_{w1} and S_{w2} work at a grid frequency, whereas S_{w3},S_{w4}, and S_{w5} are functional at high frequencies. The switch S_{w5} is open during current freewheeling period, thereby detaching the full HB inverter from the PV panels. The switch S_{w1} closes the freewheeling path, by S_{w1} and S_{w3} inverse diode for the negative half cycle, and by S_{w3} and S_{w1} inverse diode for the positive half cycle of the electrical grid. The H5 transformerless inverter topology results in high efficiency, particularly at a partial load [142]. It only requires one extra transistor compared with the full HB topology. Nevertheless, conduction losses can increase if the semiconductor is mediocre because the transistor is in series with the full HB inverter [143]. At present, several inverters available in the market use this topology, particularly those from branded patents, as an alternative to implementing transformerless PV inverters [123].

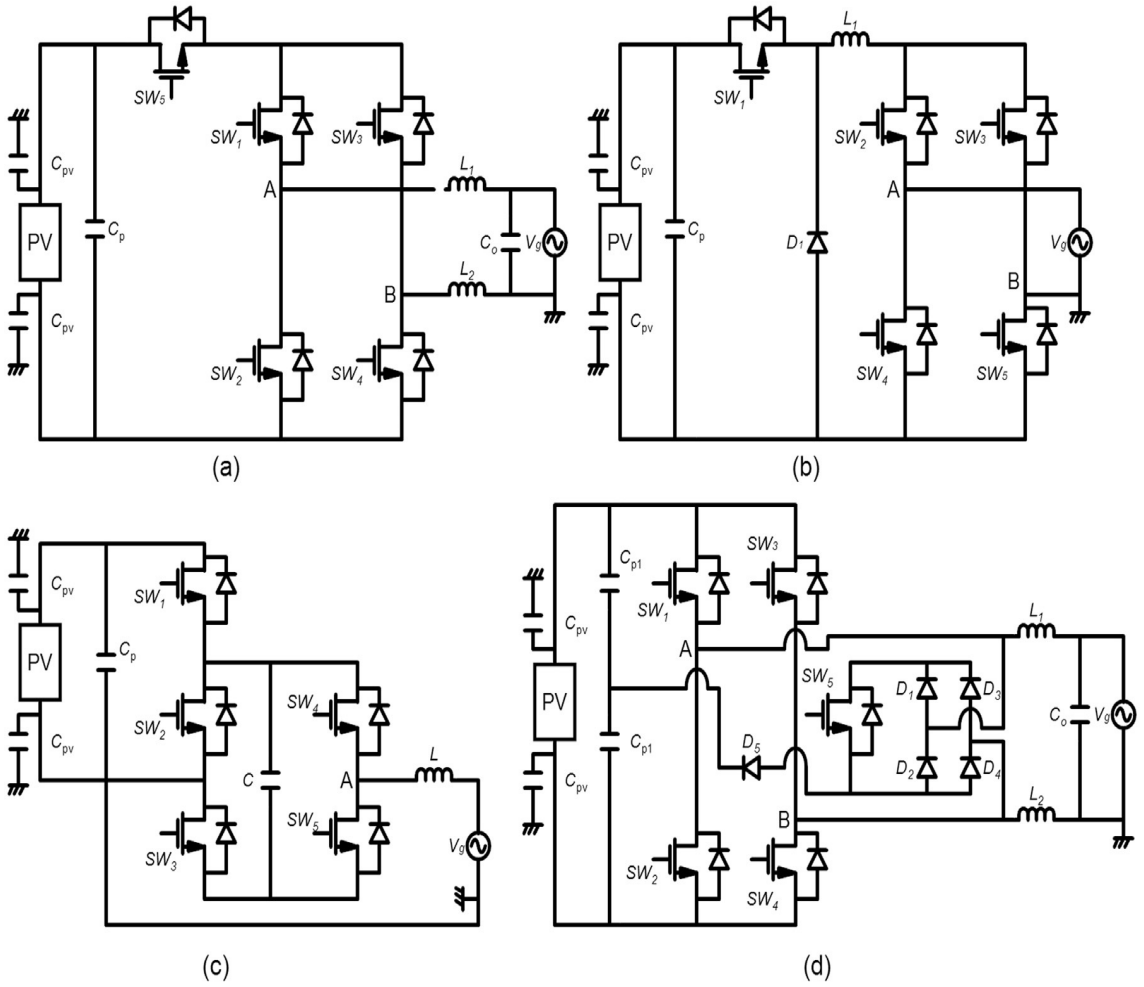

Figure 2.20: H5 topology (a), single-buck inverter topology (b), virtual DC bus topology (c), HB-ZVR topology (d).

The elementary outline for the five-switch inverter is a buck converter working at a high frequency. To develop the sinusoidal output, the high-frequency switch adopts a corrected sinusoidal reference, whereas the low-frequency switches work at the line frequency to change the waveform from a corrected sinusoid to a full-sinusoidal waveform. This topology is called a single-buck inverter (Fig. 2.20(b)) [144]. Similar to the uni-polar dual-buck inverter, the biggest advantage of the single-buck inverter is that it can use metal-oxide-semiconductor field-effect transistors (MOSFETs) reliably for a high-frequency switch. Another benefit of the single-buck inverter is that only one magnet is required, which decreases the cost [144]. When MOSFETs are utilized for full-bridge unfolders, the extra conduction loss from an extra switch in the con-

duction route is alleviated. The modulation operation of the converter is uni-polar, which reduces inductor loss. Given that the AC neutral point is linked to the DC negative point at all times, CM noise is also decreased compared with that in standard uni-polar modulation. At both negative and positive line cycles, S_{w1} works at high frequencies because the reference is a rectified sinusoid wave. The switch S_{w1} turns off the current freewheels via D1,S_{w2},and S_{w5} during the positive line cycle, whereas it turns off the current freewheels through D1,S_{w3}, and S_{w4} for the negative line cycle. The fundamental component of the CM voltage is low. Similarly, the dV/dt of the voltage transition is gradual; thus, leakage current magnitude is negligible. A short circuit is a disadvantage of a single-buck inverter. The only practical solution for this problem is to place inductors on the mid-node of the full-bridge unfolder to the AC line. Consequently, CM noise is increased, and losses occur in inductors.

Table 2.7: Parameters of five-switch topologies.

	H5 [141]	Single-Buck [146]	Virtual DC-Bus [147]	HB-ZVR [145]
Power (KW)	1	0.25	0.5	2.8
Input voltage (V)	340–700	380	400	350
Switching frequency (KHz)	20	30	20	8
Grid voltage (V)	240	240	230	230
Filter inductor (mH)	4	6	-	1.8
Filter capacitor (uF)	6.6	0.47	C1 = 470, C2= 940	2

Another five-switch transformerless inverter can be generated as displayed in Fig. 2.20(c). It is an economical PV inverter, and is called the virtual DC bus [147]. To eliminate leakage current, parasitic capacitance between the ground and the PV module is prevented via direct connection between the negative pole of the DC bus and the grid neutral line. Similarly, a virtual DC bus provides the negative level. Consequently, the inverter achieves three-level output voltage. The switch S_{w2} is always

turned off, whereas S_{w1} and S_{w3} are always turned on in the positive half cycle of the grid current. However, S_{w4} and S_{w5} commutate complementary at high frequencies. S_{w4} is always turned off, whereas S_{w5} is always turned on in the negative half cycle; S_{w2} complementary and S_{w1} and S_{w3} synchronously commutate at switching frequency [147]. The PV panel and the capacitor Cp form the real DC bus, whereas the switched capacitor C creates the virtual DC bus, which is charged to keep a constant DC voltage via S_{w1} and S_{w5}. Both double-frequency SPWM and uni-polar SPWM can be used to generate high-performance AC current. The main problem is controlling the charging of the virtual DC bus capacitor using the real bus. Similarly, the power switches are influenced by additional current stresses because of switched capacitor action, which decreases reliability and efficiency [147,148]. Fortunately, the maximum current stress can be limited to less than thrice that of basic half-bridge inverters by adopting an appropriate design.

Zero voltage rectifier topology (HB-ZVR) is another five-switch topology with AC bypass [145], in which the short-circuited output voltage is clamped to the midpoint of the DC bus during the freewheeling period via a bidirectional switch and a diode rectifier. To protect the lower DC-link capacitor from short circuiting, another diode is added (Fig. 2.20(d)). The working standard of HB-ZVR topology is considerably analogous to the highly efficient and reliable inverter concept (HERIC) topology [149], which is discussed in the following subsection. In the positive half wave, the S_{w5} gate pulse is opposite the S_{w1} and S_{w4} gate pulses, with a minor dead time to ignore grid short circuit [145,149]. The switch S_{w5} is controlled during the negative half wave by S_{w2} and S_{w3} contrary to the gate pulse that generates a zero-voltage output state by short circuiting the output of the inverter and fixing it to the midpoint of the DC bus. Diode D5 performs the clamping, which permits one-directional clamping as long as the potential of the freewheeling path is higher than the midpoint voltage of the DC link. Consequently, CM voltage fluctuation is observed when the reverse condition occurs. Another drawback of this topology is the dead time requirement that increases output current distortion. The specifications of some five switch topologies are listed in Table 2.7.

2.5.2.5 Six-switch inverters

A new topology based on the full HB inverter, known as HERIC, was developed to avoid the occurrence of leakage current while preserving the three-level output voltage [150]. In this topology, a series of branches are added parallel to the output filter (Fig. 2.21(a)). Several commercial inverters have used this topology, including Sunway's converter [123,124]. The advantages of HERIC topology include its low leakage current, high efficiency, and uni-polar PWM. Moreover, the benefits also includes its three-level output voltage that is generated using uni-polar SPWM and low current ripple in the output filter. To provide the freewheeling current path, two switches are added to the AC side. The extra branches shift at the electrical grid frequency, such that S_{w1} is in the off-state in the negative half cycle and in the on state in the positive half cycle. By contrast, S_{w2} is in the off-state in the positive half cycle and in the on-state in the negative half cycle. Consequently, diodes D1 and D2 can work as freewheeling diodes in both negative and positive half cycles, thereby inhibiting the flow of output current through the diodes. This feature separates the electrical grid from the PV panel and achieves three-level output voltage because the same one remains short circuited when D2 or D1 conducts. Through HERIC topology, the PV panel keeps a floating voltage to the ground, and consequently, attain a constant CM voltage [124]. Ground leakage current is reduced to a satisfactory level [145,149].

Furthermore, the efficiency of HERIC topology can be improved compared with that of HB topology because the current does not stream through bridge semi-conductors during freewheeling periods. This feature is considerably useful when the inverter works in light load conditions [124, 145, 151]. Another six-switch inverter, H6-type MOSFET inverter topology, which does not use insulated-gate bipolar transistors (IGBTs), has been proposed in [152] (Fig. 2.21(b)). A uni-polar SPWM with three-level output voltage can be implemented using this topology. The freewheeling current streams via S_{w5} and D1 in the positive half cycle of the grid current when S_{w1} and S_{w1} are off. By contrast, it streams through D2 and S_{w6} for the negative half cycle of the grid current when S_{w2} and S_{w3} are off. Consequently, reverse recovery is unnecessary for this topology. The European efficiency and peak efficiency of the H6-type MOS-

FET inverter on a 300 W prototype circuit with 30 kHz operating frequency are 98.1% and 98.3%, respectively [152, 153]. The grid current streams via three switches in the active mode, and thus, conduction losses remain high. Another challenge is that anti-parallel diodes are triggered when a phase shift happens between the inverter output current and voltage. Thus, the reliability of the system is reduced because of the low reverse recovery of such diodes [153, 154].

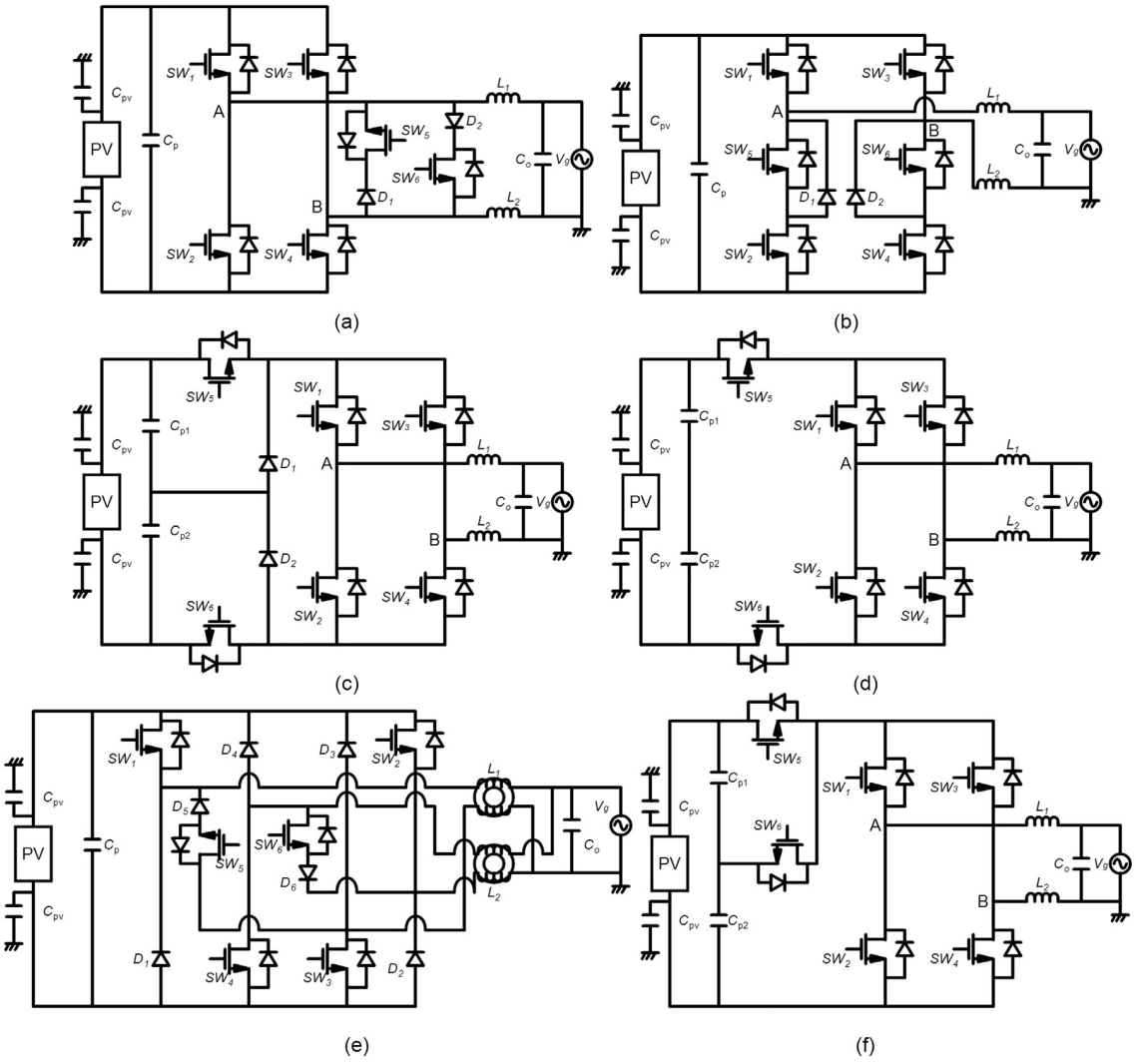

Figure 2.21: HERIC topology (a), H6-type MOSFET inverter topology (b), H6 topology (c), improved H6 topology (d), HRE topology (e), oH5 topology (f).

FB inverter with DC bypass (DCBP) topology adds a bidirectional clamping branch and two switches to the FB topology (Fig. 2.21(c)) [155]. The clamping branch has two diodes and a capacitive divider that clamps half of the DC voltage input to the CM

voltage input. S_{w1} and S_{w4} are commutated anti-parallel to S_{w2} and S_{w3} with line frequency depending on whether the grid voltage is in a negative or positive half period. D1 or D2 works during freewheeling mode depending on whether the freewheeling path potential is lower or higher than half of the DC-link voltage. The effect of leakage current removal in this topology is only contingent on the turn-on speed of the clamping diodes. The main disadvantage of DCBP topology is that conduction losses result from the flow of inductor current through four switches in active mode [155]. In another H6 topology [148], two additional S_{w5} and S_{w6} switches are symmetrically added to the FB inverter (Fig. 2.21(d)). Uni-polar SPWM and double-frequency SPWM are the modulation techniques used for this topology. CM voltage is constant when two more capacitors with 29 pF are connected to S_{w3} and S_{w4} in parallel under uni-polar SPWM. Alternatively, CM voltage remains constant under double-frequency SPWM if four additional capacitors (470 pF) are connected to S_{w1}, S_{w2}, S_{w3}, and S_{w4} in parallel. Double-frequency SPWM decreases current ripples throughout the output filter, which is half of that in the uni-polar SPWM scheme [148]. A six-switch HRE topology was proposed in [154], which uses MOSFETs as main power switches (Fig. 2.21(e)). This topology divides the AC side into two separate portions for the negative and positive half cycles of the grid current. D1–D4 diodes perform voltage clamping for active S_{w1}–S_{w4}. The freewheeling current streams via S_{w5} and D5 when S_{w1} and S_{w3} are turned off, thereby detaching the PV module from the grid for the positive half cycle. For the negative half cycle of the grid current, the freewheeling current streams via D6 and S_{w6} when S_{w2} and S_{w4} are off. As coupled inductors, L1 and L2 start working for the positive and negative half cycles, respectively. The maximum efficiency of the HRE inverter on a 5 kW prototype circuit with a switching frequency of 20 kHz is 99.3%. The main topology has six diodes and six MOSFETs that increase the initial cost and complexity. A six-switch oH5 inverter is a modified H5 topology [156]. A clamping branch that comprises a capacitor divider and a switch are added to H5 topology, which ensures that the freewheeling path potential is fixed to half of the DC bus voltage (Fig. 2.21(f)). S_{w5} and S_{w6} are commutated during the entire grid period to warrant the disconnection of the grid from the PV module. A

dead time is required between the gate signals of S_{w5} and S_{w6} to prevent the short circuiting of the CP1 input split capacitor. Consequently, CM voltage oscillates in dead time [156, 157]. Another drawback is that conduction losses remain high because inductor current streams via three switches in active mode. The specifications of some six-switch topologies are listed in Table 2.8.

Table 2.8: Parameters of six-switch topologies.

	H6 [152]	HERIC [158]	HRE [154]	oH5 [157]
Power (KW)	0.3	1	5	1
Input voltage (V)	180-200	350	360	340-700
Switching frequency (KHz)	30	8	20	20
Grid voltage (V)	120	230	240	240
Filter inductor (mH)	0.8	1.8	0.95	4
Filter capacitor (uF)	0.68	2 b	-	6.6

2.5.2.6 Multilevel inverters

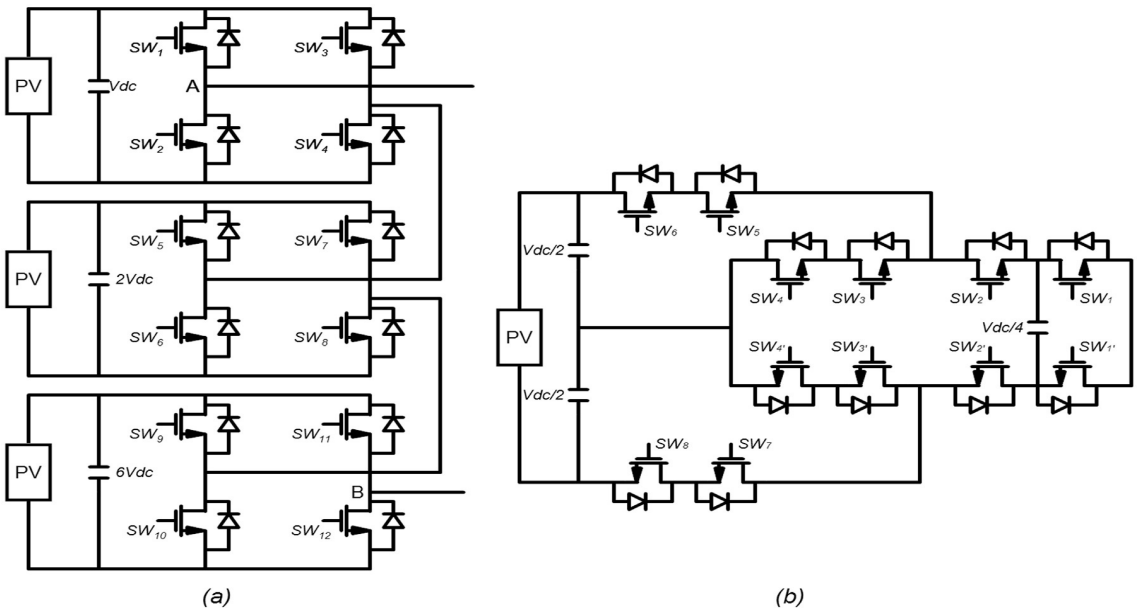

Figure 2.22: Asymmetric cascade H-bridge (ACHB) (a), 5-level ANPC (b).

The multilevel inverters are based on a number of DC voltage levels and a special arrangement of the passive components and semiconductors of the inverter [159]. The simplest multilevel inverter involves the connection of H-bridge forms in series by its AC-side, while each DC-link connected to different photovoltaic panel [160]. A cascaded H-bridge (CHB) multilevel inverter as shown in Fig. 2.22(a). A multilevel inverter called asymmetric cascaded H bridge inverter (ACHB) presented in [161]. This topology connected to unequal DC voltage levels between H-bridge forms, decreasing the switching losses and improving efficiency by switching of the higher power forms at grid frequency. Due the type and the number of existing primary energy sources, this topology could be suitable for low voltage applications or single phase. The main disadvantages of this topology include excessive switching devices, rise of the highest voltage H-bridge form by increasing the numbers of levels, complex modulation strategy and control system. The advantages include lower THD and operating at low switching frequency. By using a lot of H-bridge, the inverter can achieve high voltage levels to connect to high voltage buses without using transformers [161]. A five-level multilevel inverter called 5L-ANPC [162] includes a three-level flying capacitor (FC) power form with a three-level active NPC (ANPC) form connected between the switching devices as shown in Fig. 2.22(b). The number of inverter levels can effectively be increased with the levels of the Flying capacitor module. A five levels voltage (± Vdc/2, ± Vdc/4, and 0) can be reached by controlling FC to Vdc/4, which is connected in series to the ANPC dc-link capacitors at Vdc/2, using a suitable switching state. This topology without the series connected diodes and by just using FC forms can reach to higher level values [162]. Because of the particular configuration and the extra levels in this topology, the series loss is compensated by commutating the outer switches at lower switching frequency.

2.5.2.7 Discussion

In general, the classic half-bridge inverter removes leakage current with a basic configuration as only one inductor and two power switches are required [118]. Nevertheless, DC-link voltage should be twice the grid peak voltage, and the semiconductors must

endure high DC-link voltage stress. Furthermore, the cost and filter size of the bipolar inverter output voltage are higher. Three-level NPC inverters can reduce filter size, increase the corresponding switching frequency, and decrease semiconductor voltage stress. One of the drawbacks of these inverters is the unbalanced conduction losses among the internal and external power switches. To decrease conduction losses in low-voltage systems and maintain the main advantages of multilevel topologies, Conergy NPC inverters are used [137]. Bidirectional switches are located between the split capacitors and the midpoint of HB inverters to attain comparable clamping function and three-level output voltage in NPC inverters. Switch voltage stress is different in this topology. The two series switches in the lower and upper parts of the inverters must withstand high DC-link voltage, and active clamping switches bear only half of the high DC-link voltage. In [163], a comprehensive analysis and efficiency comparison of Conergy inverters, three-level NPC inverters, and two-level HB inverters were presented for low-voltage applications. A conclusion has been drawn that Conergy inverters and three-level NPC inverters have higher conversion efficiency comparing to two-level half-bridge inverters. In H5 topology, S_{w1} and S_{w3} are both conducting to generate zero-voltage output, whereas lower switches S_{w2} and S_{w4} and the S_{w5} blocking switch are turned off. Consequently, during zero-voltage level operation, PV panels are disconnected from the AC grid. In addition, the voltage step is only half of the DC-link voltage, and thus, the size of the filter inductor and the switching losses are reduced. However, the switching frequency of S_{w5} is twice those of other switches, which causes conduction losses and unbalanced switching. Power density is affected, which also affects the heat-sink design. In the H6 transformerless inverter, zero-voltage level realization has two probable decoupling operation modes. The first mode places S_{w1} and S_{w3} in the turn-on state. The second mode generates turn-on gate signals for S_{w2} and S_{w4}. Modulation flexibility is enhanced by the redundant switching patterns. The loss distribution for the high-frequency switches is balanced via the uni-polar SPWM. Moreover, the double frequency uni-polar SPWM is used to further decrease filter inductor size and enhance the quality of the grid current. When energy is transferred from the PV panels to the grid, four switches are in conduction

mode. The alternate operation of two blocking switches balances loss distribution for the high-frequency switches. The conduction losses of the H5 circuit are slightly more than that of the improved H6 inverter because only two switches are in conduction mode during the entire negative half cycle. Innovative HERIC-based topologies have been introduced to solve the patent problem of the HERIC inverter [125, 164, 165]. Nevertheless, these circuits are different, and rules to develop these types of transformerless inverters remain unclear. Therefore, the generation methodology and the topology derivation law are expressed in detail as follows. For HERIC topology, during the positive half cycle of the power delivery stage, S_{w2} and S_{w3} are turned off, whereas S_{w1} and S_{w4} are turned on. When S_{w6} is turned on, the operation state is similar because no current streams through it. Splitting the connection point of S_{w3} and S_{w4} (right bridge switches) is possible, and the S_{w3} emitter is connected to the S_{w6} collector. Similarly, S_{w1} and S_{w2} (left bridge switches) are disconnected, and S_{w1} and S_{w5} are in series configuration in the negative half cycle. Leakage current is suppressed via hybrid modulation, and the three-level output voltage aids in optimizing power quality and the inductor [164]. In multilevel topologies, due to the number of modules set in series, the number of output voltage levels can be increased, thus they are able to boost the AC voltage without applying a transformer or a boost converter to inject AC current into the grid. Furthermore, due to the cost of the extra power switches as needed, these devices have been mostly applied in high power applications [127]. Table 2.9 shows the comparison among different topologies described in the literature.

Table 2.9: Comparison of topologies.

Topologies	References	Leakage current	Input Voltage	Efficiency (%)	Switches	Advantage	Disadvantage
Half HB	[118]	Moderate	700 V	+	2 transistor	Low cost	High DC-link voltage stress
Conergy NPC	[119]	Very Low	800 V	++	3 transistor+ 4 diode	Low conduction losses	High device stress
Full HB	[122]	Moderate	400 V	+	4 transistor	-	High leakage current
NPC (mH)	[130]	Very Low	400 V	++	4 transistor+ 2 diode	Very low leakage current	High device stress
Dual-Buck (uF)	[123]	Low	400 V	++++	4 transistor+ 2 diode	High efficiency	Additional devices required
Three-Level NPC	[118]	Very Low	800 V	+++	4 transistor+ 2 diode	Very low leakage current	Increased complexity
H5	[141]	Low	400 V	+++	5 transistor	Low component count	Unbalanced switching
Single-Buck	[161]	Moderate	400 V	++	5 transistor+ 1 diode	Only one filter inductor	High leakage current
Virtual DC Bus	[147]	Low	400 V	++	5 transistor	Only one filter inductor	Current stress on switch 5
HB-ZVR	[145]	Low	400 V	+	5 transistor+ 5 diode	-	Low efficiency and increased complexity
HERIC	[146]	Low	400 V	+++	6 transistor+ 2 diode	Line frequency leakage current	Additional devices required
H6	[152]	Low	400 V	++	6 transistor+ 2 diode	Line frequency leakage current	Additional devices required
HRE	[154]	Low	400 V	++++	6 transistor+ 6 diode	Very high efficiency	Increased complexity
oH5	[157]	Very Low	400 V	+++	6 transistor	Very low leakage current	Additional devices required
Cascaded	[109]	Moderate	400 V	-	8 transistor	Low commutation stress and lower THD	Complex control and many switching devices

Table 2.9 shows the efficiency, leakage current, input voltage, switching voltage, number of required diodes and transistors, as well as the advantages and disadvantages of several previously validated methods. Nevertheless, determining which method is better than the others is difficult because each method has its own strengths and weaknesses. The aforementioned methods can be compared by highlighting several key features. Apparently, with regard to a high conduction path with a high switch voltage, half HB, HB-ZVR, and full HB topologies demonstrate higher power losses. Therefore, the efficiency of these inverters can be extremely low. Dual-buck and HRE topologies are the best in terms of efficiency. With regard to leakage current, all NPC, FC, and oH5 topologies perform very well. However, FC, Conergy NPC, and three-level NPC require double DC bus voltage. In multilevel inverters, the large number of switches may affect the reliability and the cost. Moreover, depending on the number of connected modules, the leakage current may also rise higher.

2.6 Review of grid connected PV inverter architectures

The type of inverters to be used depends on the installation and connection parameters of the photovoltaic modules: connection in series or in parallel, different degrees of inclination between the modules, output voltage and solar irradiance. As a result of these technical features of photovoltaic systems, the arrays configuration and the architecture of PV systems connected to the grid can have important impacts on its operation [166]. Lot of research is carried out on PV system configurations, such as Pendem et al. [167], Belhachet et al. [168], Horoufiany et al. [169]. These researches involve the study and analysis of various photovoltaic panels settings under various partial shading scenarios, to assess the performance and ability of each setting to increase output power and reduce partial shading losses.

The PV system architecture depicts how the power converters are associated with PV modules. The circuit topology of the power inverters can be changed to additionally enhance the yield energy from grid connected PV system under partial shading conditions [170]. it allows the inverter to regularly reap more energy than a string-level or arrays level inverter [171].

Given the large body of work published on inverter topologies and MPPT techniques for shaded PV arrays, such us: Dhople et al. [172], Roman et al. [173], which proposed a micro-inverter architecture to implement MPPT for strings of solar cells associated through bypass diodes in a PV module. In Wu et al. [174], another group of high-effectiveness DC/AC PV inverter with a variety of input DC voltage is proposed. A new scheme for a distributed synchronous boost converter (DMPPT) is proposed by Adinolfi et al. [175]. A system utilizing an additional full bridge inverter to perform MPPT operation is provided by Debnath et al.[176].

Different PV system architectures employing Power Conditioning Units (PCUs) with different technologies are developed by Spertino et al. [177]. Islam et al. [178] proposed an improved H5 topology for grid connected photovoltaic inverter with reduced leakage current. Common mode (CM) characteristics are studied in details. The drawback of this system is the cost of the small scale inverter. Control and circuit techniques to mitigate partial shading effects in photovoltaic arrays is presented by

Bidram et al. [179], a brief discussion of their characteristics and the approaches suggested in each category is provided.

The use of multilevel inverter is increased due to utilization of micro grid, smart grid and distributed generations to meet the huge energy demand. Various topologies of multilevel inverters (MLIs) have been published to fulfil the criteria of power requirement in an efficient and effective manner in terms of quality of power and voltage, reduced switch count, higher voltage levels with lesser number of sources, less switch stress, modular nature, less gate drive count, less use of capacitors, same and different voltage source configurations etc. Any single inverter structure is not capable to fulfil all these criteria. Each developed topology has its distinct merits and demerits.

First multilevel inverter is introduced by H. Akagi in 1981 [180]. Three standard topologies i.e. Cascaded H-Bridge (CHB), Diode-clamped multilevel inverter and Flying Capacitor (FC) have established the foundation for the multilevel inverters to expand its applications. The research is increased towards the development of various application oriented topologies such as photovoltaic (PV), fuel cell, flexible alternating current transmission system (FACTS), high-voltage direct current (HVDC), electric vehicle, hybrid vehicles, drives, uninterruptible power supply (UPS) etc. The various manufacturing companies, like ABB, Simens, General Electric, Toshiba etc. produce the power converters by using different multilevel inverter topologies for different applications. A review paper [181] on multilevel inverter topologies with reduced device counts is reported to give a better understanding about the proper selection of topology and its control strategy for particular application and requirement. A 5 level active neutral point clamped inverter with optimal modulation technique is presented in [182] with less number of active switches. A uni-polarity based cascaded multilevel inverter with reduced power switches is presented in [183] to reduce the installation space and cost. The use of series and parallel connections of DC sources for electric vehicle application is focused in [184]. An asymmetrical compact module multilevel inverter is proposed in [185] with cascaded structure to resolve the issue of current during dead time. Based on the availability of source configurations, the topology is

developed in [186] to work in symmetrical as well as asymmetrical modes.

When the renewable energy like PV is used as a source, more importance is given to the topology with asymmetrical source configuration due to the continuously variation in magnitude of source voltages. A topology reported in [187] is used for stand-alone PV applications with the range of few kilowatts. The review is carried out in [188] about the maximum power point tracking (MPPT) techniques for PV system to give an idea about appropriate use of control technique in grid-tied and stand-alone systems. The multilevel dc-link inverter is introduced in [189] with control algorithm to avoid the partial shading in PV system. A switch-ladder multilevel inverter with 47 voltage levels is presented in [190] with reduced switching losses and higher efficiency.

To improve the power quality in PV system, modular structure based multilevel inverter is developed in [191]. Three phase structure based multilevel inverter is reported in [192] for PV system with various dynamic conditions including partial shading and panel failure. A review on different multilevel inverter topologies and their modulation techniques are provided in [193] for grid connected PV systems. The researchers have focused on maximum number of levels with the asymmetric sources while developing the inverter in [194]. A modified MPPT control technique applied to multilevel DC link PV system in [195] is claiming more power and lower total harmonic distortion (THD). Capacitor also plays a vital role in the design process of inverter for high energy conversion. Its use is shown in packed U cells multilevel inverter [196]. In [197], the different source patterns are applied to capacitor based cascaded multilevel inverter to increase the voltage levels with minimum switch count. A simplified transformer based multilevel inverter topology with reduced component count is proposed in [198] for renewable energy applications. The exhaustive and benchmark work is presented in [199] with the analysis of total harmonic distortion (THD) to improve the power quality. The modified switched diode topology is proposed in [200] to improve the THD with less component counts. By combining the T-type and cross connected modules, a modified inverter in [201] has the capability to work at higher output voltage without increasing the total standing voltage and

peak inverse voltage of switches. A step-up switched-capacitor module for cascaded multilevel inverter proposed in [202] is claiming the self-balancing of capacitor voltages. A grid connected symmetrical cascaded multilevel inverter presented in [203] shows the improvement in power quality. To increase the conversion efficiency and power density, a bridge modular switched capacitor based multilevel inverter developed in [204] has more reliability and less complexity. A cascaded modified quasi-Z-source inverter with a single phase symmetrical hybrid three level inverter in [205] has higher boost ability at the load side with reduced source inductance. A transformerless single phase T- type inverter of [206] for the PV system generates 5 level voltages with asymmetric sources. A dual- asymmetrical DC port multilevel inverter is developed in [207] with minimum conversion stage and improved efficiency. The cascaded semi-half bridge cells based crisscross switched multilevel inverter is proposed in [208] with the advantages of less switch count, better modularity structure and reduced voltage stress across the switches. By using the turns ratio of transformer, the output voltage level of cascaded H-bridge multilevel inverter is increased [209]. A combination of selective harmonic elimination (SHE) technique and total harmonic distortion (THD) minimization technique is applied to a single phase multilevel inverter [210] to eliminate the lower order harmonics and minimize the voltage and current THDs. In [211], the performance analysis of a new asymmetric multilevel inverter with less switch counts is presented for a single phase grid tied PV system. A nine level multilevel inverter with one source and reduced components is proposed in [212] for high frequency AC power system distribution system with lower THD. A modified multilevel inverter based on packed U-Cell [213] for higher voltage applications is presented with the advantages of lower component counts, lower rating and blocking voltage of switches and improved performance. A multilevel inverter with variable DC link is proposed in [214] for low voltage applications. A hybrid cascaded multilevel inverter with improved symmetrical 4-level sub-module is proposed in [215] with less switch count and source count. In [216], a proposed quasi cascaded H-bridge boost inverter with less passive components results in reduction of size, cost and weight.

2.7 Conclusion

In this chapter, the principle of photovoltaic system has been described. The behaviour of the PV system under different environmental conditions is discussed. In addition, various converters that have been used for MPPT are described and analysed. Furthermore, a strategic review of MPPT techniques for PV systems under partial shading conditions is presented. Special attention is given towards the meta-heuristic based techniques due to their promising features. Among these algorithms, Bat, PSO and DE algorithms are envisaged to be very effective in dealing with MPPT problem particularly during partial shading occurrence. A comprehensive review of single-phase grid connected PV systems that adopt several transformerless schemes. The omission of transformers has led to the creation of a resonant circuit and electrification via fluctuating CM voltage that depends on topology structure and modulation scheme. Various transformerless schemes have been investigated and compared in terms of efficiency and leakage current. A classification of the transformerless schemes has been made based on the number of switches required, such as two-switch, three switch, four-switch, five-switch and six-switch and multilevel inverters. Subsequently, a discussion has been presented, and the benefits, drawbacks, and operation principle of the existing transformerless schemes have been deliberated. Moreover, a comparison table has been provided for direct comparison among different schemes. In addition, a new transformerless inverter has been proposed in this thesis. In regard to the several topologies presented in this thesis, the most important key concern is the necessity of diminishing the leakage current in the transformerless inverters. Consequently, cost-efficiency can be achieved by reducing the DC-link voltage, the number of PV panels, the switching losses. Finally, it is essential to use the system with minimum number of power switches, which reduces the power losses and cost of system by increasing the efficiency.

CHAPTER 3

PROPOSED CONTROL TECHNIQUES FOR PV SYSTEM SUBJECTED TO PARTIAL SHADING CONDITIONS: PSO-MPPT, SVPWM, FLC

Contents

3.1 Introduction

SMALL-scale PV systems (0-10 kW) are the type of renewable energy units that are mostly connected to the networks. Commercially attractive rebates and concession schemes that were introduced by the world governments for installing small scale PV systems along with price reductions in PV panels and power electronic converter systems, are the main reasons for the increased number of grid-connected small scale PV systems in LV power grids. The majority of small scale PV systems are domestic roof-top type installations and are generally single-phase systems.

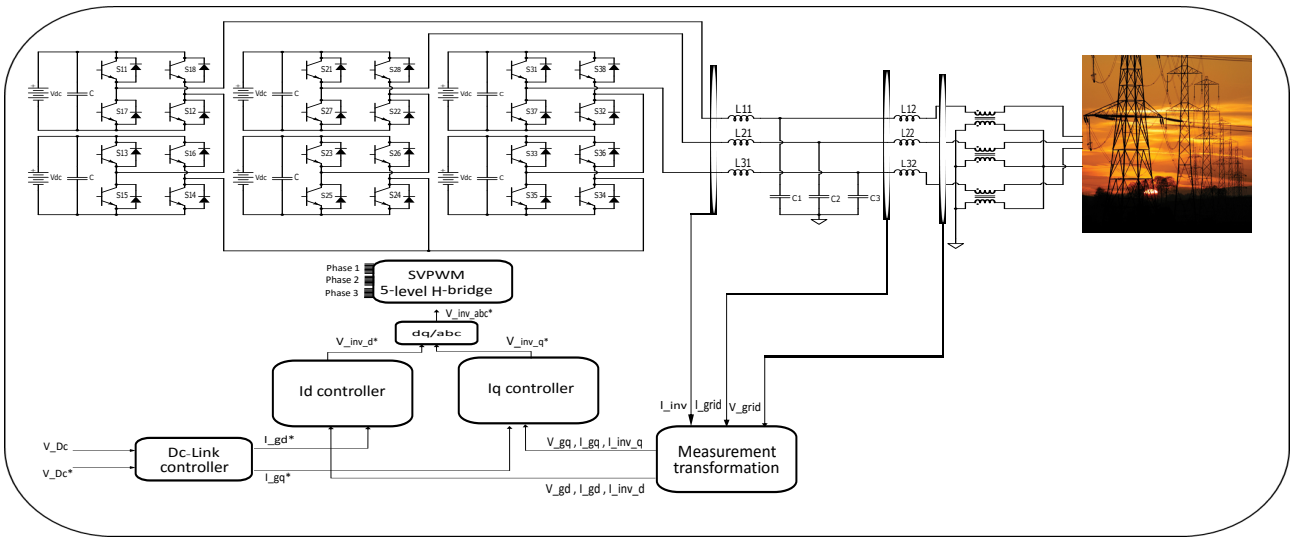

Figure 3.1: Basic structure of a grid-connected photovoltaic system.

The basic structure of a grid-connected PV system is shown in Fig. 3.1. This is a generic representation of a domestic roof-top PV system. The PV system consists of a DC-DC converter, a VSC and an LCL filter. The PCC is where the PV system is connected to the grid. In the grid-connected PV system shown in Fig. 3.1, the DC-DC converter steps up or steps down the output voltage of the PV array to a suitable level at the output of the DC-DC converter. An MPPT algorithm determines the MPP of the PV array at a given time and the DC-DC converter is controlled in such a way that the PV array is operated at the MPP. The output of the MPPT algorithm is an input to the controller of the DC-DC converter. The PV system shown in Fig. 3.1 is integrated to the grid via a VSC. A VSC with an ability to control output voltage

magnitude and phase angle with reference to the voltage at the PCC, provides a significant flexibility in controlling the active and reactive power injected to the grid. Therefore, VSCs are becoming more attractive in PV grid integration especially with the additional capability of providing reactive power support, voltage regulation and managing battery storage. The output power from a PV array is a function of solar irradiance and ambient temperature. Since solar irradiance and ambient temperature vary, the power output of a PV array is not constant. If the grid-connected PV system shown in Fig. 3.1 is controlled to inject a constant amount of power to the grid at times when power level varies at the PV array, the DC-link capacitor, C_{DC} may be charged or discharged affecting the DC-link voltage, V_{DC}. However, maintaining a constant DC-link voltage is necessary in order to minimize the appearance of low-order harmonics at the output of the VSC as a result of PWM switching of the power electronic switches of the VSC. Therefore, in a grid-connected PV system a controller is used to control the DC-link voltage at a suitable level by controlling the active power flow of the PV system.

Section 3.1. of this chapter begins by brief overview of meta-heuristics algorithms. Then, the key feature of the PSO algorithm is described. Furthermore, the formulation of MPPT as an optimization problem is presented and the application of the proposed technique for MPPT is discussed.

Section 3.2. present the SVPWM technique in general. Then presents the control of three-phase multilevel cascaded H-bridge inverter for photovoltaic (PV) grid utility system with an LCL filter using Space Vector Pulse Width Modulation (SVPWM) scheme. This technique (SVPWM) is an attractive control candidate for any multilevel inverter, since it can create a greater output power by reducing Total Harmonic Distortion (THD) and commutation losses.

In order to filter the harmonics produced by the inverter we use an LCL filter, which is a powerful solution for the interconnection between the inverter and the grid. The control of a grid-connected inverter with LCL filter is studied through conventional direct-current dq vector control strategy and presented in Section 3.3.

3.2 Particle swarm optimisation (PSO)

3.2.1 General overview on metaheuristic algorithms

Optimization is paramount in many applications, such as engineering, business activities, and industrial designs. Obviously, the aim of optimization is the searching for the optimal solution like minimizing the energy consumption and costs, to maximizing the profit, performance, and efficiency [217].

Many real-life optimization problems are difficult to solve by exact or deterministic optimization methods, due to properties, such as high dimensionality, multimodality and non-differentiability [218]. Hence, approximate or stochastic algorithms are an alternative approach for these problems. Stochastic algorithms can be decomposed into heuristics and metaheuristics. Heuristic refers to experience-based techniques for problem-solving and learning. These algorithms produce, by trial and error, acceptable solutions to a complex problem in a reasonable amount of computational time. Heuristics are problem-dependent and designed only for the solution of a particular problem. Further development of heuristic algorithms is the so-called metaheuristic algorithms. Here meta means "beyond" or "higher level", and these algorithms generally perform better than simple heuristics by using certain tradeoffs of randomization and local search. Metaheuristics can be trajectory-based or population-based. Trajectory based metaheuristics are based on a single solution at any time whereas in population-based metaheuristics, a number of solutions are updated iteratively until the termination condition is satisfied.

Two major components of any metaheuristic algorithms are intensification and diversification, or exploitation and exploration. Diversification means to generate diverse solutions so as to explore the search space on a global scale. Intensification means to focus on the search in a local region by exploiting the information that a current good solution is found in this region. This is in combination with the selection of the best solutions. The selection of the best ensures that the solutions will converge to the optimality, whereas the diversification via randomization avoids the solutions being trapped at local optima and, at the same time, increases the diversity of the

solutions. The good combination of these two major components will usually ensure that the global optimality is achievable with high accuracy [218].

Metaheuristics may be nature-inspired paradigms, stochastic, or probabilistic algorithms. Nature-inspired optimization algorithms have sparked great interest in recent years. Among them, bio-inspired especially those Swarm intelligence (SI)-based algorithms, have become very popular. In fact, these nature-inspired metaheuristic algorithms are now among the most widely used algorithms for optimization and computational intelligence [219].

Since the problem of MPP tracking in PV system can be modelled as a dynamic, multi-modal optimisation problem, bio-inspired metaheuristics are envisaged to be very effective to deal with *P-V* characteristic curve under partial shading conditions. Among them, BA, PSO and DE algorithms are very effective due to their superior efficiency with minimal control parameters, robust performance and simple structures. Then, one of these metaheuristic algorithms is proposed in this thesis to develop MPP tracker for PV system subjected to in-homogeneous irradiance.

The rest of this section discusses the key features of the PSO algorithm and describes the application of the proposed techniques for MPPT.

3.2.2 PSO algorithm

Particle swarm optimization is a population based meta-heuristic invented by Russel Eberhart (electrical engineer) and James Kennedy (socio-psychologist) in 1995 [220, 221]. This algorithm uses a population of candidate solutions to develop an optimal solution to the problem under consideration. It was originally inspired in general by the artificial life and specifically by the social behaviour of swarming animals, such as fish schooling and bird flocking. Indeed, we can observe in these animals relatively complex dynamics of displacement, whereas individually each individual has a limited "intelligence", and has only a local knowledge of its situation in the swarm. The local information and the memory of each individual are used to decide on his movement.

The swarm of particles corresponds to a population of agents, called particles.

Each particle is considered as a solution of the problem and it is assigned a position (the solution vector) and a velocity. Moreover, each particle has a memory which enables it to remember its best performance (in position and value) and the best performance achieved by the neighbouring particles: each particle has a group of informants, historically called its neighbourhood. A swarm of particles, which are potential solutions to the problem of optimization, "flies" over the search space in search of the global optimum. The velocity of a particle is then influenced by the three components: a component of inertia, a cognitive component and a social component. The first one describes the trend of the particle to follow its current direction of displacement. The second one represents the trend of the particle to move towards the best position by which it has already passed. The social component characterize the trend of the particle to rely on the experience of its congeners and, thus, to move towards the best site already reached by the swarm. The strategy for moving a particle is illustrated in Fig. 3.2.

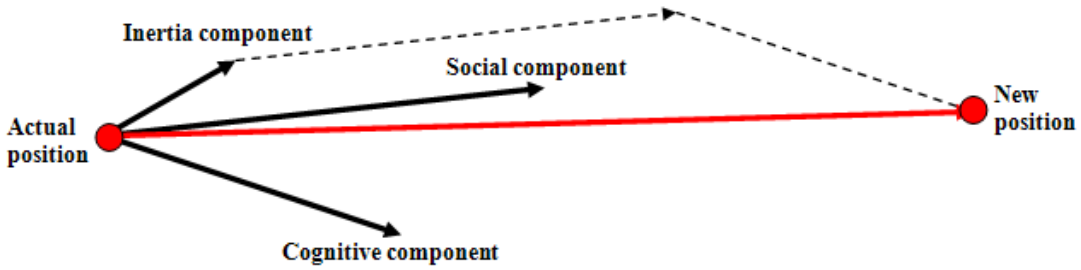

Figure 3.2: Movement of a particle.

Formalisation

In a research space of dimension D, we define a swarm of particles of size N (size of the population). The particle i of the swarm is modeled by its positron vector $x_i = (x_{i1}, x_{i2}, ..., x_{iD})$ and by its velocity $v_i = (v_{i1}, v_{i2}, ..., v_{iD})$. The quality of its position is determined by the value of the objective function of that point. This particle keeps in memory the best position by which it has already passed, that we note $Pbest_i = (Pbest_{i1}, Pbest_{i2}, ..., Pbest_{iD})$. The best position reached by the swarm is noted $Gbest =$

$(Gbest_1, Gbest_2, ..., Gbest_D)$ In our case, we are only interested in the fully connected swarm, that is, all the particles share the information; each particle knows the best position already visited by any particles in the swarm. This version of the algorithm is called, global version of PSO (Gbest), where all the particles of the swarm are considered as close to the particle i.

At the beginning of the algorithm, the particles of the swarm are initialized randomly or uniformly in the search space of the problem. Then, at each iteration, each particle moves, linearly combining the three components mentioned above. Indeed, at the iteration $t+1$, the velocity vector and the position vector are calculated from Eq. (3.1) and Eq. (3.2), respectively.

$$\begin{aligned} v_{ij}^{t+1} =& w\, v_{ij}^{t} + c_1\, r_{1_{ij}}^{t} \left(Pbest_{ij}^{t} - x_{ij}^{t} \right) \\ &+ c_2\, r_{2_{ij}}^{t} \left(Gbest_{j}^{t} - x_{ij}^{t} \right), \quad j \in \{1, 2, ..., D\} \end{aligned} \tag{3.1}$$

$$x_{ij}^{t+1} = x_{ij}^{t} + v_{ij}^{t+1}, \quad j \in \{1, 2, ..., D\} \tag{3.2}$$

with w is a constant, called the coefficient of inertia; c_1 and c_2 are two constants, called acceleration coefficients; r_1 and r_2 are two random numbers drawn uniformly in $[0, 1]$, at each iteration t and for each dimension j.

Stochastic factors allow the particles to move in the problem space randomly. This property allows for extensive exploration of the search space and increases the probability of finding the best solution with high efficiency. The three components mentioned above (i.e. of inertia, cognitive and social) are represented in Eq. (3.1) by the following terms:

wv_{ij}^{t} corresponds to the inertia component of the displacement, where the parameter w controls the influence of the direction on the future displacement;

$c_1 r_{1_{ij}}^{t} (Pbest_{ij}^{t} - x_{ij}^{t})$ corresponds to the cognitive component of displacement, where parameter c1 controls the cognitive behaviour of the particle;

$c_2 r_{2_{ij}}^{t} (Gbest_{j}^{t} - x_{ij}^{t})$ corresponds to the social component of displacement, where parameter c_2 controls the social aptitude of the particle.

PSO control parameters

The inertia weight w was firstly introduced by Yuhui Shi and Russell Eberhart [222]. This parameter plays the role of balancing the global search and local search during the search process. It can be a positive constant or even a positive linear or nonlinear function of time (or iterations). The confidence constants, c_1 and c_2, also called acceleration coefficients, represent the weighting of the stochastic acceleration limits that pull each particle towards the best global and local position. Thus, adjusting these constants changes the pressure between parameters in the system. These two parameters can be positive constants, or linearly or nonlinearly varying with time (iterations).

Convergence criteria

The stopping criterion indicates that the solution is sufficiently close to the optimum. Selecting a good termination criterion has an important role to ensure a correct convergence of the algorithm. Several criteria for halting the process of optimisation are possible. The algorithm can be stopped when the objective of optimisation is met. Indeed, in some optimization tasks, the objective function's minimum value is already known. For example, error functions for which the tolerable error is given or test functions whose minima are known. If the best vector's objective function value is within a specified tolerance of the global minimum, the optimization halts. In addition, the algorithm can be stopped after a sufficient number of iterations for the search space to be properly explored. This criterion can prove to be expensive in computing time if the number of particles to be treated in each population is important. The algorithm can also be stopped when the population is not moving fast enough.

Neighbourhood topology

The PSO algorithm is inspired by the collective behaviour of swarms. This algorithm highlights the ability of an agent to stay at an optimal distance from others in the same group and to follow a global movement affected by the local movements of its neighbours. Thus, the authors modelled the behaviour of particles by equations (3.1)

and (3.2). In practice, using Eq. (3.1), an interconnexion network must be defined in order to establish connections between the particles and allow them to exchange information with each other. This communication network between the particles is called neighbourhood topology. This topology helps to define a group of informants for each particle; this is called the neighbourhood of a particle. The neighbourhood of a particle can therefore be defined as the subset of particles of the swarm with which it has a direct communication, ie each particle can interrogate the particles in its neighbourhood (its informants), which, in turn, send it their informations. The choice of a topology (the communication network between the particles) therefore has a significant influence on the performance of PSO algorithm.

3.2.3 Application of PSO for MPPT

The PSO method is applied to realize the MPPT algorithm for PV system operating under partial shading conditions, wherein the P-V curve exhibits multiple MPPs. Flowchart of the proposed PSO based MPPT technique is shown in Fig. 3.3. The operating principles of proposed technique can be described as follows:

Step 1: PSO initialisation

In order to start the optimization, the duty cycle of the PWM signal is chosen to be the optimization variable. Thus, it is adjusted directly by the MPPT controller. Initially, a solution vector of duty cycles with N_p particles is defined. Number particles in the population should be chosen carefully. A larger number of particles results in more accurate MPP tracking even under complicated shading patterns but tracking speed reduces. As the number of particles increases, computation time also increases. Therefore, population size should be chosen in such a way that it ensure good tracking speed and accuracy. To find a tradeoff, three particles are considered in this research.

$$d = (d_i) = (d_1,\ d_2,\ d_3) \tag{3.3}$$

PSO particles are usually randomly initialized in the search space. For the proposed MPPT algorithm, the particles are initialized at fixed points, using the method

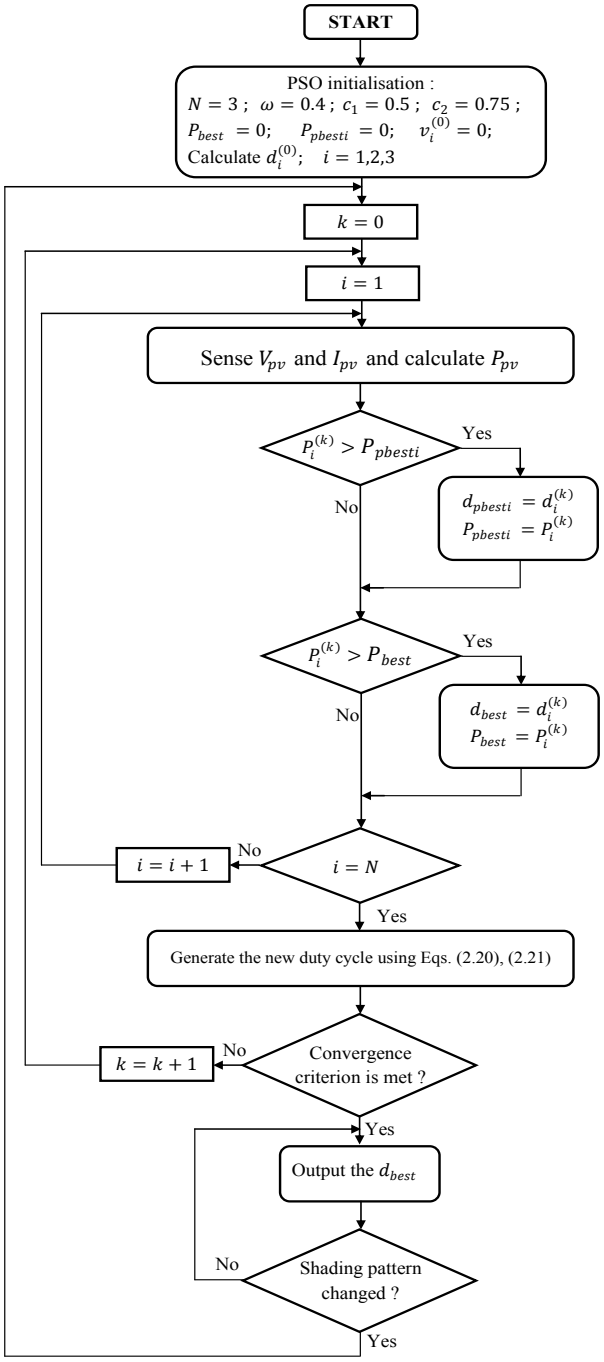

Figure 3.3: Complete flowchart of the proposed PSO method.

of the reflective impedance [223]. Then, the first vector of N duty cycles (first vector of solutions) is generated from a uniform distribution on $[0, 1]$ or it is predefined. The number of particles (N) is an important factor in the optimization process. A large number N guarantees the determination of GMPP but the convergence time can be

long while a small number N will save in convergence time but it can result in low GMPP tracking accuracy if the parameters of the MPPT algorithm are not well optimized. To ensure a compromise "convergence speed-efficiency", the number of duty cycle, N is chosen to be three (3). The first three duty cycles are calculated thus:

$$d_1 = \frac{\sqrt{\eta Z_{min}}}{\sqrt{R_{PV\_max}} + \sqrt{\eta Z_{min}}} \tag{3.4}$$

$$d_2 = \frac{\sqrt{\eta Z_{ave}}}{\sqrt{R_{PV\_STC}} + \sqrt{\eta Z_{ave}}} \tag{3.5}$$

$$d_3 = \frac{\sqrt{\eta Z_{max}}}{\sqrt{R_{PV\_min}} + \sqrt{\eta Z_{max}}} \tag{3.6}$$

where η is the converter efficiency, Z_{min}, Z_{max} and $Z_{ave} = (Z_{min} + Z_{max})/2$ are the minimum, maximum and averege values of the connected load respectively. R_{PV_min} and R_{PV_max} are the minimum and maximum values of the reflective impedances of the PV array, respectively, while R_{PV_STC} is the reflective impedances of the PV panel at STC condition. In our simulations, the values of the parameters are : $\eta = 0.96$, $Z_{min} = 40\ \Omega$, $Z_{max} = 70\ \Omega$, $R_{PV\_min} = 6\ \Omega$, $R_{PV\_STC} = 22\ \Omega$ and $R_{PV\_max} = 43\ \Omega$.

It should be mentioned that the interval $[d_1, d_3]$ serves only for a first approximation of the search space. This approach leads to prevent having major disturbances and fluctuations in the voltage of the photovoltaic panel. The BA based MPPT can then search for the MPP outside of this range. The minimum duty cycle and maximum duty cycle are defined as 0.02 and 0.98, respectively.

The current and voltage of the photovoltaic array are sensed and the corresponding power is calculated for each duty cycle. The best duty cycle, d_{best} which gives the best value of fitness (PV power) is then stored. The purpose of the optimisation process is the maximisation of power extracted from the PV panel, which is defined to be the objective function (P). The fitness value evaluation function is defined as:

$$P(d_i^k) > P(d_{pbesti}) \tag{3.7}$$

where d_{pbesti} is the personal best position of particle i.

Step 2: Update individual and global best duty cycle

For each duty cycle d_i, the corresponding PV output power $P(d_i^k)$ is calculated by multiplying the measured voltage (V_{PVi}) and current (I_{PVi}). Then, the algorithm proceeds to check whether this duty cycle value will result in a better individual fitness value (compared to old P_{besti}). In such case, the personal best position (d_{pbesti}), as well as its corresponding best individual fitness value P_{pbesti}, are updated; otherwise, P_{pbesti} retains its present value. The global best duty cycle, d_{best}, is determined by comparing fitness values of the actual population with the global best PV power achieved, P_{best}.

Step 3: Update Velocity and Position of Each Particle

After the evaluation process, velocity and position of each particle in the swarm are updated. The new duty cycles are then calculated for the each iteration by the equations:

$$v_i^{k+1} = w\, v_i^{k-1} + c_1\, r_1 \left(d_{pbesti} - d_i^k\right) + c_2\, r_2 \left(d_{best} - d_i^k\right) \tag{3.8}$$

$$d_i^{k+1} = d_i^k + v_i^{k+1} \tag{3.9}$$

Convergence criterion

The algorithm continues to calculate the new duty cycles until constraint on convergence is satisfied. In this thesis, the condition shown in the Eq. (3.10) is used as a convergence criterion. If the absolute difference between each two different duty cycles is less than a threshold Δd, then the algorithm stops the optimization process and brings out d_{best}

$$\left|d_i^k - d_j^k\right| \leq \Delta d;\ i, j = 1, 2, 3;\ i \neq j \tag{3.10}$$

Step 5: Re-initialization

In a PV system, the optimum power point is not constant and global maximum available power usually changes due to varying weather and loading conditions. In such cases, the duty cycles must be reinitialized to search for the new GMPP. If re-initialization process is no carried out properly, updating of personal best duty cycles

and global best duty cycle cannot be performed automatically for the change in operating point. As a result, the MPPT algorithm may stuck at some operating point, rather than searching for the new GMPP. The MPPT algorithm should have the ability to detect the variation of shading pattern and to search for the new global MPP. In this thesis, the search process is initialised if the following condition is satisfied

$$\frac{|P_{PV\,new} - P_{PV\,last}|}{P_{PV\,last}} > \Delta P \tag{3.11}$$

where P_{PVnew} and P_{PVlast} are the values of photovoltaic panel power in two successive sample periods and ΔP is the power tolerance, constraint given in Eq. (3.11) is utilized in the proposed PSO based MPPT to detect the irradiance and shading pattern changes and to reinitialise the search process.

3.3 Space vector PWM control for the multilevel inverter

The major feature of PWM is the low loss of power in the exchanging gadgets. Practically, there is no current when a switch is OFF. At the point when it is ON and power is being exchanged to the load, there is no voltage drop over the switch. PWM also works well with digital controls, which, on account of their on/off nature, can without difficulty set the required duty cycle [224]. PWM is vastly utilized for VSI, since it can create output power with variable frequency and variable voltage. In this work SVPWM technique is utilized to generate PWM control signals for the inverter. This technique holds strong advantages allowing higher *Dc* bus efficiency, low power losses, voltage magnitude and variable frequency control. Other points of interest of SVPWM incorporate a vast linear modulation range, fewer computations and easy implementation. Advancements in microchips diminish the calculation time and making SVPWM to become the favored PWM technique [225]. In this thesis, we suggest a scheme for a multilevel inverter to operate in over-modulation mode and right into six-step.

3.3.1 SVPWM for five level cascade H-Bridge inverter

The objective of the SVPWM technique is to estimate the reference voltage vector (V_{ref}) instantaneously by relating the switching states corresponding to the principle space vectors [226]. More precisely, for every PWM period, the reference vector (V_{ref}) is averaged by using its two adjacent space vectors for a certain duration of time and a null vector for the rest of the period. The switching state, is defined as Su, Sv, Sw and can take a value $[-2, -1, 0, 1, 2]$. There are 125 switching states for a 5-level CHB, as appeared in Fig. 3.4. Normally, in each switching period four of them are used by the switching sequence, depending on the position of the reference vector. In this thesis, a switching sequence is followed using the common-mode voltage elimination [227]. Hence, for any triangle there could be numerous switching sequences. However, one and only sequence can be executed at switching time.

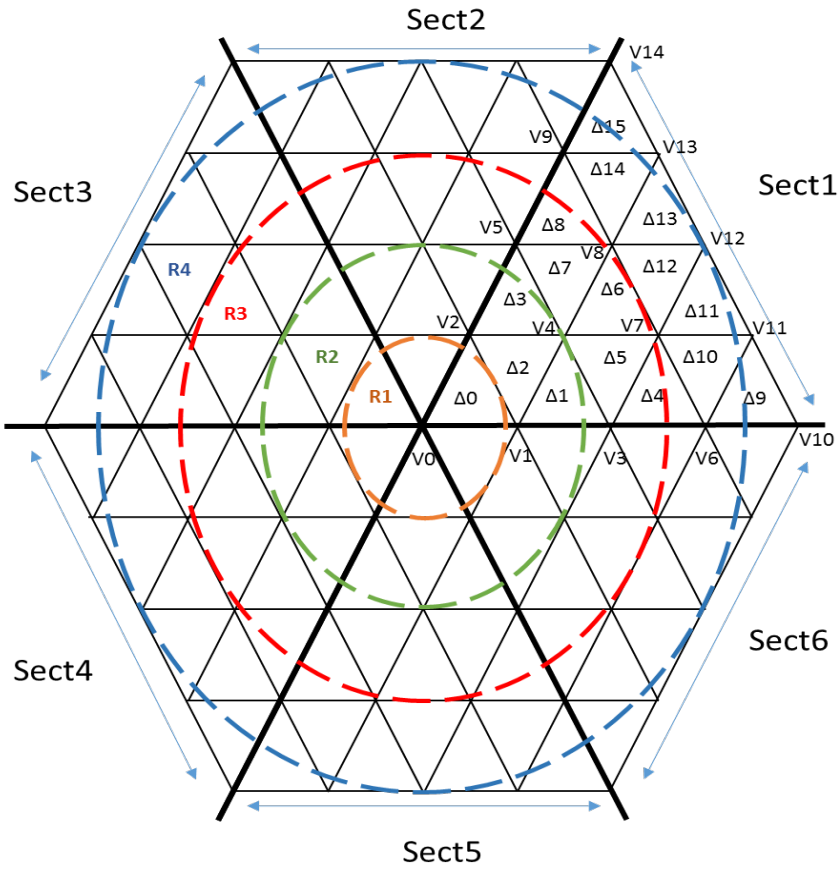

Figure 3.4: Space vector diagram for five-level inverter.

3.3.2 over-modulation mode in SVPWM

Recently, to increase the output voltage of an inverter and get a greater effective use of the DC-link voltage, an over-modulation system has been reported in the most recent literature. The modulated section of SVPWM was separated into two regions: linear region and nonlinear, allowing to the amplitude of the voltage vector. If the tip of the voltage vector path is situated in the linear region, at that time SVPWM plan is basic ; however, DC-link voltage cannot be enough used. In [228], the over-modulation section was partitioned into over-modulation types I and II. In type I, Just the amplitude of the reference vector was balanced, while in mode II, the amplitude and the angle of the reference vector were rectified. To achieve real-time and linear modulation in the nonlinear region, the two-mode over-modulation that uses restricted trajectories was introduced. In view of [228], the current work suggests a simplified SVPWM-based over-modulation methodology. The over-modulation technique is simple, suitable and exhibits only the basic function. The solutions of nonlinear equations or lookup tables are required. The proposed scheme is explained with the help of the five-level cascaded H-bridge inverter topology shown in Fig. 3.1. The scheme is then extended to an n-level inverter.

3.3.3 Modulation index and mode of modulation

An essential parameter related with SVPWM is modulation index *mi* [229], which is defined as:

$$mi = \frac{V}{V_{six-step}} \tag{3.12}$$

In Eq(3.12), V is the peak value of the fundamental voltage and ($V_{Six-Step}$) is the peak value of fundamental voltage at six-step operation.

For an NPC topology:

$$V_{Six-Step}=\frac{2}{\pi}V_{Dc} \tag{3.13}$$

where V_{Dc} is the Dc link voltage.It is same as the two-level inverter.

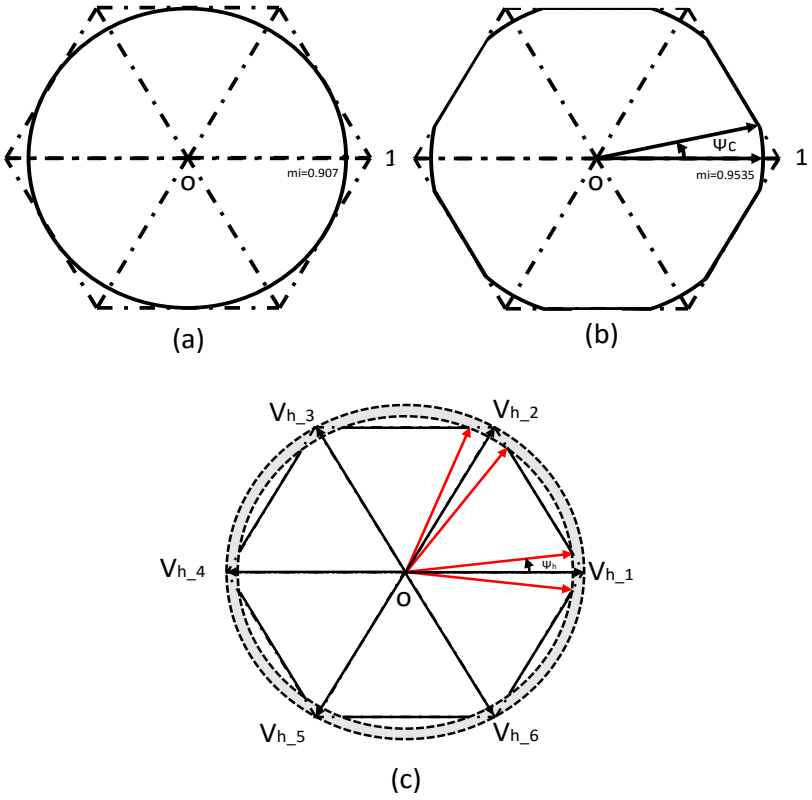

Figure 3.5: Modes of operation: (a)sinusoidal mode. (b)over-modulation mode I. (c)over-modulation mode II.

For an n-level cascaded topology:

$$V_{Six-Step}=\frac{2}{\pi}(n\text{-}1)V_{Dc} \tag{3.14}$$

The modulation region might be separated into three classifications, allowing to the magnitude of the modulation index as shown in Fig. 3.5, Firstly sinusoidal region $(0 < mi < 0.907)$, over-modulation region I$(0.907 < mi < 0.9535)$ and over-modulation II $(0.9535 < mi < 1)$. In the first classifications, the reference vector moves on a circular trajectory. In over-modulation I, the reference vector moves on a circular trajectory for some part of the sector and for the residual part, it moves on a side of the hexagon. In over-modulation region II, for the focal part of the sector, the reference vector moves on a linear trajectory while for the residual part it is held at one of the six vertices of the hexagon [229].

3.3.4 Switching times modification and over-modulation Area

The fundamental thought of SVM is to make up the requisite volt-seconds utilizing separate switching on-times created by inverter. Based on 2-level inverter, the on-time count depends on the region of the reference vector inside of the sector S_i , where "i" implies that it can take any whole number from : 1,6. Volt-second equation for the first sector is:

$$V_r T_s = V_1 T_a + V_2 T_b \tag{3.15}$$

The volt-seconds in terms of components V_α, V_β along (α, β) axis are:

$$\begin{cases} V_\alpha^r T_s = T_a + 0.5 T_b \\ V_\beta^r T_s = h T_b \\ T_s \quad = T_a + T_b + T_o \end{cases} \tag{3.16}$$

From the geometry of the sector, shown in Fig. 3.6, the on-times are calculated as:

$$\begin{cases} T_a &= T_s \left(V_\alpha^r - \dfrac{V_\beta^r}{\sqrt{3}} \right) \\ T_b &= T_s \left(\dfrac{V_\beta^r}{h} \right) \\ T_o &= T_s - T_a - T_b \end{cases} \tag{3.17}$$

In eqs (3.16)-(3.17), h is the height of a sector, which is a unity side equilateral triangle . In eqs (3.15)-(3.17), $T_s = 1/(2 * F_s)$ where F_s is the switching frequency.

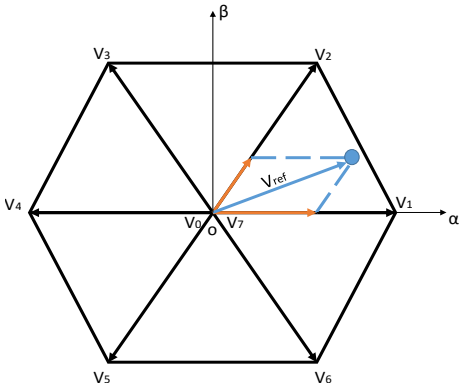

Figure 3.6: The space vector diagram for two-level inverter.

Can be divided each sector into $(n\text{-}1)^2$ triangles, where n specifies the level of the inverter. For any given reference vector, both the operation sector and the is calculated by using Eqs (3.18) and (3.19), correspondingly:

$$S_i = integer\left(\frac{\theta}{60}\right) + 1 \tag{3.18}$$

$$\gamma = reminder\left(\frac{\theta}{60}\right) \tag{3.19}$$

In eqs (3.18) and (3.19), $(0 < \theta < 360)$ is the angle of the reference vector with respect to α axis, γ is the angle within the sector and S_i is the sector operation. The space vector diagram of a three phase voltage source inverter is a hexagon, consisting of six sectors.

3.3.4.1 Sinusoidal mode$(0 < mi < 0.907)$

The inward vector limit is zero and the external reference limit is the engraved circle of the hexagon. Besides, in every sector, a triangle can be characterized into two forms according to his base side. The triangle number Δ_j can be dictated by using of two whole number factors $\jmath_1$ and $\jmath_2$, which are reliant on the position of reference vector (V_α, V_β).

$$\jmath_1 = int\left(V_\alpha + \frac{V_\beta}{\sqrt{3}}\right) \tag{3.20}$$

$$\jmath_2 = int\left(\frac{V_\beta}{h}\right) \tag{3.21}$$

Geometrically if $\jmath_1$=2, this means that the specific area is located inside $[V_3V_6V_9V_5]$ and if $\jmath_2 = 1$, this means that the specific area is located inside $[V_2V_{11}V_{12}V_5]$. The values of $\{\jmath_1 \wedge \jmath_2\}$ connote the crossing of these two regions. This crossing is a rhombus made of two triangles $[\Delta_6\Delta_7]$. Let $\left(v_\alpha^r, v_\beta^r\right)$ be the coordinates of the reference vector with respect to the origin of the rhombus.

$$v_\alpha^r = V_\alpha - \jmath_1 + 0.5\jmath_2 \tag{3.22}$$

$$v_\beta^r = V_\beta - h\jmath_2 \tag{3.23}$$

The slope $\left(v_\beta^r / v_\alpha^r\right)$ of the line between the origin of the rhombus and the reference vector can be determined by using eqs (3.22)-(3.23). This slope is compared with the slope of the diagonal of the rhombus which is $\sqrt{3}$. The slope comparison is done by evaluating the following inequality $\left(v_\beta^r \leq \sqrt{3}.v_\alpha^r\right)$.
If $\left(v_\beta^r \leq \sqrt{3}.v_\alpha^r\right)$, it indicates that the triangle is of type 1. The point P is within the triangle Δ_6 and the small vector v_r (v_α^r, v_β^r) is represented by $\overrightarrow{V_4P}$. These triangles are Analogous to the two-level inverter sector 1. Then, the triangle number Δ_j is given as:

$$\Delta_j = j_1^2 + 2.j_2 \tag{3.24}$$

If $\left(v_\beta^r \geq \sqrt{3}.v_\alpha^r\right)$, which indicates that the triangle is of type 2. The point P is within the triangle Δ_7 and the small vector v_r (v_α^r, v_β^r) is represented by $\overrightarrow{V_8P}$. These triangles are analogous to sector 2 of a two-level. Then, the triangle number Δ_j is given as:

$$\Delta_j = j_1^2 + 2.j_2 + 1 \tag{3.25}$$

3.3.4.2 over-modulation I $(0.907 < mi < 0.9535)$

The key purpose of the over-modulation strategy is to find a satisfactory modification technique to adapt the reference voltage vector. Given that the mode I over-modulation region is between the engraved circle and the hexagon, then two limit modulation indices exist. The inward one, the maximum linear modulation index happens at $m_i = 0.907$, and the external one, the maximum modulation index of over-modulation mode I happens at $m_i = 0.9535$. The thick circle in Fig. 3.5.b demonstrates the chosen reference vector path. This area is noticeable by a non-linearity. Generally, depending on the mi, the path is rectified and the actual vector tip moves on the path appeared in thick lines. First of all, it moves along the round track, then along the straight track on the side of the sector and lastly along the round track. Follows a method which modifies the switching vectors on-times on circular track to compensate for the loss in volt-seconds, instead of changing the reference vector [230]. Let Ψ_c be the angle, illustrated by the intersection of the the hexagon track and the reference vector, Fig. 3.5.b. For $(\Psi_c < \gamma < \pi/3 - \Psi_c)$, the vector proceeds onward the

hexagonal track and for the rest part of the sector on circular track. Utilizing cartesian geometry,Ψ_c is expressed as:

$$\Psi_c = \frac{\pi}{6} - \cos^{-1}\left(\frac{\pi}{2mi\sqrt{3}}\right) \tag{3.26}$$

Hexagonal Part: $(\Psi_c < \gamma < \pi/3 - \Psi_c)$ On the linear portion, in a switching period two switching states are executed. The coordinates of the vector Vr are given in function of the angle and level of the inverter as:

$$(V_\alpha, V_\beta) = \left(\frac{\sqrt{3}\,(n\text{-}1)}{\sqrt{3}+\tan\gamma}, \frac{\sqrt{3}\,(n\text{-}1)\tan\gamma}{\sqrt{3}+\tan\gamma}\right) \tag{3.27}$$

Knowing the coordinates of V_r , (3.27), we define two integers i_1, i_2 to find the triangle in which tip coordinates of actual vector lies. These two integers are given as:

$$\begin{cases} i_1 = n\text{-}2 \\ i_2 = int\left(\frac{V_\beta}{h}\right) \end{cases} \tag{3.28}$$

These triangles are of type 1. Using this point, the small vector can be directly acquired from (3.22)-(3.23). Knowing $\left(V_\alpha^r, V_\beta^r\right)$, assuming that the on-time T_o=0 for hexagonal track, equation (3.17) is used to determine the on-time T_a similar to the two-level inverter. Then T_b=T_s-T_a. Triangle number Δ_j is calculated using (3.25).

Circular Part $(0 < \gamma < \Psi_c)$ **or** $(\pi/3 - \Psi_c < \gamma < \pi/3)$ As depicted before, the on-times sinusoidal mode are gotten using(3.17). The on-times are adjusted to compensate for the loss of volt-seconds during the linear trajectory, which may ensure that the amplitude of rectified vector is equal to those of the reference vector and the voltage trajectory within the hexagon [231]. In this way, at a modulation index mi , the loss in volt-seconds over a sector is proportional to $(mi\text{-}0.907)$. The most extreme conceivable value of mi is 0.9535. Then, the maximum possible loss in volt-seconds over a sector is proportional to difference $(0.9535\text{-}0.907)$. The compensation factor φ is then:

$$\varphi = \frac{mi\text{-}0.907}{0.9535\text{-}0.907} = \frac{mi\text{-}0.907}{0.0465} \tag{3.29}$$

Based on triangle type (top-side, bottom-side), the on-time modifications are obtained as:

- if triangle are of type 1, the on-time modifications are given as:

$$\begin{cases} T_a = T_a + 0.5\varphi^2 T_o \\ T_b = T_b + 0.5\varphi^2 T_o \\ T_o = T_s - T_a - T_b \end{cases} \tag{3.30}$$

where T_a and T_b are the on-times of the two vertices that are on the hexagon side.

if triangle are of type 2, the on-time modifications are given as:

$$\begin{cases} T_a = T_a - 0.5\varphi^2 T_o \\ T_b = T_b - 0.5\varphi^2 T_o \\ T_o = T_s - T_a - T_b \end{cases} \tag{3.31}$$

where T_a and T_b are now the on-times of the two vertices that are not on the hexagon side. The on-time modifications in (3.26) adequately lessen the on-times of the internal vector utilized and increment the on-times of the external vectors. It is clarified in [230] that such plan is appropriate for fast closed loop operation.

3.3.4.3 over-modulation II $(0.9535 < mi < 1)$

Seeing that the over-modulation mode II area is outside the mode I section, the two limit conditions are the most extreme modulation index of modes II and I respectively. The switching in over-modulation II is marked by a hold angle Ψ_h, appeared by the thick red arrow in Fig. 3.5.c. For $(\Psi_h < \gamma < \pi/3\text{-}\Psi_h)$, the vector V_r proceeds onward the hexagonal track. In the over-modulation mode II, there are six substantial vectors for the total space vector chart. For $(0 < \gamma < \Psi_h)$ and $(\pi/3\text{-}\Psi_h < \gamma < \pi/3)$, the vector V_p is held on one of the substantial vectors. In this study, the hold angle Ψ_h is gotten utilizing a system like the method described by A.K.Gupta [231] where Ψ_h is calculated as:

$$\frac{\pi/3}{mi} = 2\Psi_h + \frac{(\pi/3\text{-}2\Psi_h)}{0.9535}. \tag{3.32}$$

For $(\Psi_h < \gamma < \pi/3\text{-}\Psi_h)$, the on-time estimation is the same as the mode I hexagonal trajectory. For $(0 < \gamma < \pi/3\text{-}\Psi_h)$ and $(\pi/3\text{-}\Psi_h < \gamma < \pi/3)$, the vector is held at one of the six substantial vectors. At $mi = 1$, hexagonal track disappears and vector is just held at one of the six substantial vectors consecutively. Like to the two-level inverter, this is a six-step operation. Subsequently, a multilevel inverter loses its multilevel characteristics when operated at $mi = 1$. For useful operation of a 5-level inverter, the greatest modulation factor (mi) ought to be restricted to slightly less than one (1-ε) in order to keep up the five-level output voltage waveform. Along these lines, no other calculation is necessary. It enormously streamlines the PWM procedure as switching states can be effortlessly mapped as for the triangle number. The triangle number is expressed to offer a simple way for the triangles organization, prompting to simplicity of the identification and extension to any level.

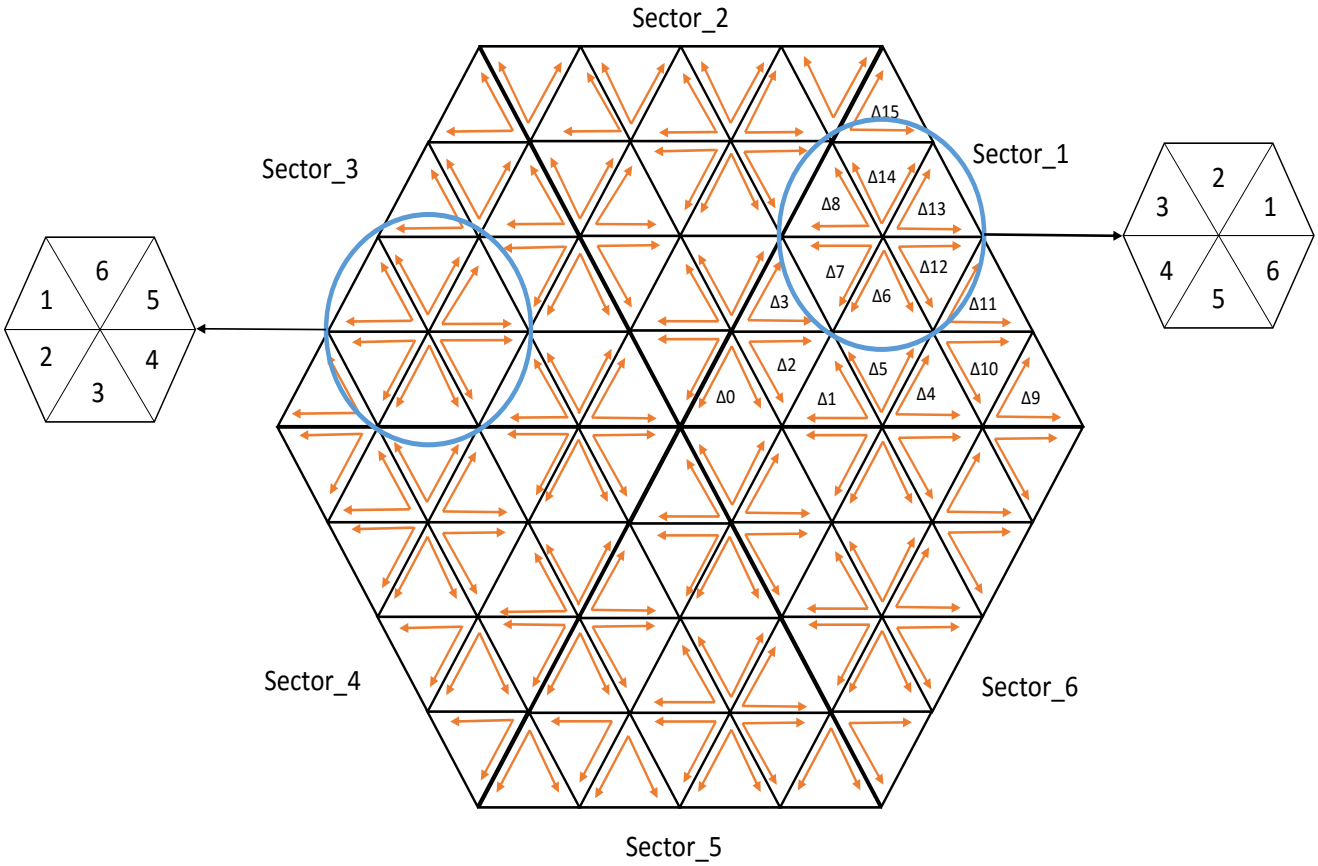

Figure 3.7: Switching Sequence diagram for 5-level space vector PWM.

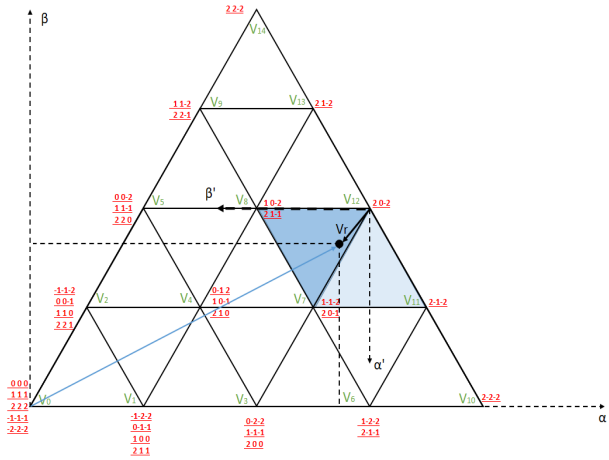

Figure 3.8: The space vector diagram of first sector of a five-level inverter.

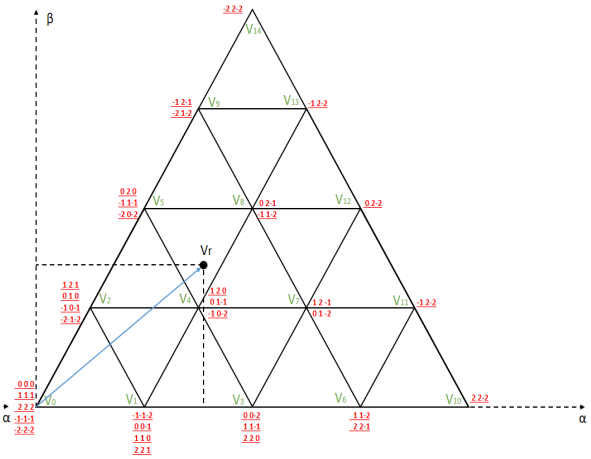

Figure 3.9: The space vector diagram of second sector of a five-level inverter.

3.3.5 Generating the switching sequence

Having determined the triangle Δ_j, the shift vector V_r is now calculated by following the switching sequences which vary from a triangle to another. For each triangle, we require an organization to order the on-times calculated t_a, t_b, t_o in desired sequence of $[t_0 \rightarrow t_a \rightarrow t_b \rightarrow t_0]$. An order is identified Figs. 3.8 and 3.9 for each triangle in Fig. 3.7. The triangle in odd sectors $[S_1, S_3, S_5]$ has the identical duty-ratios order. Also, the triangle in even sectors $[S_2, S_4, S_6]$ has the identical duty-ratios order. This structure has been applied for a five-level cascaded which can be extended to a several level. The structure can be utilized for both cascaded H-bridge inverter and NPC topologies and can be certainly stretched to include over-modulation range.

3.4 Feedback linearization control of a three-phase multilevel inverter through a LCL filter

The formal grid-tie multilevel inverter is controlled in a synchronous reference frame by a dual-loop control strategy. Firstly, based on the small signal model, the controllers are designed for a steady-state operating point by neglecting the coupling terms and high-order. Later on, in spite of their complications, these last ones are taken into account in an LCL approach filter [232]. Hypothetical examination, demon-

strating and a simulation of a grid-tie system are detailed. With a specific end goal to lessen the intricacy of the system, a linear current and voltage controllers have been established for a 3-phase grid-tie inverter. Instantaneously, the controllers regulate the current injected to the grid and the Dc link. The simulation results demonstrate that the control and dynamic performance of the inverter-grid arrangement offer high harmonic attenuation.

3.4.1 LCL filter design

The focal purpose of the LCL filter is to decrease high-order harmonics on the output side; however poor design might cause a distortion increase. Therefore, the filter must be designed appropriately and reasonably. The LCL filter transfer function, which affects the closed loop system bandwidth in the grid-connected mode, is

$$i_2 = \frac{v_i + v_g\left(1 + s^2 C_f L_i + s C_f R_i\right)}{C_f L_2^g L_i s^3 + s^2 C_f\left(L_2^g R_i + L_i R_2^g\right) + s\left(C_f R_2^g R_i + L_i + L_2^g\right) + R_2^g + R_i} \tag{3.33}$$

Based on Equation (3.33), the transfer function between the converter voltage V_i and the grid current i_2 is expressed by Equation (3.34) while neglecting the resistors effect. The LCL filter resonance frequency Allowing to this equation is given by

$$H = \frac{i_2}{v_i} = \frac{1}{C_f L_2^g L_i s^3 + s\left(L_i + L_2^g\right)} \tag{3.34}$$

$$w_{res}^2 = (2\pi f_{res})^2 = \frac{L_2^g + L_i}{L_2^g L_i C_f} \tag{3.35}$$

The LCL filter outline approach is expected to meet network code prerequisites through efficient lessening of high request current harmonic parts on the grid side. It requires the following input data : the active power P; the voltage of the grid U_g; the switching frequency of the converter f_{sw}; grid voltage frequency f_g; Then, the LCL filter constraints are adjusted allowing to the following steps.

Resonance frequency

The resonant frequency must have a distance from the grid frequency and must be minimally one half of the switching frequency, because the filter must have enough attenuation in the switching frequency of the converter. The resonant frequency for the L-C-L filter can be calculated as:

$$10f_g < \frac{f_{sw}}{6} < f_{res}\left(L_g, C_f\right) < \frac{f_{sw}}{2} \tag{3.36}$$

Maximum value of the total inductor

In order to makes the voltages drops in the filter and the losses unimportant , the total values of the LCL filter inductor should be as small as possible. To this reason, the max inductor value should be lower than 0.1 pu as appeared in Equation

$$L_T = L_i + L_2^g = 0.1\frac{U_g^2}{2\pi f_g P} \tag{3.37}$$

Then, the minimum inverter side inductor i_L can be calculated according to the equation (3.37) as below :

$$\Delta i_{max} = \frac{V_{dc}}{6L_i f_{sw}} \tag{3.38}$$

$$L_i = \frac{V_{dc}}{6f_{sw}\Delta i_{max}} \tag{3.39}$$

Maximum LCL filter capacitor value

The design of the filter capacity proceeds from the fact that the maximal power factor variation acceptable by the grid is λ% of the rated power P as shown in Equation (3.40). The filter capacity can therefore be calculated as

$$|Q_c| \leq \quad \lambda\,|P| \tag{3.40}$$

$$Q_c = -U_g^2 C_f w_g \tag{3.41}$$

Q_c signifies the reactive power expended by the filter capacitor and ˇ chosen usually equal to or lower than 0.05. According to Equations (3.40) and (3.41), the maximum value of the filter capacitor can be expressed as :

$$C_f = 0.05\frac{P}{2\pi f_g U_g^2} \tag{3.42}$$

3.4.2 Modeling of the system

The inverter, which is the key component of the framework, is associated to the grid through an LCL arrangement. The switching frequency should be far higher than the grid frequency and the parasitic parameters are ignored. In view of this supposition, the current and voltage in the system can be investigated without consideration of the high-frequency components. Fig. 3.10 shows the block diagram of 3-phase grid-connected PV inverter and its control scheme.

DC-link side

In order to control the output voltage of the PV panel and force it to the MPP value, according to the solar irradiation and cell temperature parameters, we need to control the Dc-link voltage. The voltage ripple will decrease, by using a relatively large DC-link capacitor. The following equation (3.43) govern the DC bus voltage:

$$\frac{d\hat{v}_{Dc}}{dt}=\frac{1}{C_{Dc}}.(i_{Dc}\text{-}i_{pv}) \tag{3.43}$$

An underlined supposition here, is that the power of the PV collections comprises the charging capacitor power and the Dc-link input power of the 3-phase VSI without other energy dissipation.

$$P_{pv} = P_{in} + P_{cap} \tag{3.44}$$

Where P_{in}=$\hat{V}_{Dc} * i_{Dc}$ is the Dc-link power input of the inverter and P_{cap}=$C_{Dc} * V_{Dc}$, V_{Dc} is defined as the power of the Dc-link capacitor. The AC side output and the instantaneous active power of the Dc-link input can be represented as:

$$P_{out}=(\frac{3}{2})(V_{gd} \times i_{2\_d} + V_{g\_q} \times i_{2\_q}). \tag{3.45}$$

$$P_{in}=P_{pv}- C_{Dc} \times V_{Dc} \times \frac{d\hat{V}_{Dc}}{dt}. \tag{3.46}$$

To attain steady state operation, the AC power served into the grid must be on a par with the delivered Dc power of the PV. The *Dc* voltage controller gives the set point of the AC power, the power transmission loss of both the LCL filter and the inverter is neglecting. At that time, we can consider that:

$$\frac{1}{2}C_{Dc}\frac{d\hat{v}_{Dc}^2}{dt}=P_{pv} - (\frac{3}{2})\left(V_{g\_d}i_{2\_d} + V_{g\_q}i_{2\_q}\right). \tag{3.47}$$

The resulting non-linear system, with respect to V_{Dc} will be transformed to an equivalent linear system. A new state variable is chosen $\lambda = {V_{Dc}}^2$ The equation becomes:

$$\frac{1}{2}C_{Dc}\frac{d\lambda}{dt} = P_{pv} - (\frac{3}{2})\left(V_{g\_d}i_{2\_d} + V_{g\_q}i_{2\_q}\right) \tag{3.48}$$

Output LCL filter

In the steady state, the grid phase currents I_{2a}, I_{2b}, and I_{2c} are controlled to be in phase with the consistent grid phase voltages V_{ga}, V_{gb}, and V_{gc} which are written as :

$$\begin{bmatrix} V_{ga} \\ V_{gb} \\ V_{gc} \end{bmatrix} = \begin{bmatrix} V_m cos(wt) \\ V_m cos(wt - 2\pi/3) \\ V_{\ m} cos(wt + 2\pi/3) \end{bmatrix} \tag{3.49}$$

Where w and V_m are the angular frequency and the amplitude of the phase voltage, respectively. The equations describing the current and voltage of the three phase are:

$$\begin{cases} L_1\frac{di_{1k}}{dt} = V_{ck} - R_1 i_{1k} - V_{1k} \\ C_f\frac{d\hat{V}_{ck}}{dt} = i_{1k} - i_{2k} \\ L_2\frac{di_{2k}}{dt} = V_{2k} - R_2 i_{2k} - V_{ck} \end{cases} \tag{3.50}$$

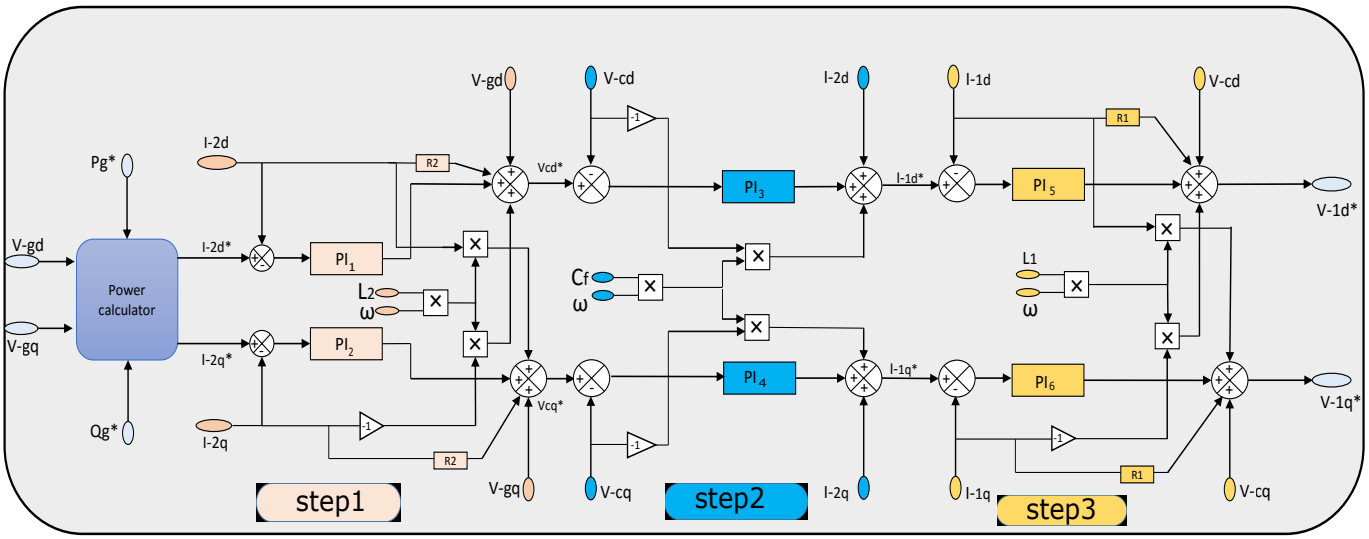

Figure 3.10: Block diagram of three phase grid-connected PV inverter control.

where k is the phase number equal to $\{1,2,3\}$. The differential equations of the LCL filter in the frame (α,β) are:

$$\frac{d}{dt}\begin{pmatrix} i_{1\_\alpha\beta} \\ \hat{V}_{c\_\alpha\beta} \\ i_{2\_\alpha\beta} \end{pmatrix} = \begin{pmatrix} -\frac{R_1}{L_1} & -\frac{1}{L_1} & 0 \\ \frac{1}{C_f} & 0 & -\frac{1}{C_f} \\ 0 & \frac{1}{L_2} & -\frac{R_2}{L_2} \end{pmatrix} \times \begin{pmatrix} i_{1\_\alpha\beta} \\ \hat{V}_{c\_\alpha\beta} \\ i_{2\_\alpha\beta} \end{pmatrix}$$

$$+ \begin{pmatrix} \frac{1}{L_1} & 0 \\ 0 & 0 \\ 0 & -\frac{1}{L_2} \end{pmatrix} \times \begin{pmatrix} V_{inv\_\alpha\beta} \\ V_{g\_\alpha\beta} \end{pmatrix} \tag{3.51}$$

In that frame, six equations can be composed (3.36)-(3.41) at w angular speed. Transformation into the $(d-q)$ frame of the state description in $(\alpha-\beta)$ frame is gotten from the transformation matrix T (Park's transformation).

Fig. 3.11 represents the averaged equivalent circuit in the synchronous (d,q) reference frame. Assuming that R_1 and R_2 are dissimilar from zero, the differential complex equations in $(d-q)$ frame are given by:

$$\frac{d\hat{V}_{c\_d}}{dt} = w\,\hat{V}_{c\_q} + \frac{1}{C_f} i_{1\_d} - \frac{1}{C_f} i_{c\_d} \tag{3.52}$$

$$\frac{d\hat{V}_{c\_q}}{dt} = -w\,\hat{V}_{c\_q} + \frac{1}{C_f} i_{1\_q} - \frac{1}{C_f} i_{c\_q} \tag{3.53}$$

$$\frac{di_{1\_d}}{dt} = -\frac{R_1}{L_1} i_{1\_d} + w\, i_{1\_q} + \frac{1}{L_1} V_{1\_d} - \frac{1}{L_1} V_{c\_d} \tag{3.54}$$

$$\frac{di_{1\_q}}{dt} = -\frac{R_1}{L_1} i_{1\_q} + w\, i_{1\_d} + \frac{1}{L_1} V_{1\_q} - \frac{1}{L_1} V_{c\_q} \tag{3.55}$$

$$\frac{di_{2\_d}}{dt} = -\frac{R_2}{L_2} i_{2\_d} + w\, i_{2\_q} + \frac{1}{L_2} V_{2\_d} - \frac{1}{L_2} V_{c\_d} \tag{3.56}$$

$$\frac{di_{2\_q}}{dt} = -\frac{R_2}{L_2} i_{2\_q} - w\, i_{2\_d} + \frac{1}{L_2} V_{2\_q} - \frac{1}{L_2} V_{c\_q} \tag{3.57}$$

The valued complex state description in(dq) frame shows that the behavior of the LCL filter output depends on the rotation direction of the vectors. There are three reactive elements L_1, C_f and L_2. The inputs are the grid voltage (V_{g-dq}) and the inverter voltage (V_{1-dq}). The output and the state variables of the system are the currents through L_1 (i_{1-dq}) and L_2 (i_{2-dq}) and additionally the capacitor voltage (V_{c-dq}).

Equations (3.48) and (3.52)-(3.57) represent the model of the LCL-inverter-PV . The control system will be designed in the next section, based on the inverter averaged circuit.

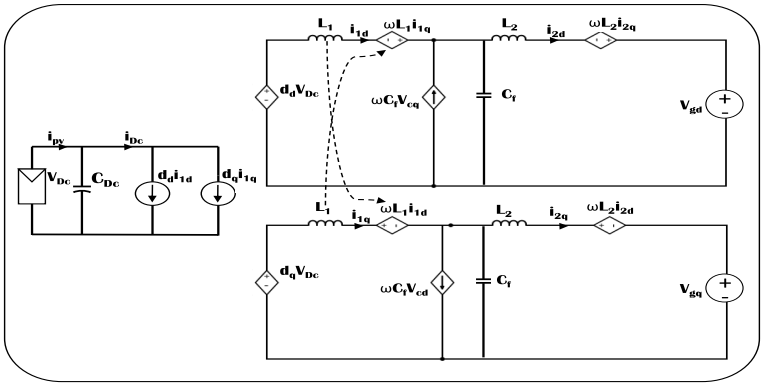

Figure 3.11: The averaged circuit in the (dq) reference frame

3.4.3 Design of simplified feedback control strategy

The PQ theory

The P-Q theory [233] is defined in three phase systems with or without a neutral conductor. From the instantaneous line current and phase voltage, the instantaneous real power P and the instantaneous imaginary power Q are defined on the (d-q) axes as :

$$\begin{bmatrix} P_g \\ Q_g \end{bmatrix} = \begin{bmatrix} v_{g\_d} & v_{g\_q} \\ -v_{g\_q} & v_{g\_d} \end{bmatrix} \begin{bmatrix} i_{2\_d} \\ i_{2\_q} \end{bmatrix} \tag{3.58}$$

In the following description, the (d-q) current will be set as function of voltages and the real and imaginary power P and Q. This is exceptionally appropriate to better clarify the physical significance of the power characterized in P-Q hypothesis. So it is conceivable to write:

$$\begin{bmatrix} \hat{i}_{2\_d} \\ \hat{i}_{2\_q} \end{bmatrix} = \frac{1}{V_{g\_d}^{\,2} + V_{g\_q}^{\,2}} \times \begin{bmatrix} v_{g\_d} & v_{g\_q} \\ -v_{g\_q} & v_{g\_d} \end{bmatrix} \times \begin{bmatrix} P_g \\ Q_g \end{bmatrix}. \tag{3.59}$$

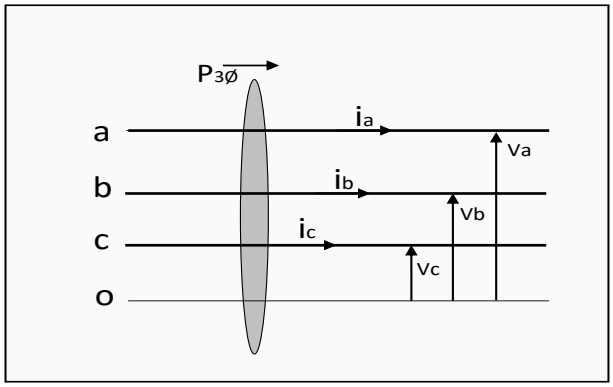

Figure 3.12: Three phase instantaneous active power.

The output active power delivered by the PV is given by:

$$\hat{P_{dc}} = \hat{i}_{inv} \quad \times \quad V_{dc} \tag{3.60}$$

The reference active power injected to the grid is

$$\hat{P_g} = \hat{P}_{dc} - \sum (P_{inv}, P_{LCL}) \tag{3.61}$$

In this thesis, we assume that active power is injected only in the network, then:

$$\hat{Q}_g = 0 \tag{3.62}$$

We also assume that the power losses in the LCL filter and inverter is equal to zero. We can then consider that:

$$\hat{P}_{dc} \approx \hat{P_g} \tag{3.63}$$

The controller of the line current involves a cascade controller model, which allows the use of PI controllers Fig. 3.10. The controller is made out of an inward current control loop for the current(i_{1_j}), a transitional voltage controller, for the capacitor voltage (V_{c_j}) and an outer current controller, for the network line current(i_{2_j}).

Step1:Network current controller side The grid current reference will generate by the combination of signal references, generated for active power and reactive power control. The grid current should follow the reference current generated by the active and reactive current components of the load, according to the basic methodology of the control. The grid current controller is especially designed to control and separate the currents of inductance L2 (i_{2_d} and i_{2_q}). Based on [24]-[25] the current controller input is divided into two terms: the feedback input (i_{2-dq}) and the reference input ($\hat{i}_{2-dq}$). Based on the standard P-I controllers, the output current inverter is achieved. The resultant state equations are:

$$\delta_{i_{2\_d}} = \hat{i}_{2\_d} - i_{2\_d} \tag{3.64}$$

$$\delta_{i_{2\_q}} = \hat{i}_{2-q} - i_{2\_q} \tag{3.65}$$

The differential equations (3.56) and (3.57) become:

$$L_2 \frac{d(\delta_{i_{2\_d}})}{dt} = L_2 \frac{d(\hat{i}_{2\_d})}{dt} + R_2 i_{2\_d} - wL_2 i_{2\_q} + V_{g\_d} - V_{c\_d} \tag{3.66}$$

$$L_2 \frac{d(\delta_{i_{2\_q}})}{dt} = L_2 \frac{d(\hat{i}_{2\_q})}{dt} + R_2 i_{2\_q} + wL_2 i_{2\_d} + V_{g\_q} - V_{c\_q} \tag{3.67}$$

where

$$\hat{V}_{c\_d} = L_2\frac{d(\hat{i}_{2\_d})}{dt} + R_2 i_{2\_d} - wL_2\hat{i}_{2\_q} + V_{g\_d} \tag{3.68}$$

$$\hat{V}_{c\_q} = L_2\frac{d(\hat{i}_{2\_q})}{dt} + R_2(i_{2\_q}) + wL_2\hat{i}_{2\_d} + V_{g\_q} \tag{3.69}$$

As indicated by (3.68) and (3.69), the voltage $\hat{V}_{c-dq}$ is consist of two terms: first one is the equivalent impedance voltage drop when it is crossed by the current i_{2-dq} and the second term, which characterizes the network voltage V_{g-dq} . The difference between the measured voltage V_{c-dq} and the reference voltage $\hat{V}_{c-dq}$ yields an error on the injected current. Then, the terms (3.68) and (3.69) must be monitored by current controllers given by the step-1 stage, Fig. 3.10.

Step 2:Voltage controller The feedback control methodology is like to the step 1 stage. We assume that the actual current i_{2-d} and i_{2-q} are equal to their reference values, for simplicity of the investigation,. The input of the voltage controller is divided into two terms: the reference input ($\hat{V}_{c-d}$,$\hat{V}_{c-q}$), and the feedback inputs (V_{c-d},V_{c-q}), according to the differential equations of the filter capacitance C_f,. The resultant state equations are:

$$\delta_{V_{c\_d}} = \hat{V}_{c\_d} - V_{c\_d} \tag{3.70}$$

$$\delta_{V_{c\_q}} = \hat{V}_{c\_q} - V_{c\_q} \tag{3.71}$$

The differential equation (3.54) and (3.55) become:

$$C_f\frac{d(\delta_{V_{c\_d}})}{dt} = C_f\frac{d(\hat{V}_{c\_d})}{dt} - C_f wV_{c\_q} + i_{2\_d} - i_{1\_d} \tag{3.72}$$

$$C_f\frac{d(\delta_{V_{c\_q}})}{dt} = C_f\frac{d(\hat{V}_{c\_q})}{dt} + C_f wV_{c\_d} + i_{2\_q} - i_{1\_q} \tag{3.73}$$

where

$$\hat{i}_{1\_d} = C_f\frac{d(\hat{V}_{c\_d})}{dt} - C_f wV_{c\_q} + i_{2\_d} \tag{3.74}$$

$$\hat{i}_{1\_q} = C_f\frac{d(\hat{V}_{c\_q})}{dt} + C_f wV_{c\_q} + i_{2\_q} \tag{3.75}$$

The difference between the measured current i_{1-dq} and the reference current $\hat{i}_{1-dq}$ yields an error on the capacitor voltage. Based on (3.74) and (3.75), each one of the current ($\hat{i}_{1-d}$,$\hat{i}_{1-q}$) is consists of two terms. First one describes the capacitor current when it is fed by V_{c-dq} , while the second describes the network current i_{1-dq} which is directly measurable. Terms (3.74) and (3.75) must be expounded by voltage controllers appeared in the step-2 stage, Fig. 3.10.

Step 3:Inverter side current controller Fig. 3.12 shows the inverter current controller side. The inductor current controller is accomplished with a PI controller. The relating state equations are:

$$\delta_{i_{1\_d}} = \hat{i}_{1\_d} - i_{1\_d} \tag{3.76}$$

$$\delta_{i_{1\_q}} = \hat{i}_{1\_q} - i_{1\_q} \tag{3.77}$$

The differential equations (3.52) and (3.53) become:

$$L_1 \frac{d(\delta_{i_{1\_d}})}{dt} = L_1 \frac{d(\hat{i}_{1\_d})}{dt} + R_1(i_{1\_d}) - wL_1 i_{1\_q} + V_{c\_d} - V_{1\_d} \tag{3.78}$$

$$L_1 \frac{d(\delta_{i_{1\_q}})}{dt} = L_1 \frac{d(\hat{i}_{1\_q})}{dt} + R_1(i_{1\_q}) + wL_1 i_{1-d} + V_{c\_q} - V_{1\_q} \tag{3.79}$$

where

$$\hat{V}_{1\_d} = L_1 \frac{d(\hat{i}_{1\_d})}{dt} + R_1(i_{1\_d}) - wL_1 i_{1\_q} + V_{c\_d} \tag{3.80}$$

$$\hat{V}_{1\_q} = L_1 \frac{d(\hat{i}_{1\_q})}{dt} + R_1(i_{1\_q}) + wL_1 i_{1\_q} + V_{c\_q} \tag{3.81}$$

The variation between the reference voltages ($\hat{V}_{1-d}$,$\hat{V}_{1-q}$) and the measured (V_{1-d},V_{1-q}) yields an error on the inverter current . The terms (3.80) and (3.81) must be controlled by the current controllers given by the step-3, Fig. 3.10.

3.5 Conclusion

In this chapter, the designing procedures of PSO based MPPT, SVPWM, FLC are described in details. The comprehensive analysis of every aspects is followed by the detail flowchart. The next chapter discusses the software implementation, the simulation results and experimental multilevel PV inverter interface with solar panels are presented at the end.

CHAPTER 4

SIMULATION AND REAL TIME IMPLEMENTATION OF THE PROPOSED SEMI MODULAR INVERTER

Contents

4.1 Introduction

This chapter proposes a new control structure for two multilevel three-phase inverter topologies for photovoltaic (PV) systems connected to the grid. This control scheme includes the use of the space vector pulse wide modulation (SVPWM) technique to control the Diode Clamped Inverter (DCI) and cascade inverter topologies, this technique (SVPWM) is an attractive control candidate for any multilevel inverter, it can create a greater output power by reducing Total Harmonic Distortion (THD) and commutation losses.

Since the energy provided by the photovoltaic (PV) system depends on the atmospheric conditions like temperature and irradiance, a stage of adaptation is inserted between the photovoltaic panel and the inverter to extract the maximum of the available power. This stage is a conjunction of a DC-DC converter and a maximum power point tracker (MPPT).

This chapter presents the GMPP tracking results for the proposed PSO MPPT controllers, during partial shading. The idea is to locate the GMPP for any type of *P-V* curve regardless of environmental variations. This is made possible due to the ability of these techniques to handle non-linear objective functions effectively using relatively simple algorithm.

A FPGA implementation of PSO based MPPT is proposed to overcome the problem of MPP tracking under partial shading conditions. This MPPT technique is validated under various PV array configurations in order to evaluate the behavior of each PV configuration under non-uniform irradiation.

Then, a comparative study of photovoltaic systems with these inverter topologies is carried out under Matlab/Simulink environment and evaluated on the basis of MPPT, harmonic distortion, cost, advantages and disadvantages.

In order to test the practical implementation of the proposed control structure, FPGA/Simulink-based Hardware in the Loop approach has been used to bring the obtained results as close as possible to reality and with a minimum of constraints. Based on the analysis of the obtained results, some experimental parameters are summarized and a comparison table is synthesized.

4.2 Simulation results of different PV configurations under partial shading conditions

In order to compare the different structures under the same operating conditions, all the constituent elements of the simulated models have been chosen so that they can be used in the case of real dimensioning. The test procedure was developed to eliminate bias when comparing systems. In this study, the modules were 55 W, 36 cells with 2 bypass diodes per module. The test used various shading conditions ranging from 20% for each panel to more than 50% for a total of 10 configurations. For each configuration, each panel had exactly the same shading pattern applied. The systems tested are composed of 5×6 identical panels, subjected to two gradient scenarios indicated in Table 4.1 for Scenario 1 and Table 4.2 for Scenario 2. The performance results are then summarized in Table 4.3, which includes the results obtained for each configuration.

Table 4.1: Shading patterns of 5×6 PV array relating to scenario 1.

	String1	**String2**	**String3**	**String4**	**String5**	**String6**
Row1	1000	1000	1000	1000	1000	1000
Row2	1000	1000	1000	800	800	1000
Row3	1000	1000	1000	600	600	1000
Row4	1000	1000	1000	800	800	1000
Row5	1000	1000	1000	1000	1000	1000

Table 4.2: Shading patterns of 5×6 PV array relating to scenario 2.

	String1	**String2**	**String3**	**String4**	**String5**	**String6**
Row1	1000	500	1000	500	800	800
Row2	800	800	800	800	800	1000
Row3	500	500	500	500	500	1000
Row4	800	800	800	800	800	1000
Row5	1000	1000	1000	1000	1000	1000

The simulation results for conventional central architectures (serie, parallel, serie-parallel) and alternative architectures (HC, BL, TCT) studied are shown in Fig. 4.1. The P-V characteristic of the power extracted from PV arrays are presented for the two scenarios, Fig. 4.1(a) for scenario 1 and Fig. 4.1(b) for scenario 2.

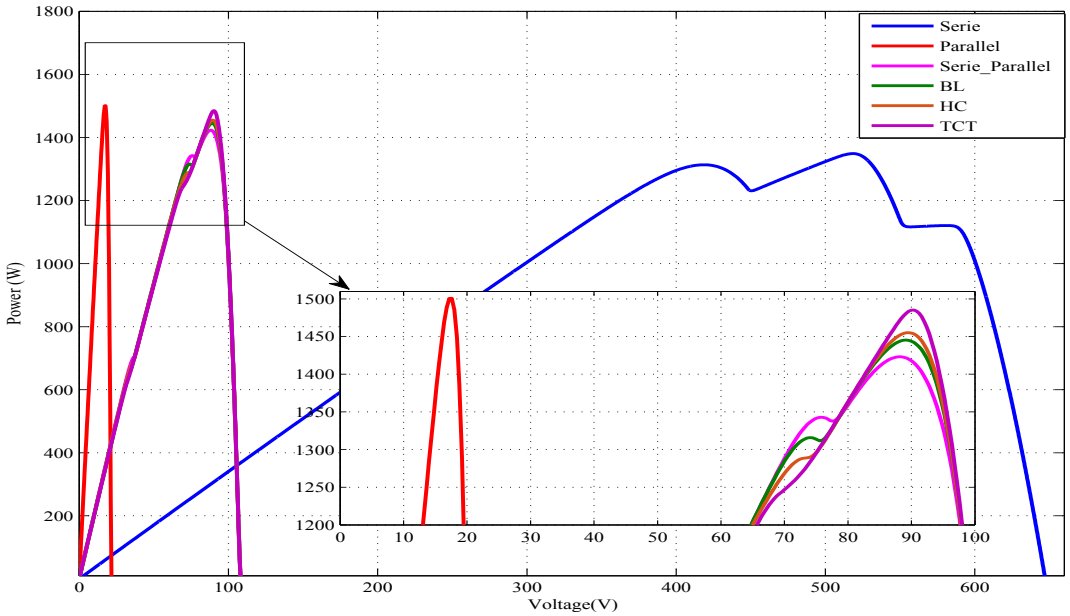

(a) Scenario 1

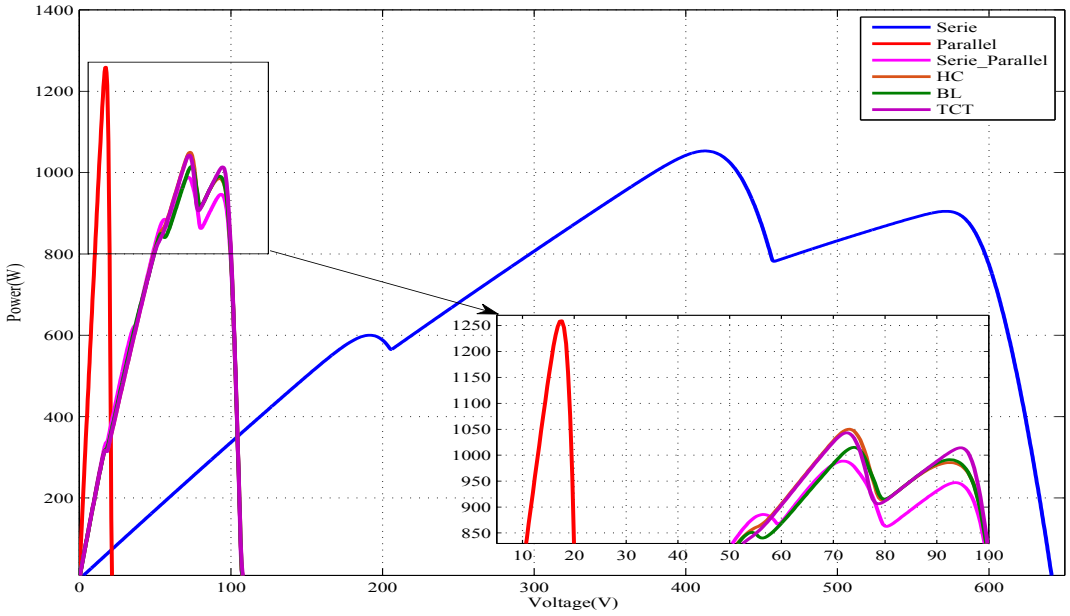

(b) Scenario 2

Figure 4.1: The P-V characteristic of PV array configurations at partial shading conditions.

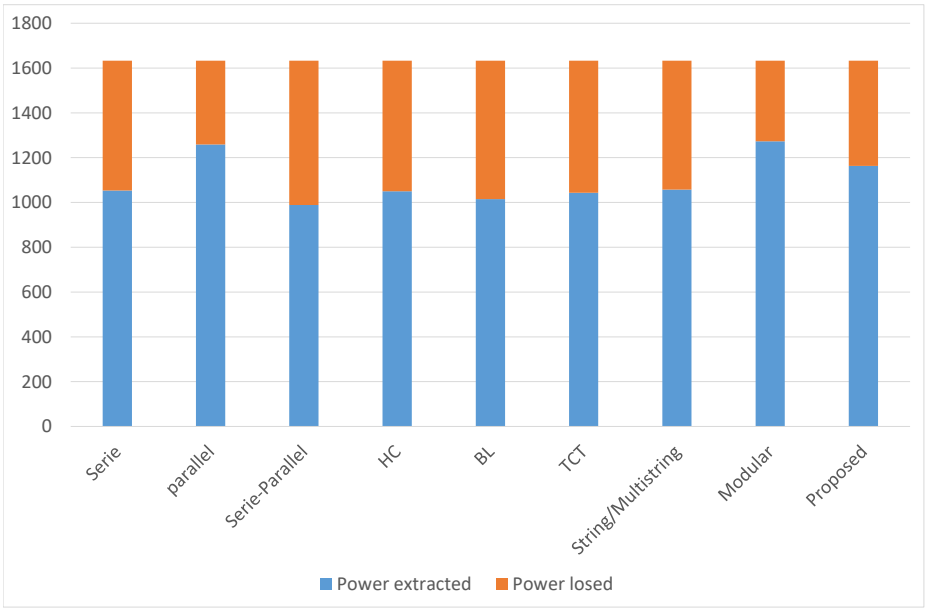

(a) Scenario 1

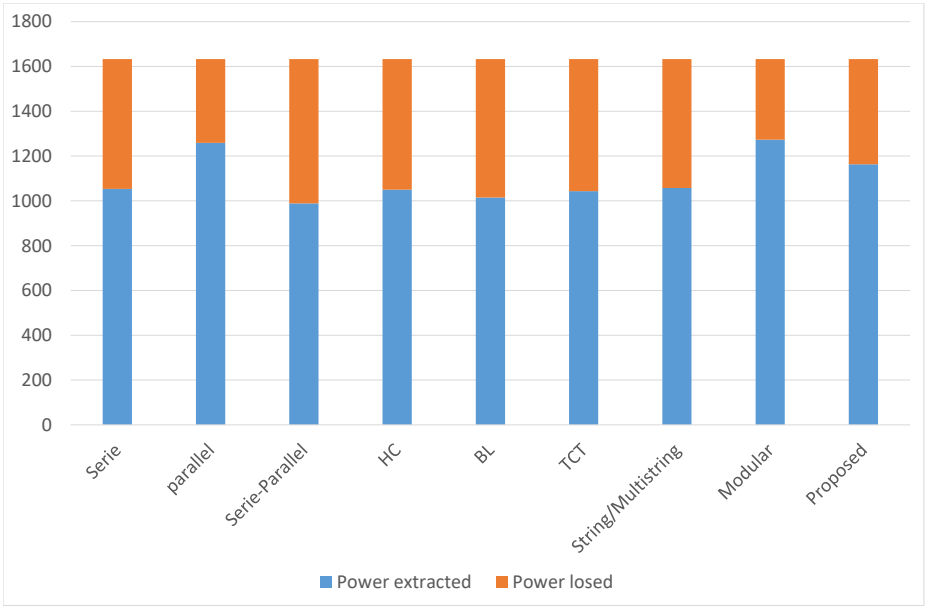

(b) Scenario 2

Figure 4.2: Power extraction against power loss for all different PV array configurations under partial shading conditions.

For the string, multi-string, modular and semi-modular architecture and for legibility reasons, the P-V characteristic can't be represented for each string and each module according to the studied architectures. For this, resulting output voltage and power extracted from photovoltaic modules, as we have explained above, are summarized in Table 4.3, to show the ranking of the different interconnection architectures and to select the optimal circuit topologies giving the highest performance, as well as to evaluate the behavior of each PV inverter due to non-uniform irradiation.

Table 4.3: Simulation results for different configurations under PSC for 2 scenario.

Iverter Topology	**PV architecture**	**scenario1**			**scenario2**		
		P (W)	**V(V)**	**I(A)**	**P(W)**	**V(V)**	**I(A)**
Central Inverter Topology	**Serie**	1349	520.8	2.59	1053.2	413.2	2.54
	Parallel	1500.4	17.6	85.2	1259.1	17.6	71.53
	Serie-Parallel	1423.9	88.4	16.10	988.5	72	13.72
	HC	1445.2	88.5	16.32	1050	73.6	14.26
	BL	1455.3	89.6	16.24	1015.2	74.4	13.64
	TCT	1485.3	90.4	16.43	1043.0	72.8	14.32
String/Multistring Inverter	**String/Multistring**	**P(W)**			**sum of output power per string**		
		1451.6		1057.6			
Modular inverter	**Modular**	1534.8		1273.3	**sum of output power per module**		
Semi-Modular Inverter	**Semi-Modular**	1507.2		1163.5	**sum of output power per section**		

Based on results illustrated in Figs. 4.1 and 4.2 and results included in Table 4.3, different architecture connections of photovoltaic inverter are compared under different shaded patterns. In these conditions, it can be seen that the modular connection is dominant. This concept certainly seems very attractive, but costs and performance are penalized. Always with the aim of discretizing production and being less sensitive to shading. The proposed semi-modular solution solves the cost problem by reducing the number of converters and cable connections while keeping the power extracted from the photovoltaic generators as high as possible.

4.3 Simulation and experimental implementation of PV-inverter under different topologies

4.3.1 Experimental implementation of PSO-MPPT

In order to validate the simulation results which carried out from Section 4.2 and to select the optimal PV systems architectures and circuit topologies offering the highest performance, we performed tests under different shading scenarios for two PV architectures: string and modular to evaluate the behaviour of each PV inverter setting due to non-uniform irradiation. A FPGA-based control circuit prototype, shown in Fig. 4.3, was developed for this purpose.

The schematic prototype of the first considered PV system architecture, string architecture, is shown in Fig. 4.4(a). The experimental results obtained for this topology under two scenarios of partial shading are shown in Figs. 4.6 and 4.7. The resulted P-V curves are characterized by the presence of multiple MPPs: for scenario 1: $P_{LMPP} = 31.9$ W and $P_{GMPP} = 49.6$ W. and for scenario 2 : $P_{LMPP1} = 25$ W and $P_{GMPP} = 81.7$ W. The GMPP is on the left of the P-V curve for the two scenarios, with $V_{GMPP} = 23.8$V in scenario 1 and $V_{GMPP} = 43.5$V in scenario 2. It can be seen that the PSO algorithm has effectively found the GMPP in the two cases and the operating point is maintained around $V = 23.8$V and $I = 2.1$ A in scenario 1 and $V = 43.5$ V and $I = 1.87$ A in scenario 2.

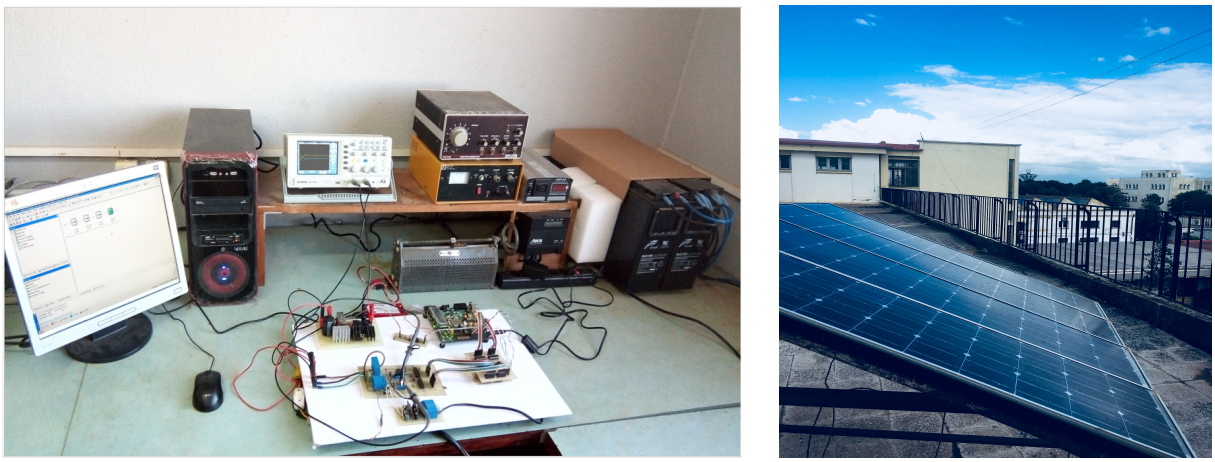

Figure 4.3: Components of PV system under test.

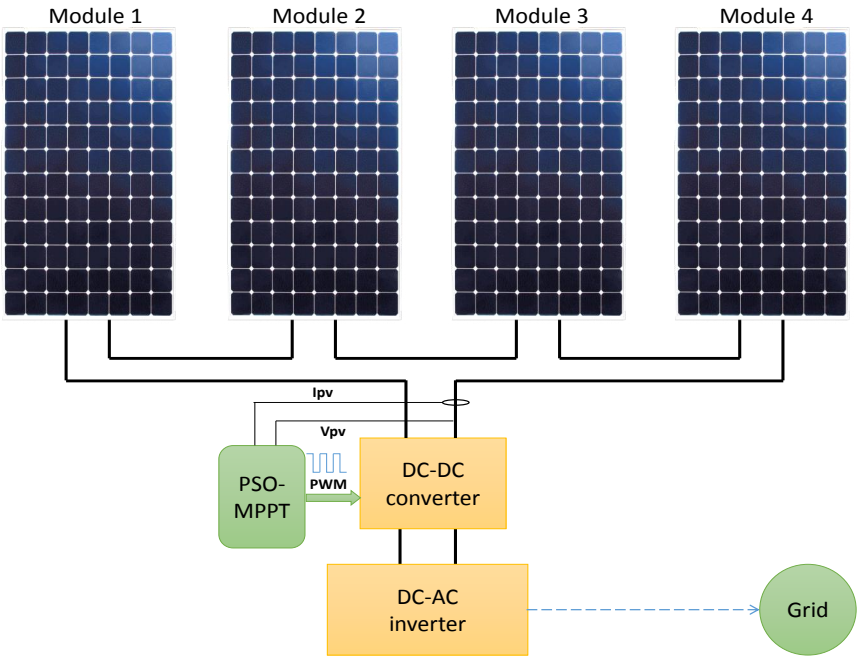

(a)

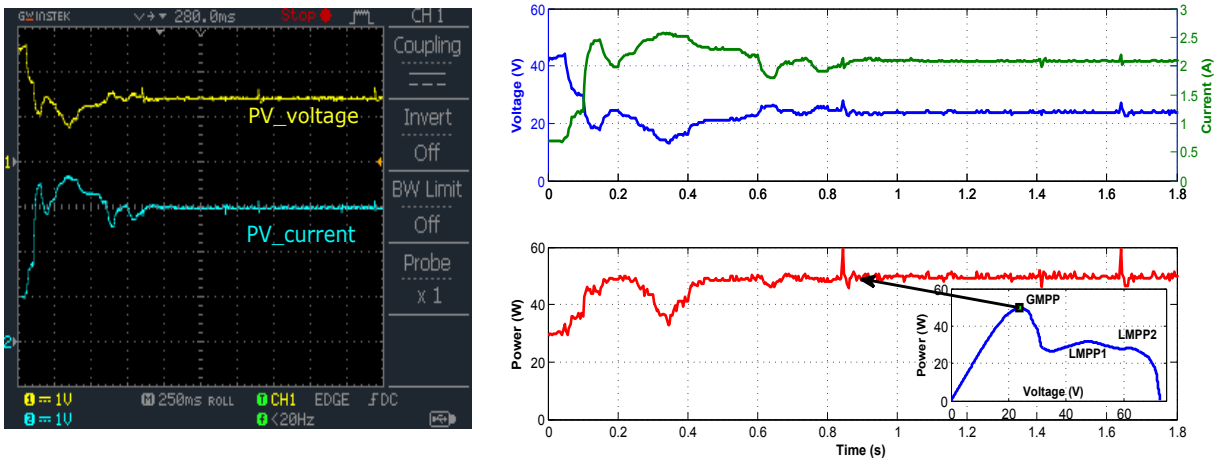

(b)

Figure 4.4: (a) Schematic prototype of the proposed central architecture control, (b) Measured array voltage, current and power waveforms during MPPT process under a shading pattern.

The schematic prototype of the second considered PV systems architectures, modular architecture is shown in Fig. 4.5(a). The experimental results obtained for this topology under two scenarios of partial shading are shown in Figs. 4.6 and 4.7. This figures show the P-V curves for each separate PV module as well as the results of the MPP tracking.

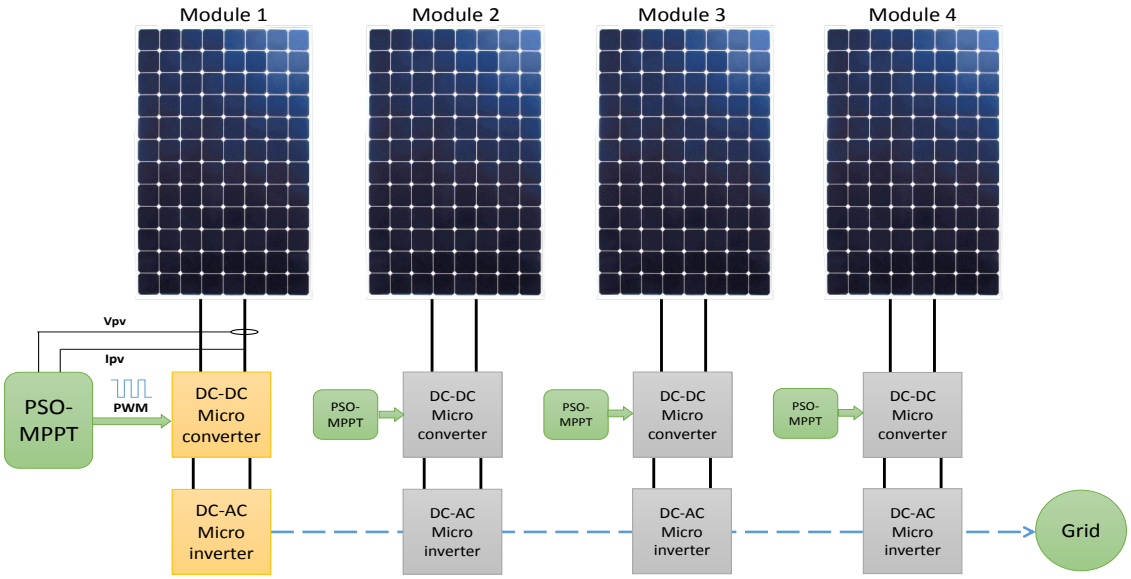

(a)

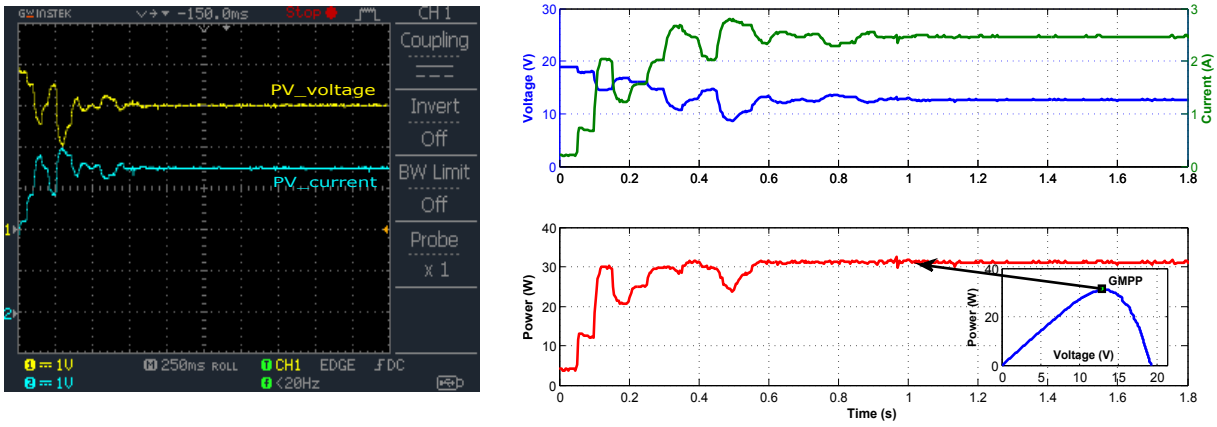

(b)

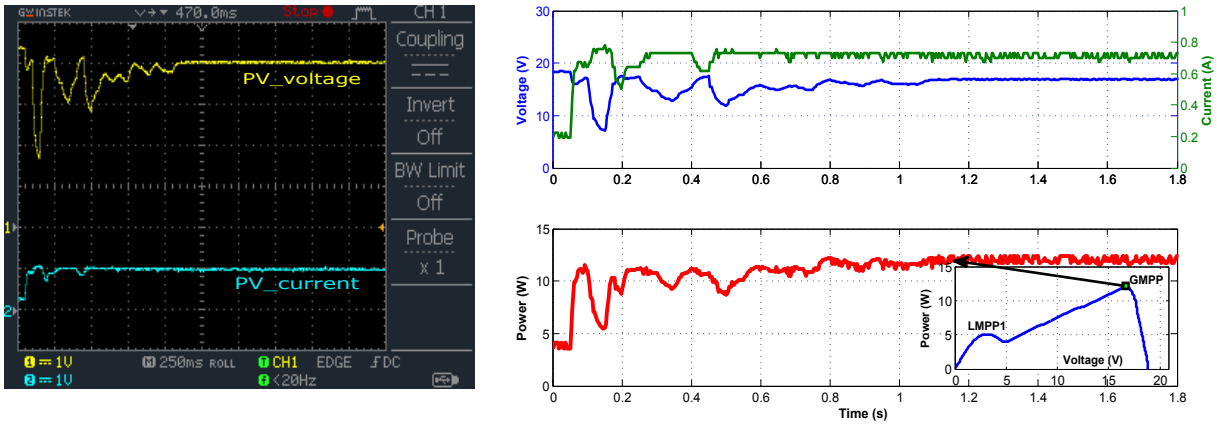

(c)

Figure 4.5: (a) Schematic prototype of the proposed modular architecture control, Measured array voltage, current and power waveforms during MPPT process under a uniform pattern:(b) for module 1, (c) for module 2.

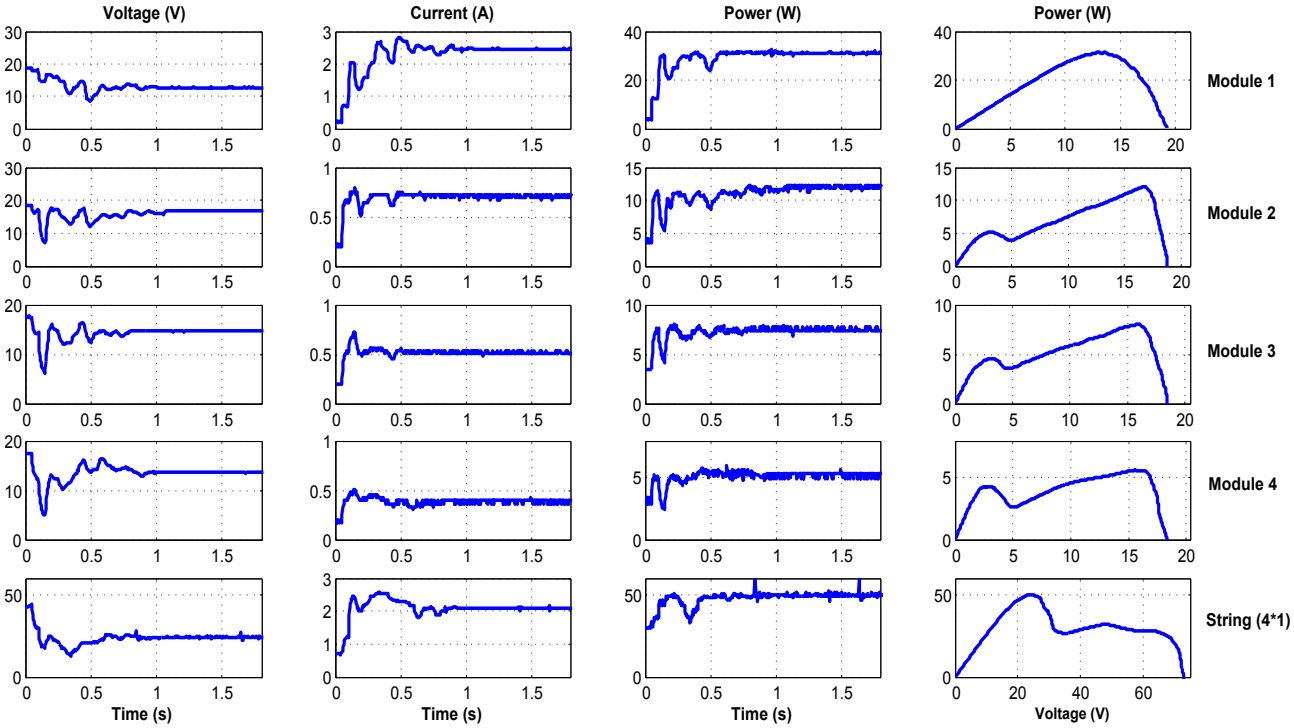

Figure 4.6: Experimental waveforms under Irradiance Condition Scenario 1 (ICS1) containing (voltage, current, power and $P-V$ characteristic curve).

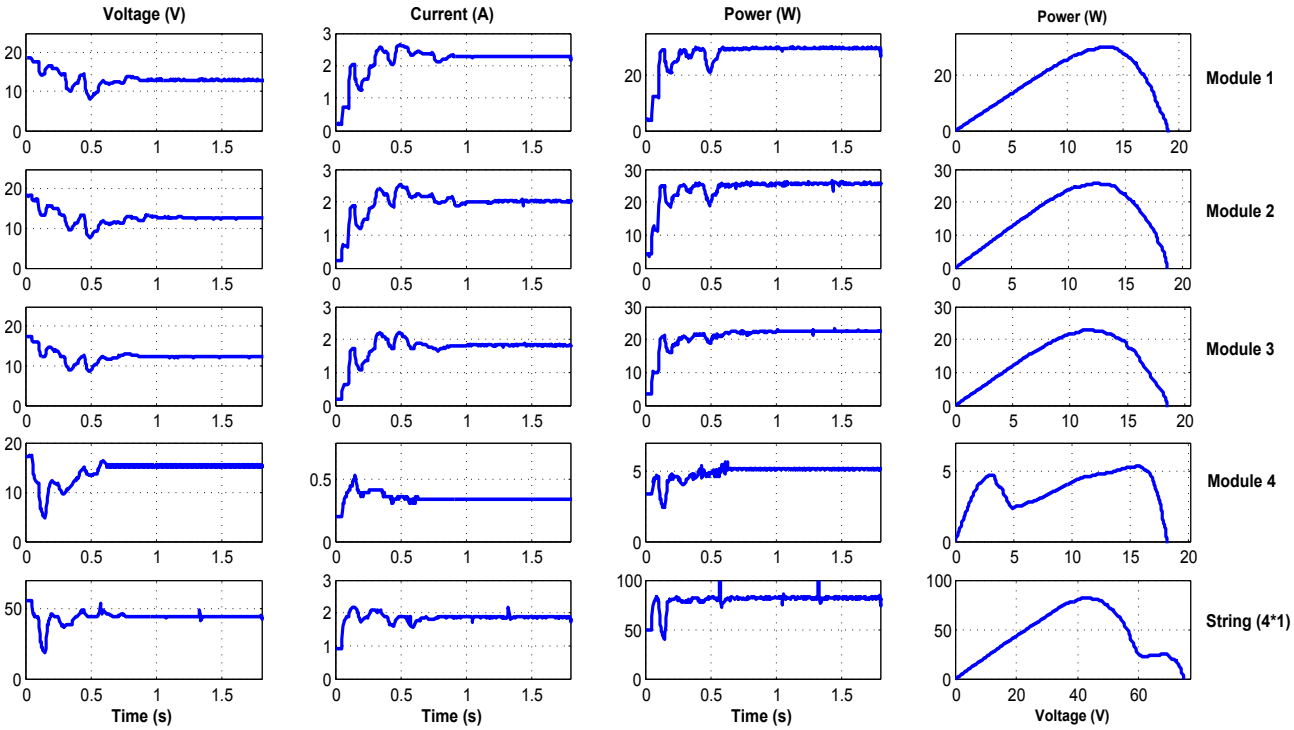

Figure 4.7: Experimental waveforms under Irradiance Condition Scenario 2 (ICS2) containing (voltage, current, power and $P-V$ characteristic curve).

Table 4.4: Experimental results of a PV system architectures under two irradiance condition scenarios

	scenario_1			scenario_2		
	Current(A)	Voltage(V)	Power(W)	Current(A)	Voltage(V)	Power(W)
Module1	2.49	13.05	32.5	2.31	13.6	31.5
Module2	0.73	17.9	13.11	2.10	12.72	26.8
Module3	0.54	14.6	8	1.88	12.42	23.4
Module4	0.41	13.6	5.7	0.42	13.57	5.7
String(4S)	2.10	23.8	**49.6**	1.8	43.52	**81.7**
Modular	**maximum power extracted= 59.31W**			**maximum power extracted= 87.4W**		

Considering the configurations of available photovoltaic system architectures: string, modular that has been examined under two possible shading scenarios, a detailed observation of Figs. 4.4 to 4.7 and the results shown in Table 4.4 , show that the performance of the PV generator is variable and the choice of the most optimal and appropriate configuration depends strongly on the shading pattern, the intensity of shading, the type of shading affecting the PV array (uniform or not) and the used configuration. In order to obtain a practically usable voltage, it is essential to use a series connection of solar cells in an array. Since there is a considerable loss of power due to non-uniform illumination in a serial array, care must be taken to ensure that all cells associated in series get a similar irradiance under different shading patterns.

A number of these strings are connected in parallel to obtain the required power. Such care will give better protection to the grid and at the same time, the total energy production will be higher. In this thesis, the string and modular connections are compared under different shaded patterns. It can be seen that the modular connection is dominant. The result show also the benefit of inserting an adaptation stage with PSO-based MPPT between the PV array and the load in order to optimize the produced power at any time. The choice of the PV inverter used to inject this power extracted into the grid depends strongly on the architecture of the photovoltaic arrays used. The following section describes how the PV inverter converts and delivers the energy produced with maximum efficiency and safety into the grid.

4.3.2 Simulation and experimental implementation of the SVPWM

Based on Matlab/Simulink, several simulations were carried out to evaluate the control and synchronization algorithms. The SVPWM output is generated from the Simulink. The developed programs determine first the position of the reference vector according to the sampling frequency $f_s = 5$ kHz and the fundamental frequency $f = 50$ Hz. On the basis of the sector selected, where the reference vector is located, the switching sequence and the operating time for different switching states are computed. Fig. 4.8 illustrates the results of the output simulation in the case of a switching frequency of 5 kHz. Moreover and in order to check the feasibility of the SVPWM that has been depicted above, implementation on FPGA circuit is used to execute the proposed control. Fig. 4.9(a) represents the block diagram of the proposed VHDL code where *clk* is the input clock and *mi* is the modulation index.

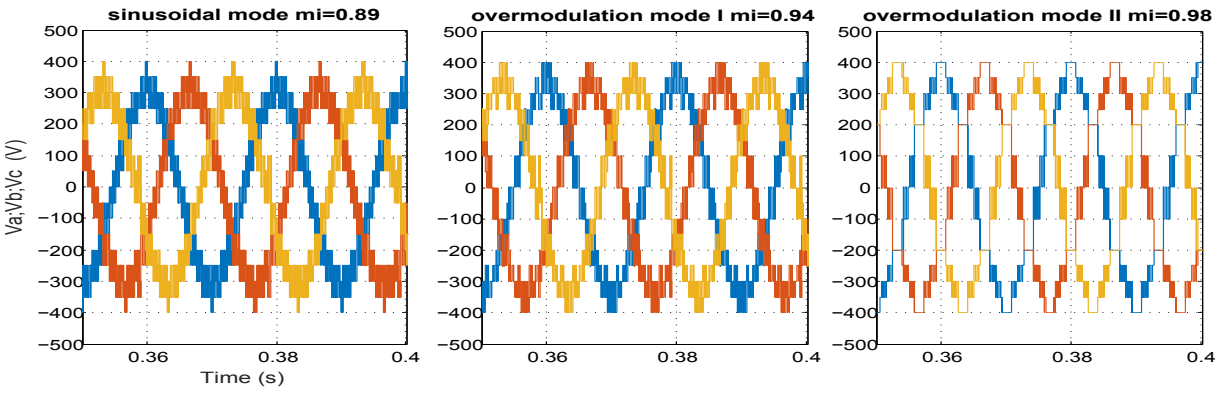

(a) Line to neutral output voltages

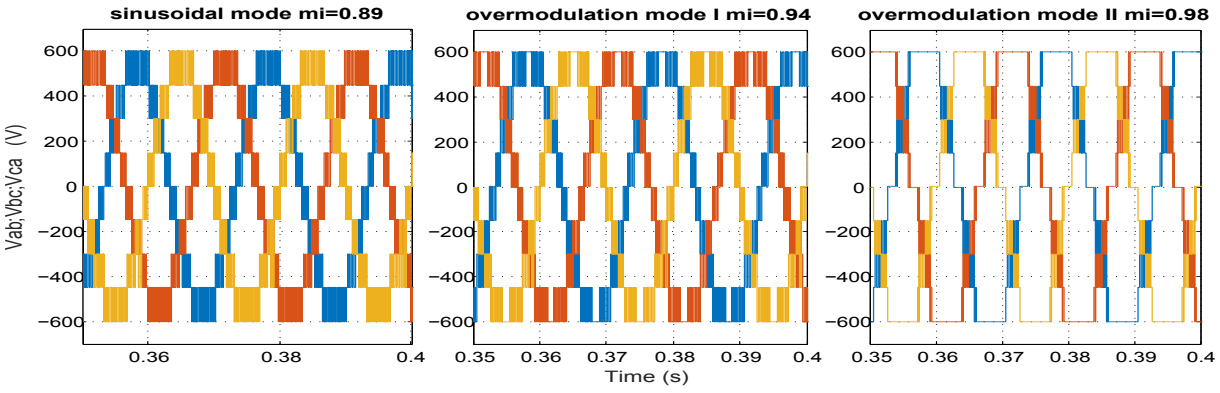

(b) line to line output voltages

Figure 4.8: Simulation results for inverter output voltages.

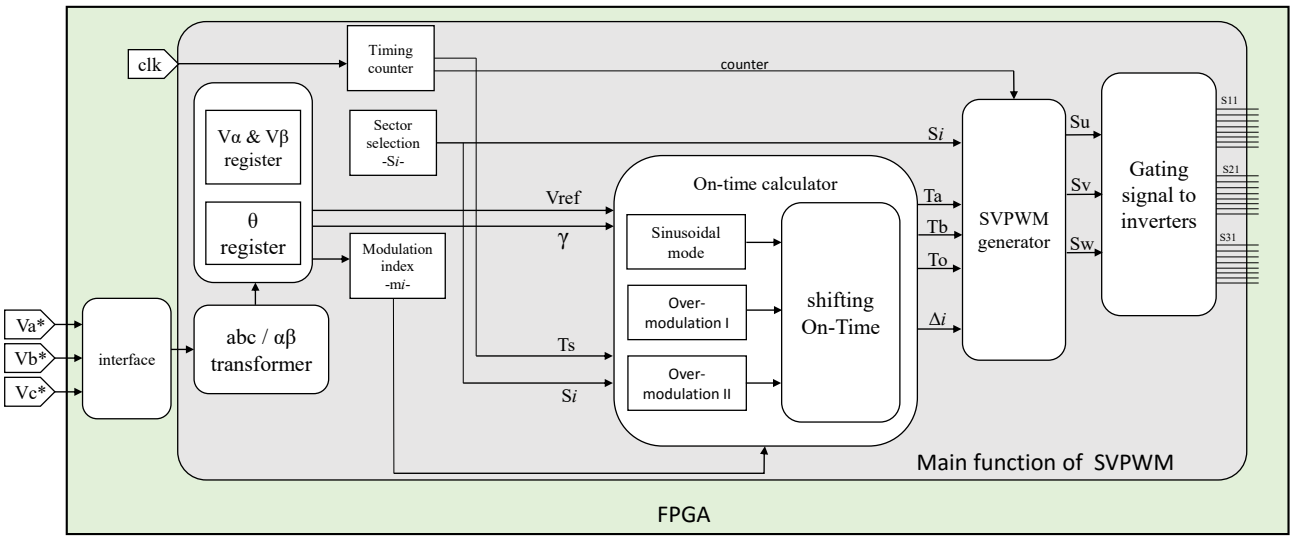

(a) Block diagram of the proposed VHDL code for SVPWM

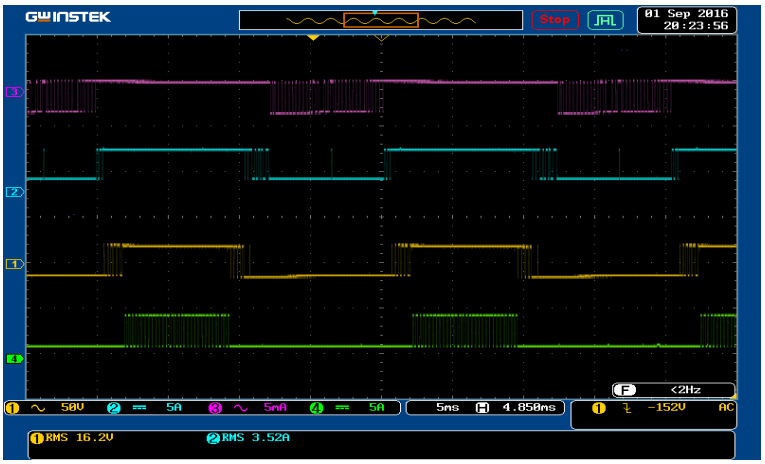

(b) mi=0.89

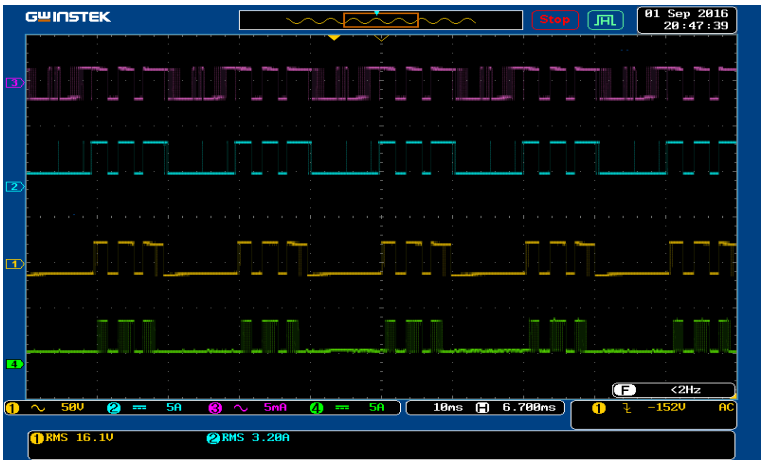

(c) mi=0.92

Figure 4.9: Experimental inverter pulses [S11-S14].

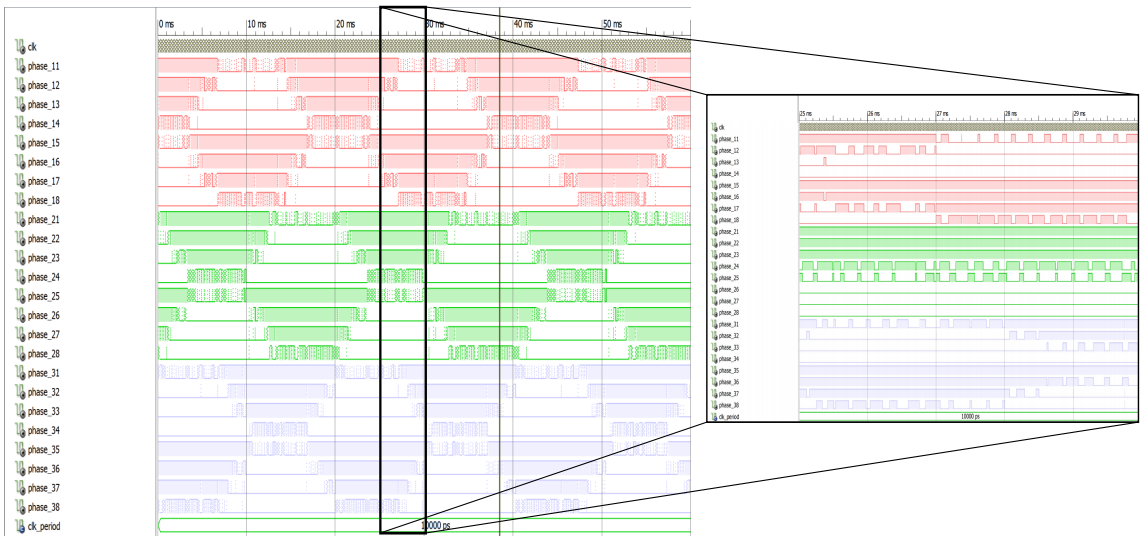

(a) Cascaded inverter.

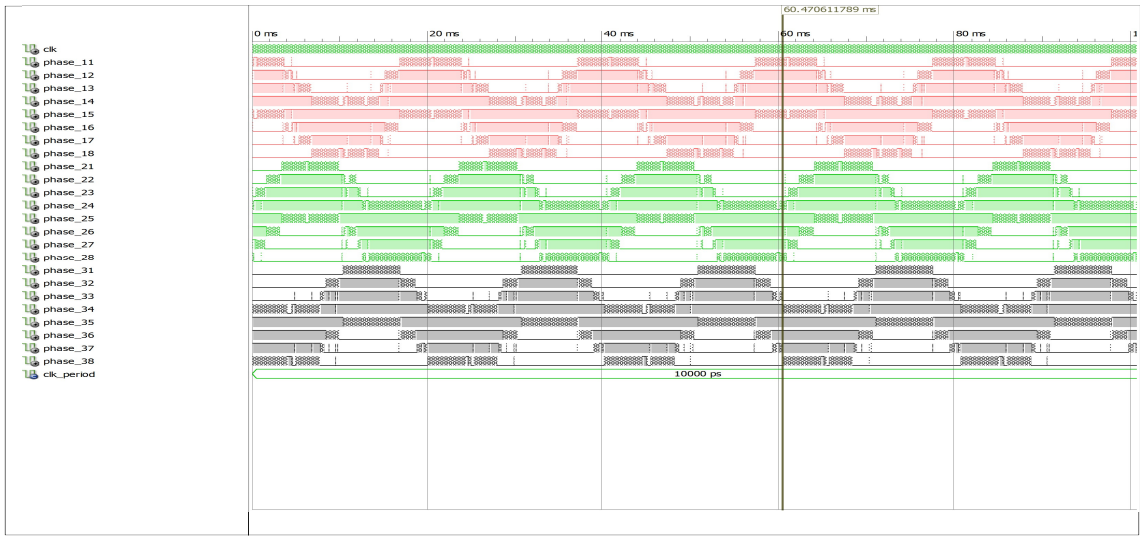

(b) Diode clamped inverter.

Figure 4.10: The simulated 24-pulses gate control signals generated by SVPWM.

The experimental inverter pulses [S11-S14] are presented in Figs. 4.9(b) and 4.9(c) for $mi = 0.82$; $mi = 0.92$. The computation process is similar for each reference vector located in any of the 96 sub-triangles; nevertheless, the resultant switching states, switching sequences of the voltage vectors, are different in each sub-triangle. All the functional blocks in Fig. 4.9(a) are described using VHDL coding. Fig. 4.10 presents the simulated 24-pulses gate control signals generated by SVPWM algorithm for cascaded inverter Fig. 4.10(a) and diode clamped inverter Fig. 4.10(b) by Xilinx

ISE. To store the switching sequences and the switching states, look up tables (LUTs) are used. Different criteria are considered, for example, simplicity, flexibility and computation accuracy, while designing the VHDL code. The VHDL code includes a number of computational blocks, such as, sector identifier, switching state selector and on-time calculator. The proposed work, takes into account some key design measures in order to simplify hardware design and enhance calculation precision.

4.3.3 Feedback linearization control for the PV inverter systems

A three-phase system is modelled by a current injector with its power regulation. The control system regulates the power injected by the PV system into the connection point as a function of the temperature and irradiance. The purpose of this control is to impose the active and reactive powers injected by the PV system at the connection point of the distribution network, by defining the desired set point values P and Q. In reality, the active power P is set by the MPPT module of the PV system and the reactive power Q is zero. Moreover, this imposition of power will directly participates through the regulation of the DC bus, to the selection of the active current (Id) sent to the network. By measuring the currents and the three-phase voltages at the connection point, it is possible to determine the currents to be injected. The process of this model is described in Fig. 3.10. From the voltages and currents measured at the grid connection point, the active and reactive powers are determined. These powers are controlled by a simple Proportional-Integral type correctors. Where V_d and V_q are the direct and quadrature components of the voltage, measured at the point of common coupling (PCC), in the Park reference. I_d and I_q are the direct and quadrature components of the reference product current by the PV system on the network to which it is connected. P and Q are the reference powers of the PV system. Therefore these currents depend on the power demands as well as on the voltage measured at the point of connection. A PLL is used to synchronize the Park transformation to the pulse of the measured voltage across the network. Thus, as shown in Figs. 4.11(a) and 4.11(b), in steady state, the quadratic component V_q is zero and the direct component V_d at the output of the Park transformation is an image of the amplitude of the

measured voltage. These currents are then converted into the three-phase reference. The amplitude and the phase shift of the currents injected into the network, shown in Fig. 4.12, will thus regulate the powers at their set value. The limit for the component I_d is chosen as a function of the maximum output current of the inverter and of the power limit of the DC source.

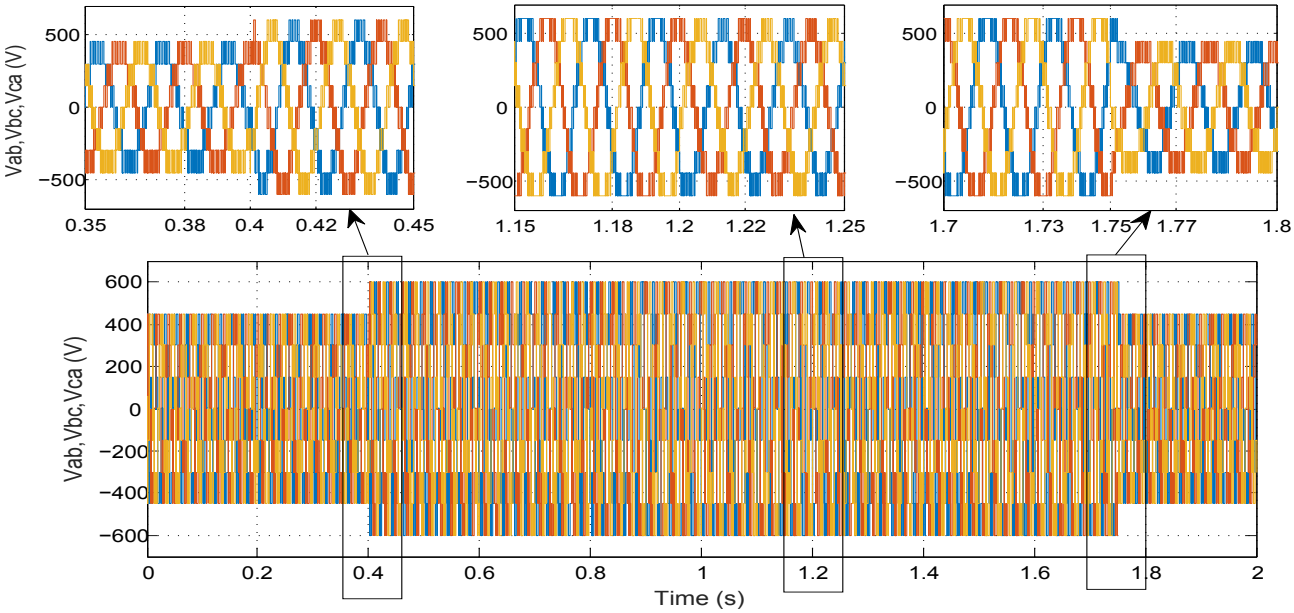

(a)

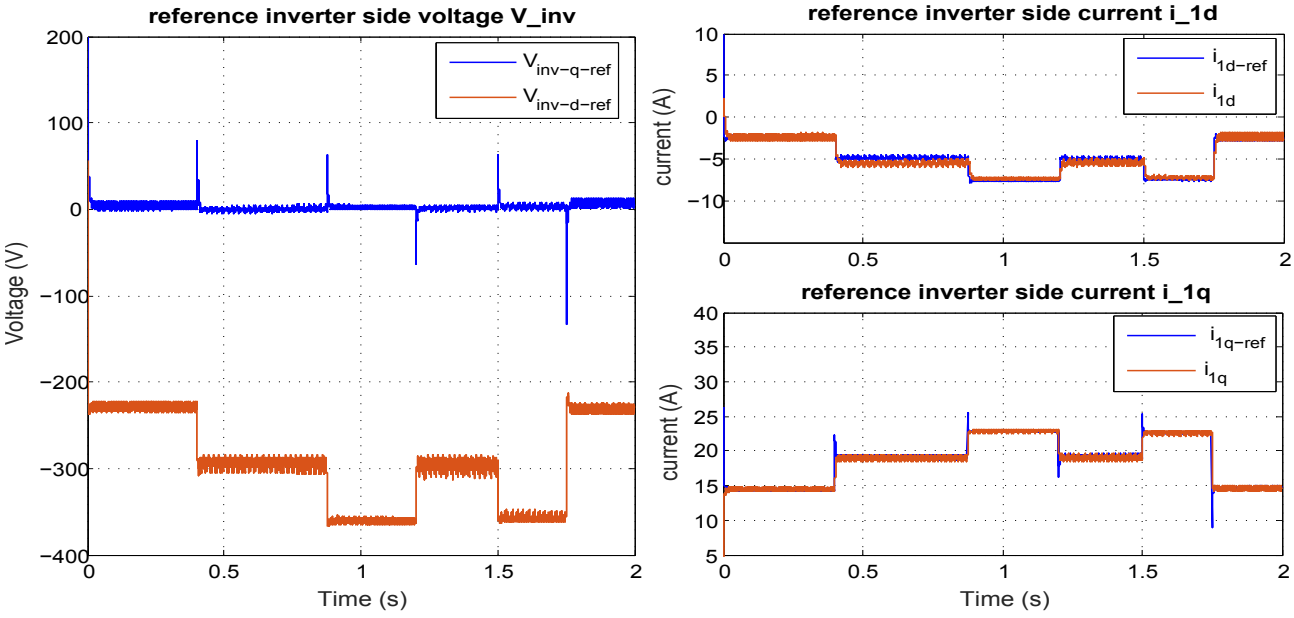

(b)

Figure 4.11: The inverter voltages and currents obtained with direct power control.

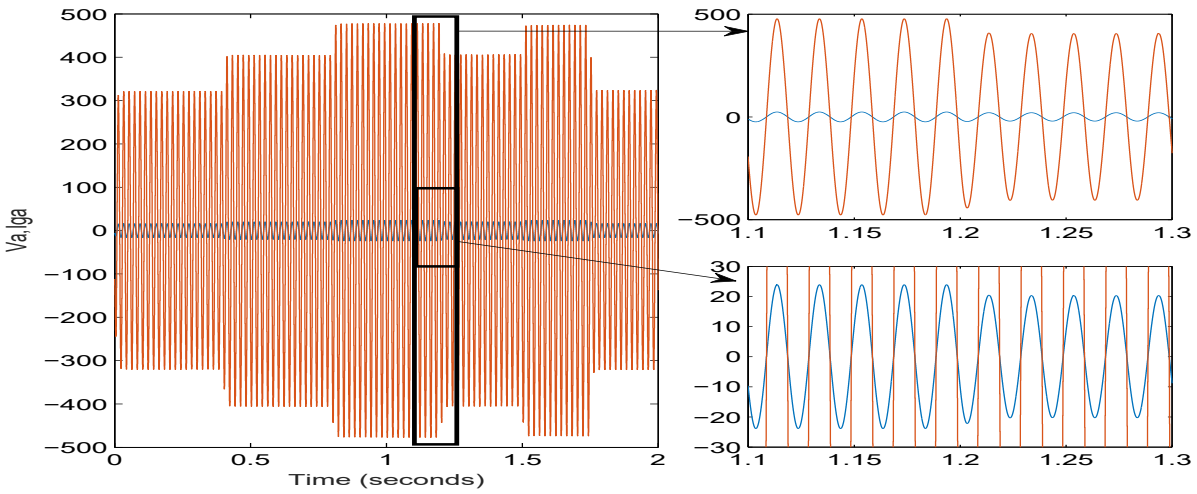

Figure 4.12: The phase angle between current injected and grid voltage at the point of common coupling (PCC).

4.3.4 Total Harmonic Distortion (THD) analysis

PV systems use power electronic inverters to connect with the distribution system, and these inverters generate harmonics and inject them to power grids during operation. Harmonic characteristics are affected by the system impedance, control system, and grid-tie filters (LCL or LC filters). Based on IEEE std. 929-2000, voltage, voltage flicker, frequency, and distortion are four parameters used to evaluate power quality in PV systems. The Total Harmonic Distortion (THD) in terms of voltages and currents are the parameters to be evaluated from the harmonics aspect.

The THD measurement for both five-level inverters is shown in Fig. 4.13. The output THD voltage for cascade inverter is presented in Fig. 4.13(a) and the output THD voltage for diode clamped inverter is presented in Fig. 4.13(b). The output THD current for cascade and diode clamped are presented respectively in Fig. 4.13(c) and Fig. 4.13(d). The simulation results in Fig. 4.13 demonstrate that the SVPWM based multilevel system has an output line-to-line voltage and current with a very low THD. When the modulation index is increased, better performance can be achieved. This demonstrates that the proposed scheme can reduce the THD which is a necessary condition in grid connected PV systems.

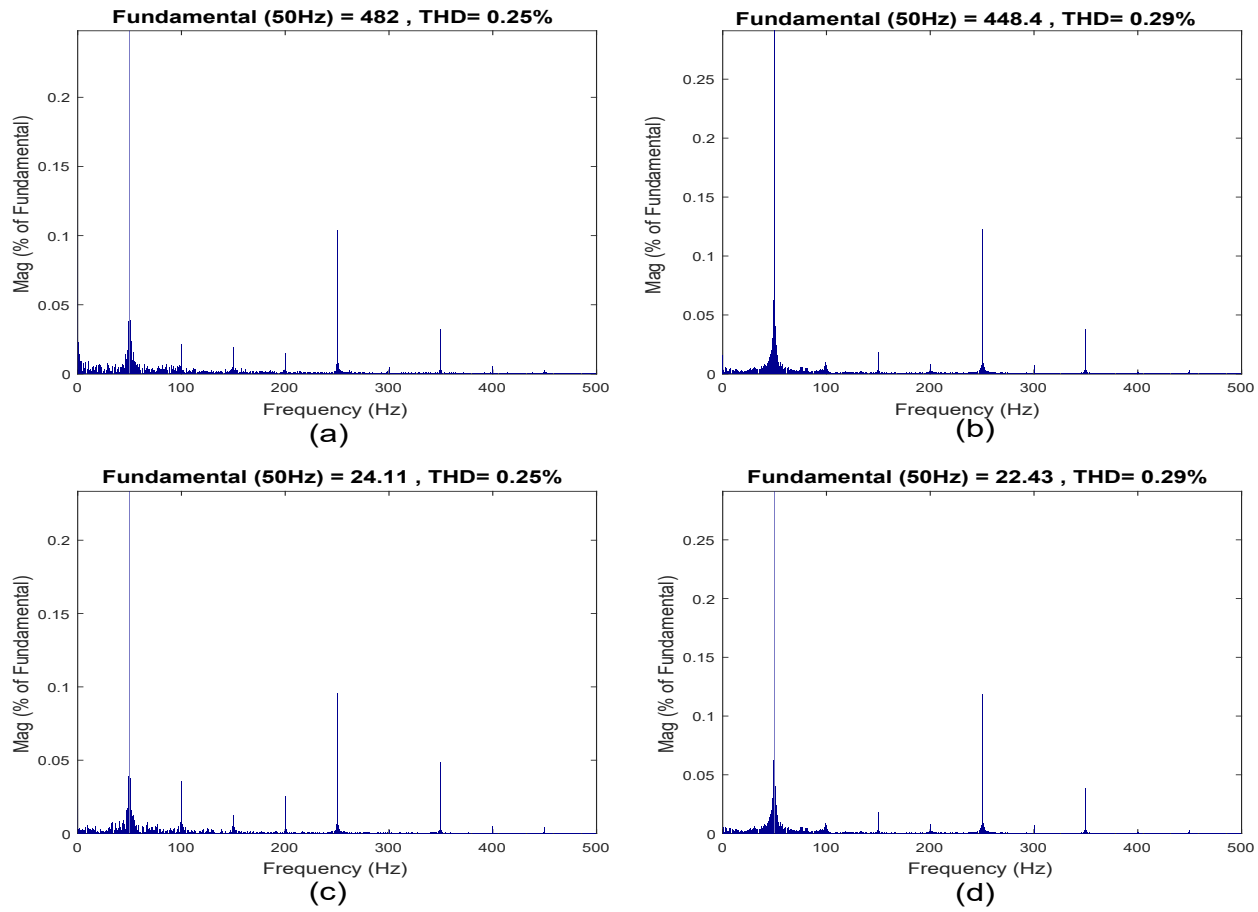

Figure 4.13: The THD measurement for five-level inverter cascade (a):voltage,(c):current and diode clamped (b):voltage, (d):current.

4.3.5 Hardware in the loop implementation (HIL) through : FPGA-MATLAB

Traditionally, industrial control tests are performed directly on physical equipment (eg, a production line), or on the entire system, or on a laboratory test-bench. These approaches have the advantage to be realistic, but they could be very costly, unsuccessful or even dangerous. The HIL test perfectly remedies to these disadvantages. In this case, the physical installation under test is replaced by a computer model, executed in real time on a simulator equipped with inputs/outputs (I/O) interfacing with the systems control and other equipments. This simulator can thus accurately

reproduce the controlled system and its dynamics, as well as its instrumentation (sensors/actuators), to test their closed-loop interactions without going through a real system. The real-time simulation of power electronics systems remains one of the most ambitious challenges of simulation with hardware in the loop (HIL). Input/output capabilities for PWM capture, closed loop simulation latency, matched resolution of coupled switches and fault injection at all levels of a complex system of power electronics, are all examples illustrating the complexity of this evolving sector [38,39]. The hardware implementation is performed in the Xilinx (XC5VLX50-1FFG676) FPGA circuit and Simulink via Ethernet cable (Fig. 4.14). The FPGA in the Loop (FIL) generates the PWM signals, used to control the three phase inverter in Simulink. As it can be seen from Fig. 4.15, the main control targets are attained.

The waveform of the output voltage is very close to that simulated in Fig. 4.1. The results of the co-simulation obtained show the correct practice of the VHDL codes developed and confirm the possibility of a practical implementation of the digital controller designed for the system.

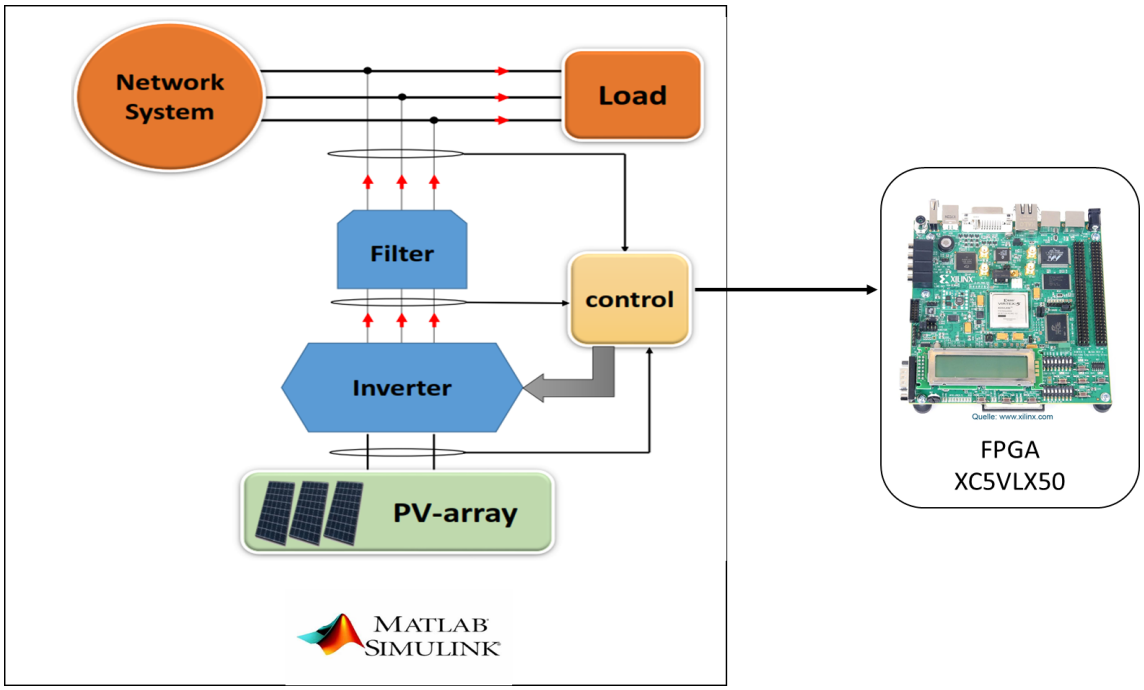

Figure 4.14: Schematic prototype of the hardware in the loop for the five-level 3-phase inverter with Matlab/FPGA.

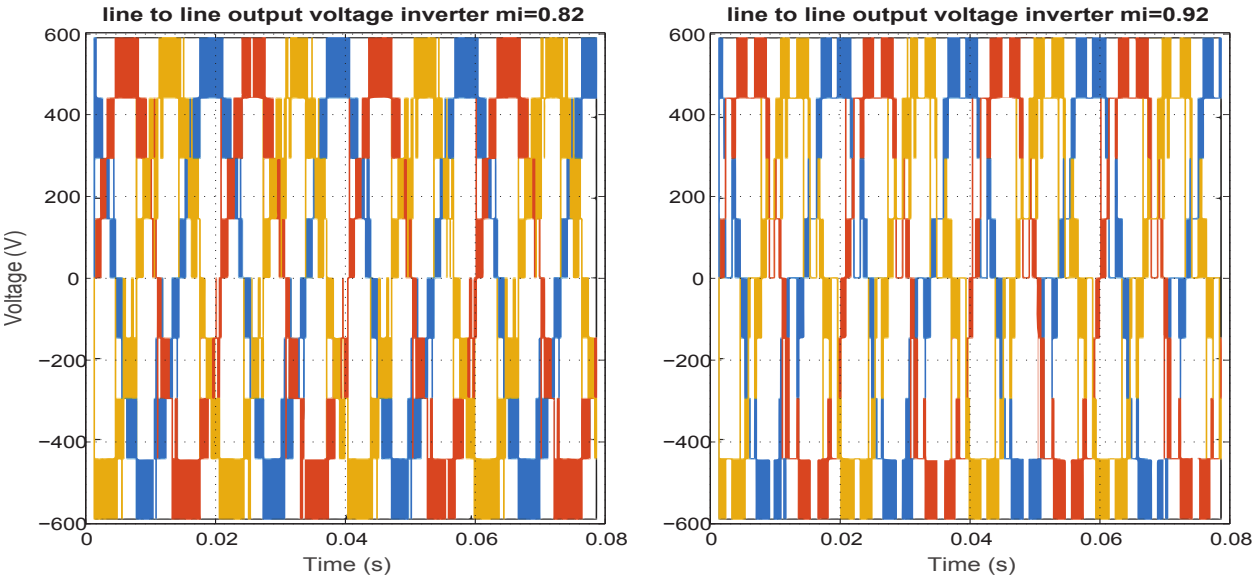

Figure 4.15: The hardware in the loop results for the five-level 3-phase inverter with Matlab/FPGA.

4.4 Experimental implementation of the proposed semi-modular photovoltaic inverter

An experimental setup is implemented to evaluate and validate the control strategies developed for the proposed semi-modular inverter. The experimental platform designed around a semi-modular multi-level converter interfaced to 4×3 PV array shown in Fig. 4.16. This figure details the different components of the test bench: the power section (inverter system and three-phase asynchronous machine in load), the measuring instruments and the control unit (FPGA and PC).

Fig. 4.17 shows the schematic of the prototype used to model the behavior of the semi-modular 5-level inverter proposed. In order to validate simulation results presented in Fig. 4.18, which illustrate the measured array current, voltage and power waveforms under shading pattern during MPPT process presented in Figs. 4.18(a) and 4.18(b), and FPGA implementation results presented in Fig. 4.19,which illustrate the experimental inverter pulses, the semi-modular three-phase inverter was used to control a three-phase asynchronous machine speed as explained in previous sections.

Figure 4.16: Components of PV system under test.

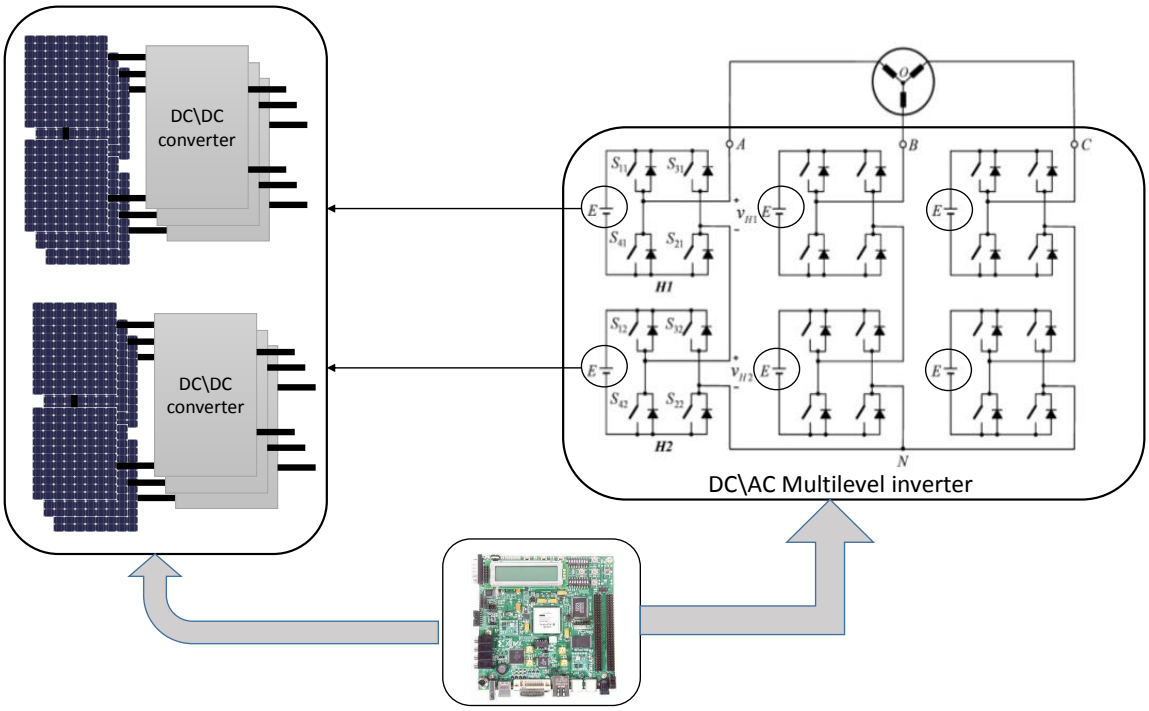

Figure 4.17: Schematic of the prototype for the proposed semi-modular inverter.

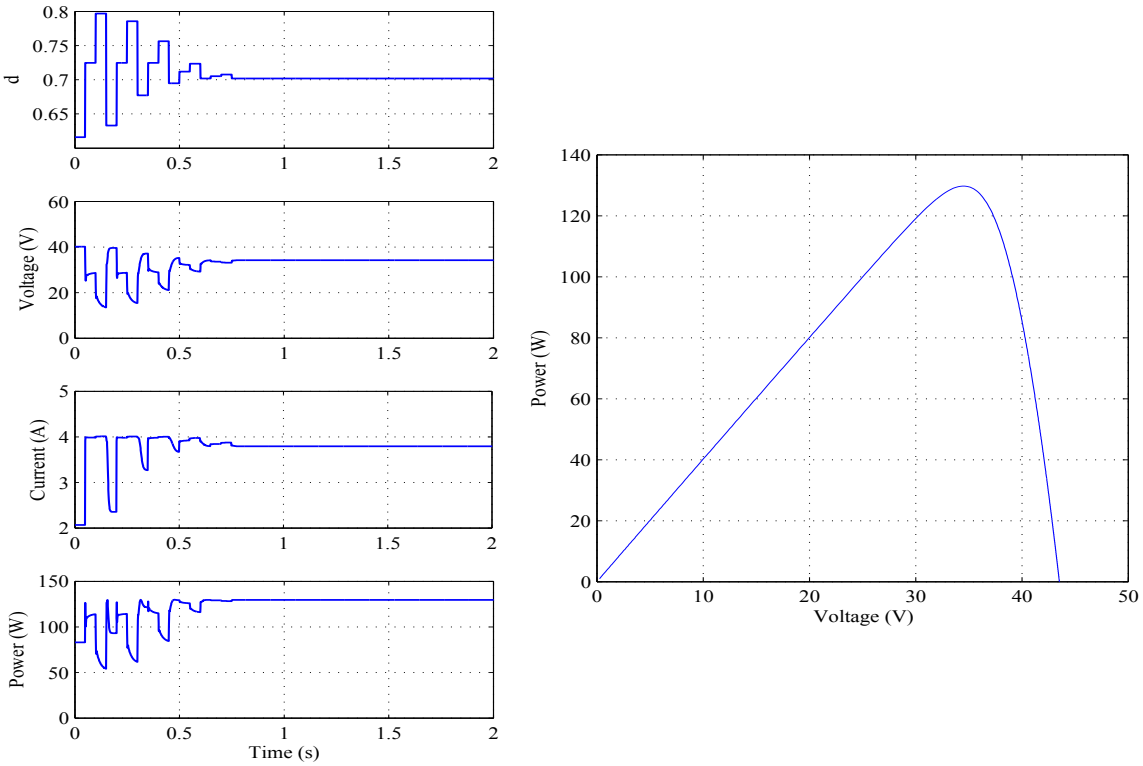

(a) Simulation results under unifrom shading pattern

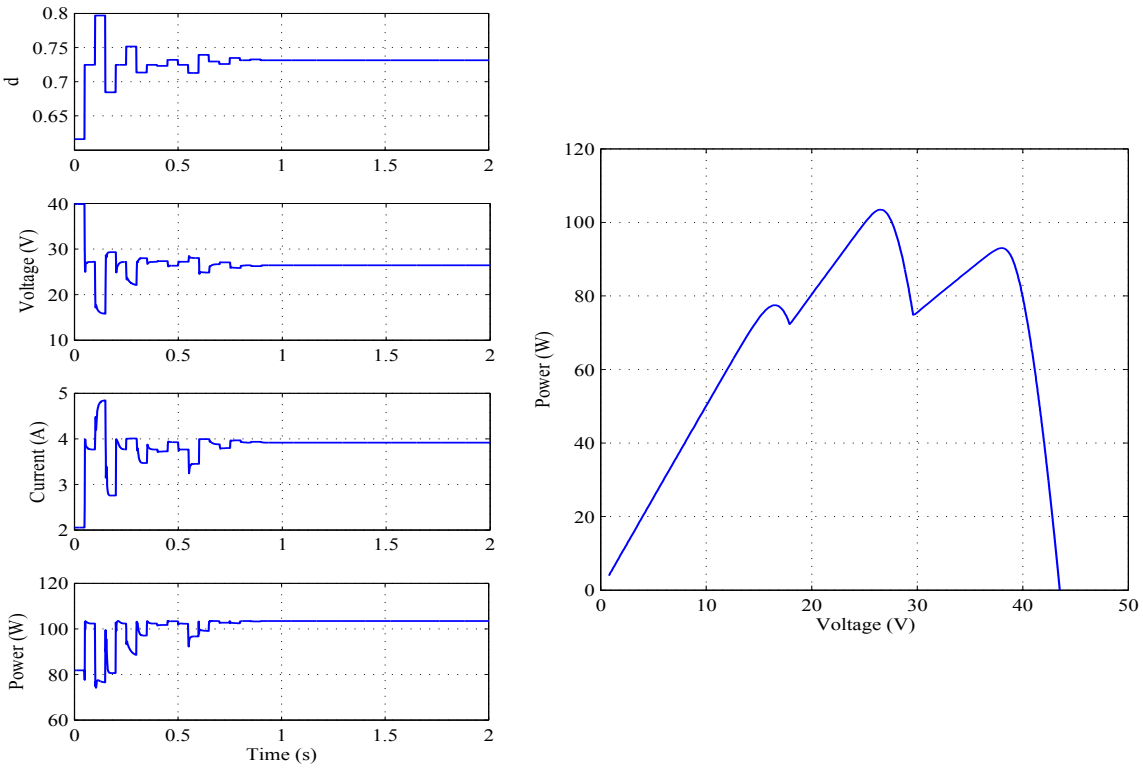

(b) Simulation results under non-unifrom shading pattern

Figure 4.18: Measured power, voltage and current of two PV modules associated in series under uniform and shading pattern during MPPT process based on PSO algorithm.

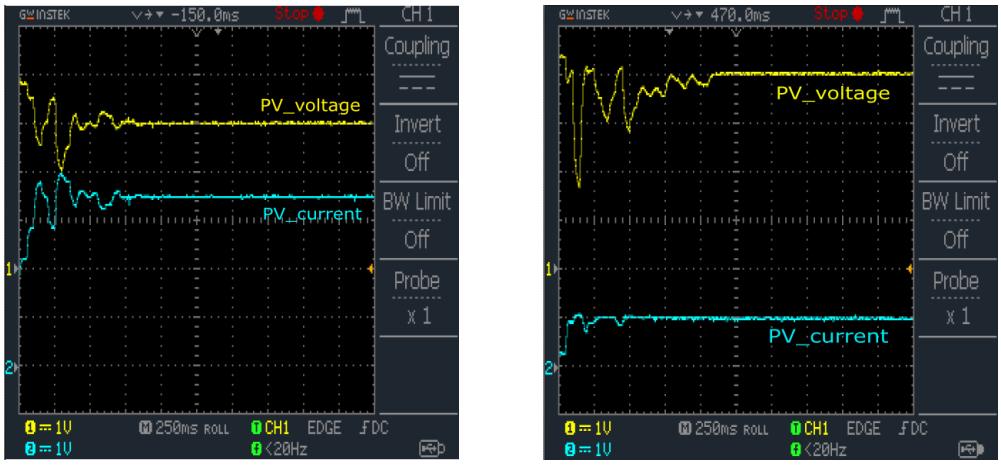

(a) experimental results under unifrom shading pattern

(b) experimental results under non-unifrom shading pattern

Figure 4.19: Measured voltage and current of two PV modules associated in series under uniform and shading pattern during MPPT process based on PSO algorithm.

The simulations results for the inverter output: line to neutral voltages (Fig. 4.8(a)) and line to line voltages (Fig. 4.8(b)) corresponding to sinusoidal mode; over-modulation I; over-modulation II, presented in Fig. 4.8 are in agreement to the experimental results shown in Figs. 4.20 and 4.21 for different modulation index (mi). Thus, to validate the efficiency of the proposed algorithm with respect to the elimination of the selected harmonics, we recorded the phase voltages of the inverter for different values of im, then we made a spectral analysis of these voltages. As a result, the experimental results confirm the efficiency and accuracy of our SVPWM implementation based on FPGA circuit for the elimination of preliminary harmonics and the control of the fundamental voltage.

the proposed semi modular can operate in unity power factor, therefore the proposed inverter has most of the features needed for a PV inverter. A full analysis of the inverter is done. Also, a suitable switching algorithm for correct operation of the inverter is presented. Moreover, the design technique for the passive elements of the topology is demonstrated. Simulation results in MATLAB plus experimental results from a laboratory prototype are added to substantiate the theoretical results.

(a) mi=0.89 (b) mi=0.92

Figure 4.20: Experimental results for inverter output pulses.

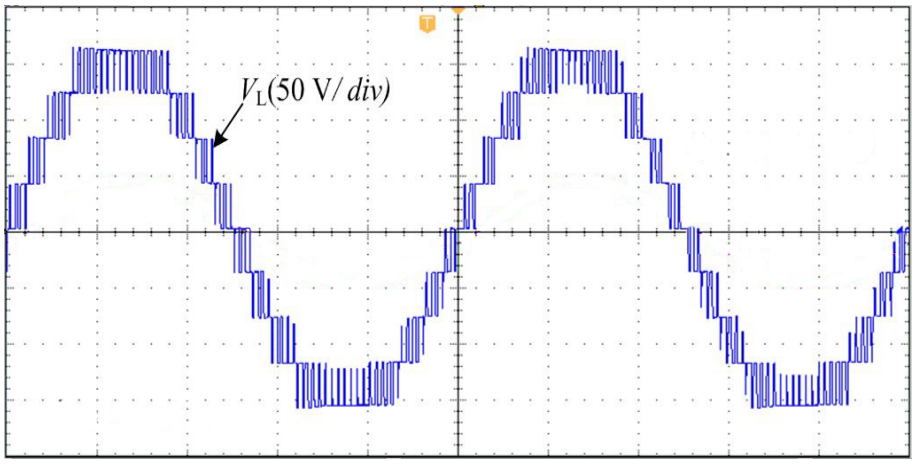

Figure 4.21: Experimental result for inverter output voltage mi =0.89.

4.5 Conclusion

This chapter analysed the performance of the proposed global search MPPT controllers based on PSO algorithm for photovoltaic systems. The Matlab/Simulink environment is used to simulate various PV architectures under various partial shading patterns and to analyse the proposed MPPT control schemes robustness and performance. To validate the control strategy for the proposed inverter, some simulations have been directed for different load power factor and input voltage conditions and

disturbances. Finally, laboratory prototypes of the semi modular inverter are designed and some experiments have been directed to examine the performance of the system and operation of proposed control flowchart and system. Experimental results are presented. Overall, the investigations show that the proposed inverter may operate well when there are different categories of high power factor loads and there is a variable input voltage. Moreover, the converter may operate satisfactorily even when the power factor of the load decreases to 0.8 as has been shown. Therefore, the utilization of the modular inverter may lead to some improvements in the application of three-phase multi-level asymmetrical five-level inverter for residential PV applications, which require step-up conversion and may be needed to supply high power factor loads with high quality.

GENERAL CONCLUSION

This work presents a new design for a three phase cascaded MLI along with simulation and experimental results that validates the practical feasibility of the proposed three-phase MLI concept. Comparison with the published papers on three phase MLI topologies shows the superiority of the proposed inverter concept over existing topologies in terms of reducing devices count without compromising the quality of the output voltage.

The main contribution and key features of this research can be highlighted as follows:

The optimisation of photovoltaic systems under partial shaded conditions is achieved thanks to the proposed MPPT technique, based on PSO algorithm, which allow the global point of the maximum power of the PV generator to be tracked with great efficiency. The objective of the maximum power point tracking (MPPT) algorithm is to optimise the operating point of the PV system at the particular point on the *I-V* curve at which the module or array yields the greatest power. However, achieving this goal is a demanding task because the MPP on the *P-V* characteristic curve is inconsistent due to continuous variation of solar irradiance and its temperature. The situation is worsened under partial shading (PS) conditions where the *P-V* curve becomes multi-modal. Thanks to the ability of metha-heuristcs to handle multi-modal functions, MPPT controller based on a PSO algorithm is proposed to deal with the multi-modal characteristic of photovoltaic panel under partial shading conditions. Simulations

are carried out under extreme shading patterns to confirm their global search ability and their good dynamic performance. Furthermore, their performances are evaluated based on the tracking efficiency, speed and steady-state oscillation and ability to handle the partial shading. The simulations results show that the proposed method tracks the GMPP with a high accuracy and yield a static efficiency above 99%. In addition, the proposed scheme outperform the P&O methods in terms of global peak tracking. FPGA implementation is presented to validate the proposed controller on real time application. The implemented architectures are designed using hand written VHDL codes for better optimization of hardware resource and a more flexible and reusable structures. Being reconfigurable, FPGAs can offer a high degree of flexibility and robustness. Since the PWM signal is generated with a high resolution, the performance of the tracking process is largely improved. Experimental results confirm the efficiency of the proposed methods in the global peak tracking and their accuracy under partial shading conditions. This work authenticates the viability of the proposed PSO algorithm for MPPT of PV system. The tests and results demonstrate that the proposed controllers are capable of effectively and accurately locating MPP even under challenging and extreme conditions where many basic algorithms fail.

The ultimate goal of this research is to develop a generalized technique to reduce the number of devices of three phase multilevel inverter; this goal is achieved in a systematic process. An extensive literature study has been done on different cascaded multilevel inverter topologies and their control strategies. Besides, the shortcomings of the existing multilevel inverter topologies are highlighted.

An H-bridge cascade topology with non-isolated dc-voltage supplies is developed and proposed at the early stage of this research. The switching pulses of this topology are controlled by Space Vector Pulse Width Modulation (SVPWM) strategy. Besides, the proposed topology has been investigated under a number of case studies, different load power factor, dynamic load, and variable carrier frequency and modulation index. Moreover, the performance of the topology is tested while a PV-array is connected as an input dc-voltage supply. The proposed cascaded multilevel inverter is compared with a number of half- bridge inverter topologies in the literatures and it

has been found that the proposed architecture optimises the number of levels in the output voltage. The feasibility of the proposed inverter is confirmed through simulation and experimental analyses at different operating conditions. Since the number of inverter components is directly related to the cost, complexity and installation area, the new three phase concept offers a cost effective technique that is expected to have a great potential in renewable power generation systems and smart grid applications. The high frequency magnetic link provides galvanic isolation between input and output of the inverter that ensures more safety in grid connected inverter operation.

Future work Extend the study to other meta-heuristics : it would be interesting to investigate the possibility of tracking during partially shaded conditions with other meta-heuristics such as Ant Colony Optimization (ACO) , Cuckoo search (CS) and Firefly algorithm (FA). The implementation of these algorithms in FPGA could also be envisaged.

It is expected that the proposed cascaded MLI will play significant role in grid connected renewable energy conversion systems. Potential future research in this area could be:

While this thesis investigated the proposed MLIs using an open loop control algorithm, the inverter can be precisely controlled with a closed loop algorithm which can extend its applications in real time.

While real time PV generator units are utilised as input source, wind turbine generators can be connected as input sources to investigate the performance of the inverter when connected to real systems.

While staircase space vector modulation technique is utilized as a control strategy in the proposed CMLI, it may raise abnormal situation when the inverter is designed for bi- directional power conversion and hence, standard pulse width modulation/Sine pulse width modulation can be developed and investigated.

BIBLIOGRAPHY

[1] L. Hassaine, E. OLias, J. Quintero, V. Salas, Overview of power inverter topologies and control structures for grid connected photovoltaic systems, Renewable and Sustainable Energy Reviews 30 (2014) 796–807.

[2] F. Belhachat, C. Larbes, Global maximum power point tracking based on anfis approach for pv array configurations under partial shading conditions, Renewable and Sustainable Energy Reviews 77 (2017) 875–889.

[3] A. Mellit, S. Kalogirou, L. Hontoria, S. Shaari, Artificial intelligence techniques for sizing photovoltaic systems: A review, Renewable and Sustainable Energy Reviews 13 (2) (2009) 406–419.

[4] B. S. Kumar, K. Sudhakar, Performance evaluation of 10 mw grid connected solar photovoltaic power plant in india, Energy Reports 1 (2015) 184–192.

[5] A. Woyte, J. Nijs, R. Belmans, Partial shadowing of photovoltaic arrays with different system configurations: literature review and field test results, Solar Energy 74 (3) (2003) 217–233.

[6] G. Notton, V. Lazarov, L. Stoyanov, Optimal sizing of a grid-connected pv system for various pv module technologies and inclinations, inverter efficiency characteristics and locations, Renewable Energy 35 (2) (2010) 541–554.

[7] M. E. Meral, F. Dincer, A review of the factors affecting operation and efficiency of photovoltaic based electricity generation systems, Renewable and Sustainable Energy Reviews 15 (5) (2011) 2176–2184.

[8] F. Blaabjerg, U. Jaeger, S. Munk-Nielsen, Power losses in pwm-vsi inverter using npt or pt igbt devices, IEEE Transactions on power electronics 10 (3) (1995) 358–367.

[9] M. Singh, V. Khadkikar, A. Chandra, R. K. Varma, Grid interconnection of renewable energy sources at the distribution level with power-quality improvement features, IEEE transactions on power delivery 26 (1) (2011) 307–315.

[10] S. Bacha, D. Picault, B. Burger, I. Etxeberria-Otadui, J. Martins, Photovoltaics in microgrids: An overview of grid integration and energy management aspects, IEEE Industrial Electronics Magazine 9 (1) (2015) 33–46.

[11] S. Europe, Global market outlook for solar power 2018–2022, SolarPower Europe: Brussels, Belgium.

[12] C. S. Solanki, Solar photovoltaics: fundamentals, technologies and applications, PHI Learning Pvt. Ltd., 2015.

[13] A. Dolara, G. C. Lazaroiu, S. Leva, G. Manzolini, Experimental investigation of partial shading scenarios on pv (photovoltaic) modules, Energy 55 (2013) 466–475.

[14] R. Eke, C. Demircan, Shading effect on the energy rating of two identical pv systems on a building façade, Solar Energy 122 (2015) 48–57.

[15] J. Ahmed, Z. Salam, A critical evaluation on maximum power point tracking methods for partial shading in pv systems, Renewable and Sustainable Energy Reviews 47 (2015) 933–953.

[16] R. González, J. Lopez, P. Sanchis, L. Marroyo, Transformerless inverter for single-phase photovoltaic systems, IEEE Transactions on Power Electronics 22 (2) (2007) 693–697.

[17] S.-M. Chen, K.-R. Hu, T.-J. Liang, Y.-H. Hsieh, L.-S. Yang, Implementation of high step-up solar power optimizer for dc micro grid application, in: 2012 Twenty-Seventh Annual IEEE Applied Power Electronics Conference and Exposition (APEC), IEEE, 2012, pp. 28–32.

[18] T. K. S. Freddy, N. A. Rahim, W.-P. Hew, H. S. Che, Comparison and analysis of single-phase transformerless grid-connected pv inverters, IEEE Transactions on Power Electronics 29 (10) (2014) 5358–5369.

[19] G. Velasco-Quesada, F. Guinjoan-Gispert, R. Piqué-López, M. Román-Lumbreras, A. Conesa-Roca, Electrical pv array reconfiguration strategy for energy extraction improvement in grid-connected pv systems, IEEE Transactions on Industrial Electronics 56 (11) (2009) 4319–4331.

[20] T. M. Blooming, D. J. Carnovale, Application of ieee std 519-1992 harmonic limits, in: Conference Record of 2006 Annual Pulp and Paper Industry Technical Conference, IEEE, 2006, pp. 1–9.

[21] C. R. Reddy, K. H. Reddy, A passive islanding detection method for neutral point clamped multilevel inverter based distributed generation using rate of change of frequency analysis, International journal of electrical and computer engineering 8 (4) (2018) 1967.

[22] H.-C. Seo, C.-H. Kim, Y.-M. Yoon, C.-S. Jung, Dynamics of grid-connected photovoltaic system at fault conditions, in: 2009 Transmission & Distribution Conference & Exposition: Asia and Pacific, IEEE, 2009, pp. 1–4.

[23] Y. Bae, T.-K. Vu, R.-Y. Kim, Implemental control strategy for grid stabilization of grid-connected pv system based on german grid code in symmetrical low-to-medium voltage network, IEEE Transactions on Energy Conversion 28 (3) (2013) 619–631.

[24] A. Yazdani, R. Iravani, Voltage-sourced converters in power systems: modeling, control, and applications, John Wiley & Sons, 2010.

[25] X. Bao, F. Zhuo, Y. Tian, P. Tan, Simplified feedback linearization control of three-phase photovoltaic inverter with an lcl filter, Power Electronics, IEEE Transactions on 28 (6) (2013) 2739–2752.

[26] M. Ebrahimi, S. A. Khajehoddin, M. Karimi-Ghartemani, Fast and robust single-phase *dq* current controller for smart inverter applications, IEEE transactions on power electronics 31 (5) (2016) 3968–3976.

[27] J. Twidell, T. Weir, Renewable energy resources, Routledge, 2015.

[28] S. Kouro, J. I. Leon, D. Vinnikov, L. G. Franquelo, Grid-connected photovoltaic systems: An overview of recent research and emerging pv converter technology, IEEE Industrial Electronics Magazine 9 (1) (2015) 47–61.

[29] N.-G. Park, T. Miyasaka, M. Grätzel, Organic-inorganic halide perovskite photovoltaics, Cham, Switzerland: Springer.

[30] A. Sorokin, S. Bobashev, T. Feigl, K. Tiedtke, H. Wabnitz, M. Richter, Photoelectric effect at ultrahigh intensities, Physical review letters 99 (21) (2007) 213002.

[31] R. Miles, K. Hynes, I. Forbes, Photovoltaic solar cells: An overview of state-of-the-art cell development and environmental issues, Progress in crystal growth and characterization of materials 51 (1-3) (2005) 1–42.

[32] G. N. Tiwari, S. Dubey, Fundamentals of Photovoltaic Modules and Their Applications, no. 2, Royal Society of Chemistry, 2010.

[33] S. Bhatia, 4 - solar thermal energy, in: S. Bhatia (Ed.), Advanced Renewable Energy Systems, Woodhead Publishing India, 2014, pp. 94 – 143.

[34] A. Mellit, S. A. Kalogirou, Artificial intelligence techniques for photovoltaic applications: A review, Progress in energy and combustion science 34 (5) (2008) 574–632.

[35] V. Salas, E. Olias, A. Barrado, A. Lazaro, Review of the maximum power point tracking algorithms for stand-alone photovoltaic systems, Solar energy materials and solar cells 90 (11) (2006) 1555–1578.

[36] M. A. Eltawil, Z. Zhao, Grid-connected photovoltaic power systems: Technical and potential problems—a review, Renewable and Sustainable Energy Reviews 14 (1) (2010) 112–129.

[37] A. Makki, S. Omer, H. Sabir, Advancements in hybrid photovoltaic systems for enhanced solar cells performance, Renewable and sustainable energy reviews 41 (2015) 658–684.

[38] K. Ishaque, Z. Salam, et al., A comprehensive matlab simulink pv system simulator with partial shading capability based on two-diode model, Solar energy 85 (9) (2011) 2217–2227.

[39] F. Belhachat, C. Larbes, A review of global maximum power point tracking techniques of photovoltaic system under partial shading conditions, Renewable and Sustainable Energy Reviews 92 (2018) 513–553.

[40] N. Belhaouas, M.-S. A. Cheikh, P. Agathoklis, M.-R. Oularbi, B. Amrouche, K. Sedraoui, N. Djilali, Pv array power output maximization under partial shading using new shifted pv array arrangements, Applied energy 187 (2017) 326–337.

[41] A. Kouchaki, H. Iman-Eini, B. Asaei, A new maximum power point tracking strategy for pv arrays under uniform and non-uniform insolation conditions, Solar Energy 91 (2013) 221–232.

[42] J. Ahmed, Z. Salam, A critical evaluation on maximum power point tracking methods for partial shading in pv systems, Renewable and Sustainable Energy Reviews 47 (2015) 933–953.

[43] T. L. Nguyen, K.-S. Low, A global maximum power point tracking scheme employing direct search algorithm for photovoltaic systems, IEEE transactions on Industrial Electronics 57 (10) (2010) 3456–3467.

[44] K. Lian, J. Jhang, I. Tian, A maximum power point tracking method based on perturb-and-observe combined with particle swarm optimization, IEEE journal of photovoltaics 4 (2) (2014) 626–633.

[45] R.-Y. Kim, J.-H. Kim, An improved global maximum power point tracking scheme under partial shading conditions, in: Journal of International Conference on Electrical Ma-

chines and Systems, Vol. 2, Journal of International Conference on Electrical Machines and Systems, 2013, pp. 65–68.

[46] B. N. Alajmi, K. H. Ahmed, S. J. Finney, B. W. Williams, A maximum power point tracking technique for partially shaded photovoltaic systems in microgrids, IEEE Transactions on Industrial Electronics 60 (4) (2013) 1596–1606.

[47] R. Boukenoui, H. Salhi, R. Bradai, A. Mellit, A new intelligent mppt method for standalone photovoltaic systems operating under fast transient variations of shading patterns, Solar Energy 124 (2016) 124–142.

[48] R. Balasankar, G. T. Arasu, J. C. M. Raj, A global mppt technique invoking partitioned estimation and strategic deployment of p&o to tackle partial shading conditions, Solar Energy 143 (2017) 73–85.

[49] K. S. Tey, S. Mekhilef, M. Seyedmahmoudian, B. Horan, A. T. Oo, A. Stojcevski, Improved differential evolution-based mppt algorithm using sepic for pv systems under partial shading conditions and load variation, IEEE Transactions on Industrial Informatics 14 (10) (2018) 4322–4333.

[50] J. H. Holland, et al., Adaptation in natural and artificial systems: an introductory analysis with applications to biology, control, and artificial intelligence, MIT press, 1992.

[51] D. B. Fogel, An introduction to simulated evolutionary optimization, IEEE transactions on neural networks 5 (1) (1994) 3–14.

[52] A. Ostermeier, A. Gawelczyk, N. Hansen, Step-size adaptation based on non-local use of selection information, in: International Conference on Parallel Problem Solving from Nature, Springer, 1994, pp. 189–198.

[53] K. S. Tey, S. Mekhilef, H.-T. Yang, M.-K. Chuang, A differential evolution based mppt method for photovoltaic modules under partial shading conditions, International Journal of Photoenergy 2014.

[54] D. Simon, Biogeography-based optimization, IEEE transactions on evolutionary computation 12 (6) (2008) 702–713.

[55] I. Fister Jr, X.-S. Yang, I. Fister, J. Brest, D. Fister, A brief review of nature-inspired algorithms for optimization, arXiv preprint arXiv:1307.4186.

[56] J. H. Holland, Genetic algorithms and the optimal allocation of trials, SIAM Journal on Computing 2 (2) (1973) 88–105.

[57] M. B. Smida, A. Sakly, Genetic based algorithm for maximum power point tracking (mppt) for grid connected pv systems operating under partial shaded conditions, in:

2015 7th International Conference on Modelling, Identification and Control (ICMIC), IEEE, 2015, pp. 1–6.

[58] R. Ramaprabha, B. Mathur, Genetic algorithm based maximum power point tracking for partially shaded solar photovoltaic array, Int J Res Rev Inf Sci (IJRRIS) 2 (1) (2012) 161–163.

[59] H. R. Mohajeri, M. P. Moghaddam, M. Shahparasti, M. Mohamadian, Development a new algorithm for maximum power point tracking of partially shaded photovoltaic arrays, in: 20th Iranian Conference on Electrical Engineering (ICEE2012), IEEE, 2012, pp. 489–494.

[60] Y. Shaiek, M. B. Smida, A. Sakly, M. F. Mimouni, Comparison between conventional methods and ga approach for maximum power point tracking of shaded solar pv generators, Solar energy 90 (2013) 107–122.

[61] G. Shankar, V. Mukherjee, Mpp detection of a partially shaded pv array by continuous ga and hybrid pso, Ain Shams Engineering Journal 6 (2) (2015) 471–479.

[62] R. Storn, Differrential evolution-a simple and efficient adaptive scheme for global optimization over continuous spaces, Technical report, International Computer Science Institute 11.

[63] H. Taheri, Z. Salam, K. Ishaque, et al., A novel maximum power point tracking control of photovoltaic system under partial and rapidly fluctuating shadow conditions using differential evolution, in: 2010 IEEE Symposium on Industrial Electronics and Applications (ISIEA), IEEE, 2010, pp. 82–87.

[64] M. F. N. Tajuddin, S. M. Ayob, Z. Salam, Tracking of maximum power point in partial shading condition using differential evolution (de), in: 2012 IEEE International Conference on Power and Energy (PECon), IEEE, 2012, pp. 384–389.

[65] M. Seyedmahmoudian, R. Rahmani, S. Mekhilef, A. M. T. Oo, A. Stojcevski, T. K. Soon, A. S. Ghandhari, Simulation and hardware implementation of new maximum power point tracking technique for partially shaded pv system using hybrid depso method, IEEE transactions on sustainable energy 6 (3) (2015) 850–862.

[66] Z.-F. Hao, G.-H. Guo, H. Huang, A particle swarm optimization algorithm with differential evolution, in: 2007 international conference on machine learning and cybernetics, Vol. 2, IEEE, 2007, pp. 1031–1035.

[67] W.-J. Zhang, X.-F. Xie, Depso: hybrid particle swarm with differential evolution operator, in: SMC'03 Conference Proceedings. 2003 IEEE International Conference on Systems, Man and Cybernetics. Conference Theme-System Security and Assurance (Cat. No. 03CH37483), Vol. 4, IEEE, 2003, pp. 3816–3821.

[68] R. Xu, J. Xu, D. C. Wunsch, A comparison study of validity indices on swarm-intelligence-based clustering, IEEE Transactions on Systems, Man, and Cybernetics, Part B (Cybernetics) 42 (4) (2012) 1243–1256.

[69] K. S. Tey, S. Mekhilef, M. Seyedmahmoudian, B. Horan, A. M. T. Oo, A. Stojcevski, Improved differential evolution-based mppt algorithm using sepic for pv systems under partial shading conditions and load variation, IEEE Transactions on Industrial Informatics.

[70] R. Eberhart, J. Kennedy, A new optimizer using particle swarm theory, in: MHS'95. Proceedings of the Sixth International Symposium on Micro Machine and Human Science, Ieee, 1995, pp. 39–43.

[71] M. Miyatake, M. Veerachary, F. Toriumi, N. Fujii, H. Ko, Maximum power point tracking of multiple photovoltaic arrays: a pso approach, IEEE Transactions on Aerospace and Electronic Systems 47 (1) (2011) 367–380.

[72] J. Shi, W. Zhang, Y. Zhang, F. Xue, T. Yang, Mppt for pv systems based on a dormant pso algorithm, Electric Power Systems Research 123 (2015) 100–107.

[73] K. Ishaque, Z. Salam, M. Amjad, S. Mekhilef, An improved particle swarm optimization (pso)–based mppt for pv with reduced steady-state oscillation, IEEE transactions on Power Electronics 27 (8) (2012) 3627–3638.

[74] K. Ishaque, Z. Salam, A deterministic particle swarm optimization maximum power point tracker for photovoltaic system under partial shading condition, IEEE transactions on industrial electronics 60 (8) (2013) 3195–3206.

[75] K. Kaced, C. Larbes, S. M. Ait-Chikh, M. Bounabi, Z. E. Dahmane, Fpga implementation of pso based mppt for pv systems under partial shading conditions, in: Systems and Control (ICSC), 2017 6th International Conference on, IEEE, 2017, pp. 150–155.

[76] S. M. Mirhassani, S. Z. M. Golroodbari, S. M. M. Golroodbari, S. Mekhilef, An improved particle swarm optimization based maximum power point tracking strategy with variable sampling time, International Journal of Electrical Power & Energy Systems 64 (2015) 761–770.

[77] K. Lian, J. Jhang, I. Tian, A maximum power point tracking method based on perturb-and-observe combined with particle swarm optimization, IEEE journal of photovoltaics 4 (2) (2014) 626–633.

[78] M. Kermadi, Z. Salam, J. Ahmed, E. M. Berkouk, An effective hybrid maximum power point tracker of photovoltaic arrays for complex partial shading conditions, IEEE Transactions on Industrial Electronics.

[79] M. Bounabi, K. Kaced, M. S. Ait-Cheikh, C. Larbes, Z. e. Dahmane, N. Ramzan, Modelling and performance analysis of different multilevel inverter topologies using pso-mppt technique for grid connected photovoltaic systems, Journal of Renewable and Sustainable Energy 10 (4) (2018) 043507.

[80] K. Kaced, C. Larbes, N. Ramzan, M. Bounabi, Z. elabadine Dahmane, Bat algorithm based maximum power point tracking for photovoltaic system under partial shading conditions, Solar Energy 158 (2017) 490–503.

[81] M. Dorigo, Optimization, learning and natural algorithms, PhD Thesis, Politecnico di Milano.

[82] M. Dorigo, L. M. Gambardella, M. Birattari, A. Martinoli, R. Poli, T. Stützle, Ant Colony Optimization and Swarm Intelligence: 5th International Workshop, ANTS 2006, Brussels, Belgium, September 4-7, 2006, Proceedings, Vol. 4150, Springer, 2006.

[83] K. Socha, M. Dorigo, Ant colony optimization for continuous domains, European journal of operational research 185 (3) (2008) 1155–1173.

[84] T. Liao, T. Stützle, M. A. M. de Oca, M. Dorigo, A unified ant colony optimization algorithm for continuous optimization, European Journal of Operational Research 234 (3) (2014) 597–609.

[85] L. L. Jiang, D. L. Maskell, J. C. Patra, A novel ant colony optimization-based maximum power point tracking for photovoltaic systems under partially shaded conditions, Energy and Buildings 58 (2013) 227–236.

[86] S. Titri, C. Larbes, K. Y. Toumi, K. Benatchba, A new mppt controller based on the ant colony optimization algorithm for photovoltaic systems under partial shading conditions, Applied Soft Computing 58 (2017) 465–479.

[87] J. Ahmed, Z. Salam, A maximum power point tracking (mppt) for pv system using cuckoo search with partial shading capability, Applied Energy 119 (2014) 118–130.

[88] J. Ahmed, Z. Salam, A soft computing mppt for pv system based on cuckoo search algorithm, in: 4th International Conference on Power Engineering, Energy and Electrical Drives, IEEE, 2013, pp. 558–562.

[89] S. Berrazouane, K. Mohammedi, Parameter optimization via cuckoo optimization algorithm of fuzzy controller for energy management of a hybrid power system, Energy conversion and management 78 (2014) 652–660.

[90] G. Velasco-Quesada, F. Guinjoan-Gispert, R. Piqué-López, M. Román-Lumbreras, A. Conesa-Roca, Electrical pv array reconfiguration strategy for energy extraction im-

provement in grid-connected pv systems, IEEE Transactions on Industrial Electronics 56 (11) (2009) 4319–4331.

[91] D. Nguyen, B. Lehman, A reconfigurable solar photovoltaic array under shadow conditions, in: Applied Power Electronics Conference and Exposition, 2008. APEC 2008. Twenty-Third Annual IEEE, IEEE, 2008, pp. 980–986.

[92] L. Gao, R. A. Dougal, S. Liu, A. P. Iotova, Parallel-connected solar pv system to address partial and rapidly fluctuating shadow conditions, IEEE Transactions on industrial Electronics 56 (5) (2009) 1548–1556.

[93] D. Nguyen, B. Lehman, An adaptive solar photovoltaic array using model-based reconfiguration algorithm, IEEE Transactions on Industrial Electronics 55 (7) (2008) 2644–2654.

[94] J. M. Myrzik, M. Calais, String and module integrated inverters for single-phase grid connected photovoltaic systems-a review, in: 2003 IEEE Bologna Power Tech Conference Proceedings,, Vol. 2, Citeseer, 2003, pp. 8–pp.

[95] S. A. Khajehoddin, A. Bakhshai, P. Jain, A novel topology and control strategy for maximum power point trackers and multi-string grid-connected pv inverters, in: 2008 Twenty-Third Annual IEEE Applied Power Electronics Conference and Exposition, IEEE, 2008, pp. 173–178.

[96] J. Jana, H. Saha, K. D. Bhattacharya, A review of inverter topologies for single-phase grid-connected photovoltaic systems, Renewable and Sustainable Energy Reviews 72 (2017) 1256–1270.

[97] B. Sahan, A. N. Vergara, N. Henze, A. Engler, P. Zacharias, A single-stage pv module integrated converter based on a low-power current-source inverter, IEEE Transactions on Industrial Electronics 55 (7) (2008) 2602–2609.

[98] S. Vighetti, Systèmes photovoltaïques raccordés au réseau: Choix et dimensionnement des étages de conversion, Ph.D. thesis, Institut National Polytechnique de Grenoble-INPG (2010).

[99] C. Cabal, L. Martínez-Salamero, L. Séguier, C. Alonso, F. Guinjoan, Maximum power point tracking based on sliding-mode control for output-series connected converters in photovoltaic systems, IET Power Electronics 7 (4) (2013) 914–923.

[100] G. P. Adam, O. Anaya-Lara, G. M. Burt, D. Telford, B. Williams, J. McDonald, Modular multilevel inverter: Pulse width modulation and capacitor balancing technique, IET power electronics 3 (5) (2010) 702–715.

[101] T. Chen, C. K. Lee, R. Hui, A general design procedure for multi-parallel modular grid-tied inverters system to prevent common and interactive instability, IEEE Transactions on Power Electronics.

[102] C. Verdugo, J. I. Candela, F. Blaabjerg, P. Rodriguez, Three-phase isolated multi-modular converter in renewable energy distribution systems, IEEE Journal of Emerging and Selected Topics in Power Electronics.

[103] S. B. Kjaer, J. K. Pedersen, F. Blaabjerg, A review of single-phase grid-connected inverters for photovoltaic modules, IEEE transactions on industry applications 41 (5) (2005) 1292–1306.

[104] M. Amjad, Z. Salam, M. Facta, S. Mekhilef, Analysis and implementation of transformerless lcl resonant power supply for ozone generation, IEEE transactions on power electronics 28 (2) (2013) 650–660.

[105] F. Blaabjerg, R. Teodorescu, M. Liserre, A. V. Timbus, Overview of control and grid synchronization for distributed power generation systems, IEEE Transactions on industrial electronics 53 (5) (2006) 1398–1409.

[106] M. Islam, S. Mekhilef, High efficiency transformerless mosfet inverter for grid-tied photovoltaic system, in: 2014 IEEE Applied Power Electronics Conference and Exposition-APEC 2014, IEEE, 2014, pp. 3356–3361.

[107] V. Salas, E. Olías, Overview of the state of technique for pv inverters used in low voltage grid-connected pv systems: Inverters above 10 kw, Renewable and Sustainable Energy Reviews 15 (2) (2011) 1250–1257.

[108] S. Rollier, B. Richard, M. Keller, Earth leakage control in solar inverters, Power System Design Europe.

[109] S. B. Kjaer, Design and control of an inverter for photovoltaic applications, Institute of Energy Technology, Aalborg University, 2005.

[110] S. Mekhilef, A. Omar, K. Muhammad, An improved topology of digitally-controlled single-phase single-stage high dc voltage converter, in: 2006 37th IEEE Power Electronics Specialists Conference, IEEE, 2006, pp. 1–5.

[111] T. Ishikawa, Grid-connected photovoltaic power systems: survey of inverter and related protection equipments, Report IEA PVPS T5-05 2006.

[112] L. Gertmar, P. Karlsson, O. Samuelsson, On dc injection to ac grids from distributed generation, in: 2005 European Conference on Power Electronics and Applications, IEEE, 2005, pp. 10–pp.

[113] M. Meinhardt, Improvement of photovoltaic inverter efficiency–targets, methods, limits, SMA Technologie AG.

[114] H. Haeberlin, L. Borgia, M. Kaempfer, U. Zwahle, New tests at grid-connected pv inverters: Overview over test results and measured values of total efficiency ηtot, in: 21st European Photovoltaic Solar Energy Conference, Dresden, 2006.

[115] H. Haeberlin, Evolution of inverters for grid connected pv-systems from 1989 to 2000, measurement 2 (1).

[116] Q. Jiang, J. Brown, Comparison of electromagnetic compatibility of different pv inverter, in: 4th IEEE International Conference on Power Electronics and Drive Systems. IEEE PEDS 2001-Indonesia. Proceedings (Cat. No. 01TH8594), Vol. 1, IEEE, 2001, pp. 420–424.

[117] C.-L. Shen, S.-T. Peng, A half-bridge pv system with bi-direction power flow controlling and power quality improvement, in: 2007 7th International Conference on Power Electronics and Drive Systems, IEEE, 2007, pp. 725–731.

[118] R. González, E. Gubía, J. López, L. Marroyo, Transformerless single-phase multilevel-based photovoltaic inverter, IEEE Transactions on Industrial Electronics 55 (7) (2008) 2694–2702.

[119] A. Hasanzadeh, C. S. Edrington, J. Leonard, Reduced switch npc-based transformerless pv inverter by developed switching pattern, in: 2012 Twenty-Seventh Annual IEEE Applied Power Electronics Conference and Exposition (APEC), IEEE, 2012, pp. 359–360.

[120] L. Ma, T. Kerekes, R. Teodorescu, X. Jin, D. Floricau, M. Liserre, The high efficiency transformer-less pv inverter topologies derived from npc topology, in: 2009 13th European Conference on Power Electronics and Applications, IEEE, 2009, pp. 1–10.

[121] I. Patrao, E. Figueres, F. González-Espín, G. Garcerá, Transformerless topologies for grid-connected single-phase photovoltaic inverters, Renewable and Sustainable Energy Reviews 15 (7) (2011) 3423–3431.

[122] D. M. Baker, V. G. Agelidis, C. Nayer, A comparison of tri-level and bi-level current controlled grid-connected single-phase full-bridge inverters, in: ISIE'97 Proceeding of the IEEE International Symposium on Industrial Electronics, Vol. 2, IEEE, 1997, pp. 463–468.

[123] S. V. Araújo, P. Zacharias, R. Mallwitz, Highly efficient single-phase transformerless inverters for grid-connected photovoltaic systems, IEEE Transactions on Industrial Electronics 57 (9) (2010) 3118–3128.

[124] B. Burger, D. Kranzer, Extreme high efficiency pv-power converters, in: 2009 13th European Conference on Power Electronics and Applications, IEEE, 2009, pp. 1–13.

[125] L. Ma, F. Tang, F. Zhou, X. Jin, Y. Tong, Leakage current analysis of a single-phase transformer-less pv inverter connected to the grid, in: 2008 IEEE International Conference on Sustainable Energy Technologies, IEEE, 2008, pp. 285–289.

[126] O. Lopez, R. Teodorescu, J. Doval-Gandoy, Multilevel transformerless topologies for single-phase grid-connected converters, in: IECON 2006-32nd annual conference on IEEE industrial electronics, IEEE, 2006, pp. 5191–5196.

[127] O. Lopez, R. Teodorescu, F. Freijedo, J. Doval-Gandoy, Eliminating ground current in a transformerless photovoltaic application, in: 2007 IEEE Power Engineering Society General Meeting, IEEE, 2007, pp. 1–5.

[128] K. Zhang, Y. Zhou, Y. Zhang, Y. Kang, Reduction of common mode emi in a full-bridge converter through automatic tuning of gating signals, in: 2006 CES/IEEE 5th International Power Electronics and Motion Control Conference, Vol. 1, IEEE, 2006, pp. 1–5.

[129] H. Hinz, P. Mutschler, Single phase voltage source inverters without transformer in photovoltaic applications, in: Proc. Int. Power Electron. Motion Control Conf.(PEMC), 1996, pp. 161–165.

[130] J. Rodriguez, S. Bernet, P. K. Steimer, I. E. Lizama, A survey on neutral-point-clamped inverters, IEEE transactions on Industrial Electronics 57 (7) (2010) 2219–2230.

[131] M. Calais, V. G. Agelidis, Multilevel converters for single-phase grid connected photovoltaic systems-an overview, in: IEEE International Symposium on Industrial Electronics. Proceedings. ISIE'98 (Cat. No. 98TH8357), Vol. 1, IEEE, 1998, pp. 224–229.

[132] Z. Zheng-Yi, Z. Chang-Jiang, H. Yu, X. Ting, Z. Liang-Bing, Analysis on voltage unbalance between the inner and outer devices in three level igbt converters, in: Proceedings of the IEEE 1999 International Conference on Power Electronics and Drive Systems. PEDS'99 (Cat. No. 99TH8475), Vol. 1, IEEE, 1999, pp. 218–224.

[133] T. Bruckner, S. Bernet, H. Guldner, The active npc converter and its loss-balancing control, IEEE Transactions on Industrial Electronics 52 (3) (2005) 855–868.

[134] H. Xiao, S. Xie, Transformerless split-inductor neutral point clamped three-level pv grid-connected inverter, IEEE transactions on power electronics 27 (4) (2012) 1799–1808.

[135] W. Wu, Y. He, T. Tang, F. Blaabjerg, A new design method for the passive damped lcl and llcl filter-based single-phase grid-tied inverter, IEEE Transactions on Industrial Electronics 60 (10) (2013) 4339–4350.

[136] B. Chen, P. Sun, C. Liu, C.-L. Chen, J.-S. Lai, W. Yu, High efficiency transformerless photovoltaic inverter with wide-range power factor capability, in: 2012 Twenty-Seventh

Annual IEEE Applied Power Electronics Conference and Exposition (APEC), IEEE, 2012, pp. 575–582.

[137] S. Kouro, M. Malinowski, K. Gopakumar, J. Pou, L. G. Franquelo, B. Wu, J. Rodriguez, M. A. Pérez, J. I. Leon, Recent advances and industrial applications of multilevel converters, IEEE Transactions on industrial electronics 57 (8) (2010) 2553–2580.

[138] A. Lesnicar, R. Marquardt, An innovative modular multilevel converter topology suitable for a wide power range, in: 2003 IEEE Bologna Power Tech Conference Proceedings,, Vol. 3, IEEE, 2003, pp. 6–pp.

[139] S. Daher, J. Schmid, F. L. Antunes, Multilevel inverter topologies for stand-alone pv systems, IEEE transactions on industrial electronics 55 (7) (2008) 2703–2712.

[140] X. Kou, K. A. Corzine, Y. Familiant, A unique fault-tolerant design for flying capacitor multilevel inverters, in: IEEE International Electric Machines and Drives Conference, 2003. IEMDC'03., Vol. 1, IEEE, 2003, pp. 531–538.

[141] M. Victor, Method of converting a dc voltage of a dc source, in particular of a photovoltaic dc source, in an ac voltage, European Patent, EP1626494, DE10204030912.

[142] G. Vazquez, T. Kerekes, A. Rolan, D. Aguilar, A. Luna, G. Azevedo, Losses and cmv evaluation in transformerless grid-connected pv topologies, in: 2009 IEEE International Symposium on Industrial Electronics, IEEE, 2009, pp. 544–548.

[143] F. Schimpf, L. E. Norum, et al., Grid connected converters for photovoltaic, state of the art, ideas for improvement of transformerless inverters, in: Nordic Workshop on Power and Industrial Electronics (NORPIE/2008), June 9-11, 2008, Espoo, Finland, Helsinki University of Technology, 2008.

[144] M. Shayestegan, M. Shakeri, H. Abunima, S. S. Reza, M. Akhtaruzzaman, B. Bais, S. Mat, K. Sopian, N. Amin, An overview on prospects of new generation single-phase transformerless inverters for grid-connected photovoltaic (pv) systems, Renewable and Sustainable Energy Reviews 82 (2018) 515–530.

[145] T. Kerekes, R. Teodorescu, P. Rodríguez, G. Vázquez, E. Aldabas, A new high-efficiency single-phase transformerless pv inverter topology, IEEE Transactions on industrial electronics 58 (1) (2011) 184–191.

[146] J. Dominic, Comparison and design of high efficiency microinverters for photovoltaic applications, Ph.D. thesis, Virginia Tech (2014).

[147] Y. Gu, W. Li, Y. Zhao, B. Yang, C. Li, X. He, Transformerless inverter with virtual dc bus concept for cost-effective grid-connected pv power systems, IEEE Transactions on Power Electronics 28 (2) (2013) 793–805.

[148] B. Yang, W. Li, Y. Gu, W. Cui, X. He, Improved transformerless inverter with common-mode leakage current elimination for a photovoltaic grid-connected power system, IEEE transactions on power electronics 27 (2) (2012) 752–762.

[149] H. Schmidt, S. Christoph, J. Ketterer, Current inverter for direct/alternating currents, has direct and alternating connections with an intermediate power store, a bridge circuit, rectifier diodes and a inductive choke, German Patent DE10 221 (592) (2003) A1.

[150] M. Shayestegan, M. Shakeri, H. Abunima, S. S. Reza, M. Akhtaruzzaman, B. Bais, S. Mat, K. Sopian, N. Amin, An overview on prospects of new generation single-phase transformerless inverters for grid-connected photovoltaic (pv) systems, Renewable and Sustainable Energy Reviews 82 (2018) 515–530.

[151] J. M. Myrzik, M. Calais, String and module integrated inverters for single-phase grid connected photovoltaic systems-a review, in: 2003 IEEE Bologna Power Tech Conference Proceedings,, Vol. 2, Citeseer, 2003, pp. 8–pp.

[152] W. Yu, J.-S. J. Lai, H. Qian, C. Hutchens, High-efficiency mosfet inverter with h6-type configuration for photovoltaic nonisolated ac-module applications, IEEE Transactions on Power Electronics 26 (4) (2011) 1253–1260.

[153] W. Yu, J.-S. Lai, H. Qian, C. Hutchens, J. Zhang, G. Lisi, A. Djabbari, G. Smith, T. Hegarty, High-efficiency inverter with h6-type configuration for photovoltaic non-isolated ac module applications, in: 2010 Twenty-Fifth Annual IEEE Applied Power Electronics Conference and Exposition (APEC), IEEE, 2010, pp. 1056–1061.

[154] B. Gu, J. Dominic, J.-S. Lai, C.-L. Chen, T. LaBella, B. Chen, High reliability and efficiency single-phase transformerless inverter for grid-connected photovoltaic systems, IEEE Transactions on Power Electronics 28 (5) (2013) 2235–2245.

[155] R. González, J. Lopez, P. Sanchis, L. Marroyo, Transformerless inverter for single-phase photovoltaic systems, IEEE Transactions on Power Electronics 22 (2) (2007) 693–697.

[156] H. Xiao, S. Xie, Y. Chen, R. Huang, An optimized transformerless photovoltaic grid-connected inverter, IEEE Transactions on Industrial Electronics 58 (5) (2011) 1887–1895.

[157] J. Wang, B. Ji, J. Zhao, J. Yu, From h4, h5 to h6—standardization of full-bridge single phase photovoltaic inverter topologies without ground leakage current issue, in: 2012 IEEE Energy Conversion Congress and Exposition (ECCE), IEEE, 2012, pp. 2419–2425.

[158] T. Kerekes, Analysis and modeling of transformerless photovoltaic inverter systems, Institute of Energy Technology, Aalborg University, 2009.

[159] O. Lopez, R. Teodorescu, J. Doval-Gandoy, Multilevel transformerless topologies for single-phase grid-connected converters, in: IECON 2006-32nd annual conference on IEEE industrial electronics, IEEE, 2006, pp. 5191–5196.

[160] B. Chen, J.-S. Lai, A family of single-phase transformerless inverters with asymmetric phase-legs, in: 2015 IEEE Applied Power Electronics Conference and Exposition (APEC), IEEE, 2015, pp. 2200–2205.

[161] S. P. Pimentel, R. M. M. Martinez, J. A. Pomilio, Single-phase distributed generation system based on asymmetrical cascaded multilevel inverter, in: 2009 Brazilian Power Electronics Conference, IEEE, 2009, pp. 346–353.

[162] J. I. Leon, L. G. Franquelo, S. Kouro, B. Wu, S. Vazquez, Simple modulator with voltage balancing control for the hybrid five-level flying-capacitor based anpc converter, in: 2011 IEEE International Symposium on Industrial Electronics, IEEE, 2011, pp. 1887–1892.

[163] M. Schweizer, J. W. Kolar, Design and implementation of a highly efficient three-level t-type converter for low-voltage applications, IEEE Transactions on Power Electronics 28 (2) (2013) 899–907.

[164] B. Ji, J. Wang, J. Zhao, High-efficiency single-phase transformerless pv h6 inverter with hybrid modulation method, IEEE Transactions on Industrial Electronics 60 (5) (2013) 2104–2115.

[165] L. Zhang, K. Sun, Y. Xing, M. Xing, H6 transformerless full-bridge pv grid-tied inverters, IEEE Transactions on Power Electronics 29 (3) (2014) 1229–1238.

[166] M. B. Latran, A. Teke, Investigation of multilevel multifunctional grid connected inverter topologies and control strategies used in photovoltaic systems, Renewable and Sustainable Energy Reviews 42 (2015) 361–376.

[167] S. R. Pendem, S. Mikkili, Modelling and performance assessment of pv array topologies under partial shading conditions to mitigate the mismatching power losses, Solar Energy 160 (2018) 303–321.

[168] F. Belhachat, C. Larbes, Modeling, analysis and comparison of solar photovoltaic array configurations under partial shading conditions, Solar Energy 120 (2015) 399 – 418.

[169] M. Horoufiany, R. Ghandehari, Optimization of the sudoku based reconfiguration technique for pv arrays power enhancement under mutual shading conditions, Solar Energy 159 (2018) 1037–1046.

[170] L. Hassaine, E. Olías, J. Quintero, A. Barrado, Power control for grid connected applications based on the phase shifting of the inverter output voltage with respect to the grid voltage, International Journal of Electrical Power & Energy Systems 57 (2014) 250–260.

[171] S. S. Letha, T. Thakur, J. Kumar, Harmonic elimination of a photo-voltaic based cascaded h-bridge multilevel inverter using pso (particle swarm optimization) for induction motor drive, Energy 107 (2016) 335–346.

[172] S. V. Dhople, J. L. Ehlmann, A. Davoudi, P. L. Chapman, Multiple-input boost converter to minimize power losses due to partial shading in photovoltaic modules, in: Energy Conversion Congress and Exposition (ECCE), 2010 IEEE, IEEE, 2010, pp. 2633–2636.

[173] E. Roman, R. Alonso, P. Ibañez, S. Elorduizapatarietxe, D. Goitia, Intelligent pv module for grid-connected pv systems, IEEE Transactions on Industrial electronics 53 (4) (2006) 1066–1073.

[174] W. Wu, J. Ji, F. Blaabjerg, Aalborg inverter-a new type of buck in buck, boost in boost grid-tied inverter, IEEE Transactions on power electronics 30 (9) (2015) 4784–4793.

[175] G. Adinolfi, G. Graditi, P. Siano, A. Piccolo, Multiobjective optimal design of photovoltaic synchronous boost converters assessing efficiency, reliability, and cost savings, IEEE Transactions on Industrial Informatics 11 (5) (2015) 1038–1048.

[176] D. Debnath, K. Chatterjee, Two-stage solar photovoltaic-based stand-alone scheme having battery as energy storage element for rural deployment, IEEE Transactions on Industrial Electronics 62 (7) (2015) 4148–4157.

[177] F. Spertino, G. Graditi, Power conditioning units in grid-connected photovoltaic systems: A comparison with different technologies and wide range of power ratings, Solar Energy 108 (2014) 219–229.

[178] M. Islam, S. Mekhilef, An improved transformerless grid connected photovoltaic inverter with reduced leakage current, Energy Conversion and Management 88 (2014) 854–862.

[179] A. Bidram, A. Davoudi, R. S. Balog, Control and circuit techniques to mitigate partial shading effects in photovoltaic arrays, IEEE Journal of Photovoltaics 2 (4) (2012) 532–546.

[180] A. Nabae, I. Takahashi, H. Akagi, A new neutral-point-clamped pwm inverter, IEEE Transactions on industry applications (5) (1981) 518–523.

[181] K. K. Gupta, A. Ranjan, P. Bhatnagar, L. K. Sahu, S. Jain, Multilevel inverter topologies with reduced device count: a review, IEEE Transactions on Power Electronics 31 (1) (2016) 135–151.

[182] H. Wang, L. Kou, Y.-F. Liu, P. C. Sen, A seven-switch five-level active-neutral-point-clamped converter and its optimal modulation strategy, IEEE Transactions on Power Electronics 32 (7) (2017) 5146–5161.

[183] E. Babaei, S. Laali, Z. Bayat, A single-phase cascaded multilevel inverter based on a new basic unit with reduced number of power switches, IEEE Transactions on industrial electronics 62 (2) (2015) 922–929.

[184] Y. Hinago, H. Koizumi, A single-phase multilevel inverter using switched series/parallel dc voltage sources, IEEE transactions on industrial electronics 57 (8) (2010) 2643–2650.

[185] S. S. Lee, M. Sidorov, N. R. N. Idris, Y. E. Heng, A symmetrical cascaded compact-module multilevel inverter (ccm-mli) with pulsewidth modulation, IEEE Transactions on Industrial Electronics 65 (6) (2018) 4631–4639.

[186] A. K. Sadigh, M. Abarzadeh, K. A. Corzine, V. Dargahi, A new breed of optimized symmetrical and asymmetrical cascaded multilevel power converters, IEEE Journal of Emerging and Selected Topics in Power Electronics 3 (4) (2015) 1160–1170.

[187] S. Daher, J. Schmid, F. L. Antunes, Multilevel inverter topologies for stand-alone pv systems, IEEE transactions on industrial electronics 55 (7) (2008) 2703–2712.

[188] B. Subudhi, R. Pradhan, A comparative study on maximum power point tracking techniques for photovoltaic power systems, IEEE transactions on Sustainable Energy 4 (1) (2013) 89–98.

[189] I. Abdalla, J. Corda, L. Zhang, Multilevel dc-link inverter and control algorithm to overcome the pv partial shading, IEEE Transactions on Power Electronics 28 (1) (2013) 14–18.

[190] E. Esfandiari, N. B. Mariun, Experimental results of 47-level switch-ladder multilevel inverter, IEEE Transactions on Industrial Electronics 60 (11) (2013) 4960–4967.

[191] A. Alexander, M. Thathan, Modelling and analysis of modular multilevel converter for solar photovoltaic applications to improve power quality, IET renewable power Generation 9 (1) (2014) 78–88.

[192] R. R. Karasani, V. B. Borghate, P. M. Meshram, H. M. Suryawanshi, S. Sabyasachi, A three-phase hybrid cascaded modular multilevel inverter for renewable energy environment, IEEE Transactions on Power Electronics 32 (2) (2017) 1070–1087.

[193] A. Sinha, K. C. Jana, M. K. Das, An inclusive review on different multi-level inverter topologies, their modulation and control strategies for a grid connected photo-voltaic system, Solar Energy 170 (2018) 633–657.

[194] E. Samadaei, S. A. Gholamian, A. Sheikholeslami, J. Adabi, An envelope type (e-type) module: asymmetric multilevel inverters with reduced components, IEEE Transactions on Industrial Electronics 63 (11) (2016) 7148–7156.

[195] M. Mao, L. Zhang, Q. Duan, B. Chong, Multilevel dc-link converter photovoltaic system with modified pso based on maximum power point tracking, Solar Energy 153 (2017) 329–342.

[196] Y. Ounejjar, K. Al-Haddad, L.-A. Gregoire, Packed u cells multilevel converter topology: theoretical study and experimental validation, IEEE Transactions on Industrial Electronics 58 (4) (2011) 1294–1306.

[197] R. Barzegarkhoo, E. Zamiri, N. Vosoughi, H. M. Kojabadi, L. Chang, Cascaded multilevel inverter using series connection of novel capacitor-based units with minimum switch count, IET Power Electronics 9 (10) (2016) 2060–2075.

[198] S. Behara, N. Sandeep, U. R. Yaragatti, Simplified transformer-based multilevel inverter topology and generalisations for renewable energy applications, IET Power Electronics 11 (4) (2017) 708–718.

[199] A. Ruderman, About voltage total harmonic distortion for single-and three-phase multilevel inverters, IEEE Transactions on Industrial Electronics 62 (3) (2015) 1548–1551.

[200] R. R. Karasani, V. B. Borghate, P. M. Meshram, H. Suryawanshi, A modified switched-diode topology for cascaded multilevel inverters, Journal of Power Electronics 16 (5) (2016) 1706–1715.

[201] M. Khenar, A. Taghvaie, J. Adabi, M. Rezanejad, Multi-level inverter with combined t-type and cross-connected modules, IET Power Electronics 11 (8) (2018) 1407–1415.

[202] M. Saeedian, S. M. Hosseini, J. Adabi, Step-up switched-capacitor module for cascaded mli topologies, IET Power Electronics 11 (7) (2018) 1286–1296.

[203] A. Mortezaei, M. G. Simões, T. D. C. Busarello, F. P. Marafão, A. Al-Durra, Grid-connected symmetrical cascaded multilevel converter for power quality improvement, IEEE Transactions on Industry Applications 54 (3) (2018) 2792–2805.

[204] L. He, C. Cheng, A bridge modular switched-capacitor-based multilevel inverter with optimized spwm control method and enhanced power-decoupling ability, IEEE Transactions on Industrial Electronics 65 (8) (2018) 6140–6149.

[205] A.-V. Ho, T.-W. Chun, Single-phase modified quasi-z-source cascaded hybrid five-level inverter, IEEE Transactions on Industrial Electronics 65 (6) (2018) 5125–5134.

[206] G. E. Valderrama, G. V. Guzman, E. I. Pool-Mazún, P. R. Martinez-Rodriguez, M. J. Lopez-Sanchez, J. M. S. Zuñiga, A single-phase asymmetrical t-type five-level transformerless pv inverter, IEEE Journal of Emerging and Selected Topics in Power Electronics 6 (1) (2018) 140–150.

[207] H. Wu, L. Zhu, F. Yang, T. Mu, H. Ge, Dual-dc-port asymmetrical multilevel inverters with reduced conversion stages and enhanced conversion efficiency, IEEE Transactions on Industrial Electronics 64 (3) (2017) 2081–2091.

[208] N. Arun, M. M. Noel, Crisscross switched multilevel inverter using cascaded semi-half-bridge cells, IET Power Electronics 11 (1) (2017) 23–32.

[209] J.-S. Lee, H.-W. Sim, J. Kim, K.-B. Lee, Combination analysis and switching method of a cascaded h-bridge multilevel inverter based on transformers with the different turns ratio for increasing the voltage level, IEEE Transactions on Industrial Electronics 65 (6) (2018) 4454–4465.

[210] M. Srndovic, A. Zhetessov, T. Alizadeh, Y. L. Familiant, G. Grandi, A. Ruderman, Simultaneous selective harmonic elimination and thd minimization for a single-phase multilevel inverter with staircase modulation, IEEE Transactions on Industry Applications 54 (2) (2018) 1532–1541.

[211] M. K. Das, K. C. Jana, A. Sinha, Performance evaluation of an asymmetrical reduced switched multi-level inverter for a grid-connected pv system, IET Renewable Power Generation 12 (2) (2017) 252–263.

[212] J. Liu, J. Wu, J. Zeng, H. Guo, A novel nine-level inverter employing one voltage source and reduced components as high-frequency ac power source, IEEE Transactions on Power Electronics 32 (4) (2017) 2939–2947.

[213] A. N. Babadi, O. Salari, M. J. Mojibian, M. T. Bina, Modified multilevel inverters with reduced structures based on packedu-cell, IEEE Journal of Emerging and Selected Topics in Power Electronics 6 (2) (2018) 874–887.

[214] M. Norambuena, S. Kouro, S. Dieckerhoff, J. Rodriguez, Reduced multilevel converter: A novel multilevel converter with a reduced number of active switches, IEEE Transactions on Industrial Electronics 65 (5) (2018) 3636–3645.

[215] S. S. Lee, M. Sidorov, C. S. Lim, N. R. N. Idris, Y. E. Heng, Hybrid cascaded multilevel inverter (hcmli) with improved symmetrical 4-level submodule, IEEE Transactions on Power Electronics 33 (2) (2018) 932–935.

[216] M.-K. Nguyen, T.-T. Tran, Quasi cascaded h-bridge five-level boost inverter, IEEE Transactions on industrial electronics 64 (11) (2017) 8525–8533.

[217] X.-S. Yang, Chapter 1 - introduction to algorithms, in: X.-S. Yang (Ed.), Nature-Inspired Optimization Algorithms, Elsevier, Oxford, 2014, pp. 1 – 21.

[218] K.-L. Du, M. Swamy, et al., Search and optimization by metaheuristics, Springer, 2016.

[219] X.-S. Yang, Chapter 2 - analysis of algorithms, in: X.-S. Yang (Ed.), Nature-Inspired Optimization Algorithms, Elsevier, Oxford, 2014, pp. 23 – 44.

[220] J. KENNEDY, Particle swarm optimization, in: Proc. of 1995 IEEE Int. Conf. Neural Networks,(Perth, Australia), Nov. 27-Dec., Vol. 4, 1995, pp. 1942–1948.

[221] R. Eberhart, J. Kennedy, A new optimizer using particle swarm theory, in: Micro Machine and Human Science, 1995. MHS'95., Proceedings of the Sixth International Symposium on, IEEE, 1995, pp. 39–43.

[222] Y. Shi, R. Eberhart, A modified particle swarm optimizer, in: Evolutionary Computation Proceedings, 1998. IEEE World Congress on Computational Intelligence., The 1998 IEEE International Conference on, IEEE, 1998, pp. 69–73.

[223] T. L. Nguyen, K.-S. Low, A global maximum power point tracking scheme employing direct search algorithm for photovoltaic systems, IEEE transactions on Industrial Electronics 57 (10) (2010) 3456–3467.

[224] A. K. Gupta, A. M. Khambadkone, A general space vector pwm algorithm for multilevel inverters, including operation in overmodulation range, Power Electronics, IEEE Transactions on 22 (2) (2007) 517–526.

[225] Y. Deng, K. H. Teo, C. Duan, T. G. Habetler, R. G. Harley, A fast and generalized space vector modulation scheme for multilevel inverters, Power Electronics, IEEE Transactions on 29 (10) (2014) 5204–5217.

[226] E. Pouresmaeil, D. Montesinos-Miracle, O. Gomis-Bellmunt, J. Bergas-Jané, A multiobjective control strategy for grid connection of dg (distributed generation) resources, Energy 35 (12) (2010) 5022–5030.

[227] A. K. Gupta, A. M. Khambadkone, A space vector modulation scheme to reduce common mode voltage for cascaded multilevel inverters, Power Electronics, IEEE Transactions on 22 (5) (2007) 1672–1681.

[228] S. K. Mondal, B. K. Bose, V. Oleschuk, J. O. Pinto, Space vector pulse width modulation of three-level inverter extending operation into overmodulation region, Power Electronics, IEEE Transactions on 18 (2) (2003) 604–611.

[229] J. Holtz, W. Lotzkat, A. M. Khambadkone, On continuous control of pwm inverters in the overmodulation range including the six-step mode, Power Electronics, IEEE Transactions on 8 (4) (1993) 546–553.

[230] A. Tripathi, A. M. Khambadkone, S. K. Panda, Direct method of overmodulation with integrated closed loop stator flux vector control, Power Electronics, IEEE Transactions on 20 (5) (2005) 1161–1168.

[231] A. K. Gupta, A. M. Khambadkone, A general space vector pwm algorithm for multi-level inverters, including operation in overmodulation range, Power Electronics, IEEE Transactions on 22 (2) (2007) 517–526.

[232] X. Bao, F. Zhuo, Y. Tian, P. Tan, Simplified feedback linearization control of three-phase photovoltaic inverter with an lcl filter, Power Electronics, IEEE Transactions on 28 (6) (2013) 2739–2752.

[233] N. Pogaku, M. Prodanović, T. C. Green, Modeling, analysis and testing of autonomous operation of an inverter-based microgrid, Power Electronics, IEEE Transactions on 22 (2) (2007) 613–625.